

WAVE SLAMMING ON A HORIZONTAL PLATE

by

SHANKAR SUBRAYA BHAT

**B.E., Karnataka University, India, 1984
M.Tech., Mangalore University, 1986**

**A THESIS SUBMITTED IN PARTIAL FULFILLMENT OF
THE REQUIREMENTS FOR THE DEGREE OF
MASTER OF APPLIED SCIENCE**

in

**THE FACULTY OF GRADUATE STUDIES
DEPARTMENT OF CIVIL ENGINEERING**

**We accept this thesis as conforming
to the required standard**

THE UNIVERSITY OF BRITISH COLUMBIA

August, 1994

© Shankar S. Bhat, 1994

In presenting this thesis in partial fulfillment of the requirements for an advanced degree at the University of British Columbia, I agree that the Library shall make it freely available for reference and study. I further agree that permission for extensive copying of this thesis for scholarly purposes may be granted by the head of my department or by his or her representatives. It is understood that copying or publication of this thesis for financial gain shall not be allowed without my written permission.

(Signature)

Department of Civil Engineering

The University of British Columbia
Vancouver, Canada

Date September 29th, 1994

Abstract

The design of coastal and offshore structures requires a thorough understanding of environmental loading, particularly due to waves. Structural elements such as decks located in the splash zone encounter intermittent contact with the water, and the loads associated with the water impact may be several times larger than those experienced by elements when fully submerged. These forces may give rise to localized damage and to fatigue problems.

Such structures should clearly be designed to account for wave impact, in addition to more general wave loading. Several studies have reported the related problems of ship bottom slamming, missile entry and sea plane landing. Although previous studies have contributed to an improved understanding of wave impact, there is still considerable uncertainty in the estimation of impact loads on structural elements near the water surface. In this context, the present study has been carried out to examine the wave loads on a fixed horizontal plate located near the still water level.

Experiments were conducted in the wave flume of the Hydraulics Laboratory of the Department of Civil Engineering at the University of British Columbia. A plate, 60.0 cm long, 20.0 cm wide and 6.25 mm thick, was instrumented with load-cells to measure the vertical force on the plate due to waves. The plate was supported by two vertical rods through the load-cells which were connected to a cross shaft mounted on bearings at the ends.

Tests were conducted over a range of wave periods and wave heights in combination with different plate clearances above the still water level. The vertical reactions at the two supports were measured, and the time histories of vertical force and its line of action are

thereby obtained. The wave surface elevations at the leading and rear end of the plate were measured with the plate absent. Results are presented in the form of force time histories, their lines of action and the associated water surface elevation. An analysis of these time histories is carried out to obtain various parameters of wave impact which include, the peak upward and downward force, their lines of action and times of occurrence, and the associated wetted lengths. The influence of incident wave parameters on these is investigated. Video images are studied to understand the impact process and to identify the difficulties involved in the investigation. An attempt is also made to predict the vertical force based on the hydrodynamic impact, drag and buoyancy forces.

Table of Contents

	Page
Abstract.....	ii
Table of Contents	iv
List of Tables.....	vii
List of Figures.....	viii
List of Symbols	xii
Acknowledgments.....	xv
Chapter 1 Introduction	1
1.1 General.....	1
1.2 Literature Review	2
1.2.1 Water Entry Problem	2
1.2.2 Horizontal Cylinder	4
1.2.3 Horizontal Plate.....	5
1.3 Scope of the Present Investigation.....	7
Chapter 2 Theoretical Development.....	8
2.1 Dimensional Analysis.....	8

2.2 Vertical Force Formulation.....	10
2.2.1 Wave Theory and Associated Kinematics	14
2.2.2 Superposition of Force Components	16
2.3 Dynamic Response of SDOF System	19
Chapter 3 Experimental Investigation.....	21
3.1 Introduction.....	21
3.2 The Plate	21
3.3 Wave Flume and Generator	22
3.4 Control and Data Acquisition.....	23
3.5 Measurements	23
3.6 Experimental Procedures.....	24
3.7 Dynamic Characteristics of the Assembly.....	25
3.8 Data Processing	27
Chapter 4 Results and Discussion.....	29
4.1 Vertical Force.....	30
4.2 Vertical Force and Incident Waves.....	32
4.3 Video Records.....	34
4.4 Force Predictions.....	35

Chapter 5 Conclusions and Recommendations 38

References 40

Appendix A Static Analysis 42

List of Tables

Table 2.1 Added mass constant for a thin rectangular plate.

Table 3.1 Regular wave parameters used in experiments.

Table 4.1 Summary of test conditions and principal results.

Table 4.2 Computed values of the factor α in selected tests.

List of Figures

- Fig. 1.1 Photographs of typical jetty facilities, Jericho beach, Vancouver.
- Fig. 2.1 Definition sketch.
- Fig. 2.2 Stages of wave propagation past a horizontal plate. (a) initial contact, $t = t_0$; (b) submergence of upwave portion of plate, $t_0 < t < t_1$; (c) complete submergence of plate, $t_1 < t < t_2$; (d) submergence of downwave portion of plate, $t_2 < t < t_3$; (e) wave detaching from plate, $t = t_3$.
- Fig. 2.3 Sketch of ideal force components variation over a wave cycle. (a) free surface elevation; (b) wetted length λ ; (c) proposed variation of $\partial\lambda/\partial t$ as a *velocity* c' ; (d) force components: inertia force, F_{a1} ; added mass force, F_{a2} ; drag force, F_d ; buoyancy force, F_b ; (e) total vertical force: actual force, predicted force.
- Fig. 2.4 Variation of added mass functions with plate aspect ratio λ/b . (a) $f_1(\lambda/b)$; (b) $f_2(\lambda/b)$.
- Fig. 2.5 Variation of dimensionless added mass with plate aspect ratio λ/b . (a) Eq. 2.7; (b) Eq. 2.26.
- Fig. 2.6 Definition sketch of a single degree of freedom (SDOF) system.
- Fig. 2.7 Sketch of an idealized force as a triangular pulse.
- Fig. 2.8 Dynamic amplification factor and relative rise-time as a function of T_r/T_n for applied impulsive force with $T_d/T_r = 1$. (Isaacson and Prasad, 1993).
- Fig. 3.1 Photographs of the plate assembly. (a) side view; (b) top view indicating the details of supports and load-cell arrangements.
- Fig. 3.2 Experimental setup showing the details of the plate and the load-cell arrangement. (a) elevation; (b) cross-section.
- Fig. 3.3 Sketch showing the wave flume and the test location.
- Fig. 3.4 Flow chart indicating the wave generation and the data control setup.
- Fig. 3.5 Response of load-cells A and B to a step load of 117.7 N (12 kg) tested in air. (a) time history; (b) spectral density.
- Fig. 3.6 Response of load-cells A and B to a step load of 58.9 N (6 kg) tested for a submerged condition. (a) time history; (b) spectral density.
- Fig. 3.7 Time histories of the measured vertical force showing the effect of filtering ($h = 1.4$ cm, $T = 2.02$ sec, $H = 17.5$ cm). (a) unfiltered force signal; (b) filtered force signal at 15 Hz cut-off.

- Fig. 3.8 Time histories of total vertical force and its line of action showing the effect of filtering ($h = 1.4$ cm, $T = 2.02$ sec, $H = 17.5$ cm). (a) unfiltered force (b) filtered force with 15 Hz cut-off.
- Fig. 3.9 Time histories of (a) free surface elevation; (b) vertical force and its line of action. ($h = 1.4$ cm, $T = 2.02$ sec, $H = 17.5$ cm).
- Fig. 3.10 Flow chart indicating the sequence of analysis of the measured force and wave elevation time histories.
- Fig. 4.1 Time histories of free surface elevation, wetted length, vertical force measured at the supports, total vertical force and the associated line of action during one wave cycle for $h = 0.8$ cm, $T = 1.68$ sec, $H = 14.2$ cm. (a) free surface elevation and wetted length; (b) vertical force; (c) total vertical force and line of action.
- Fig. 4.2 Time histories of free surface elevation, wetted length, vertical force measured at the supports, total vertical force and the associated line of action during one wave cycle for $h = 0.8$ cm, $T = 1.70$ sec, $H = 10.5$ cm. (a) free surface elevation and wetted length; (b) vertical force; (c) total vertical force and line of action.
- Fig. 4.3 Time histories of free surface elevation, wetted length, vertical force measured at the supports, total vertical force and the associated line of action during one wave cycle for $h = 0.8$ cm, $T = 1.70$ sec, $H = 6.80$ cm. (a) free surface elevation and wetted length; (b) vertical force; (c) total vertical force and line of action.
- Fig. 4.4 Time histories of free surface elevation, wetted length, vertical force measured at the supports, total vertical force and the associated line of action during one wave cycle for $h = 1.4$ cm, $T = 1.68$ sec, $H = 14.2$ cm. (a) free surface elevation and wetted length; (b) vertical force; (c) total vertical force and line of action.
- Fig. 4.5 Time histories of free surface elevation, wetted length, vertical force measured at the supports, total vertical force and the associated line of action during one wave cycle for $h = 1.4$ cm, $T = 1.68$ sec, $H = 10.5$ cm. (a) free surface elevation and wetted length; (b) vertical force; (c) total vertical force and line of action.
- Fig. 4.6 Time histories of free surface elevation, wetted length, vertical force measured at the supports, total vertical force and the associated line of action during one wave cycle for $h = 0$ cm, $T = 2.02$ sec, $H = 17.5$ cm. (a) free surface elevation and wetted length; (b) vertical force; (c) total vertical force and line of action.
- Fig. 4.7 Time histories of free surface elevation, wetted length, vertical force measured at the supports, total vertical force and the associated line of action during one wave cycle for $h = 1.4$ cm, $T = 2.02$ sec, $H = 17.5$ cm. (a) free surface elevation and wetted length; (b) vertical force; (c) total vertical force and line of action.

- Fig. 4.8 Time histories of free surface elevation, wetted length, vertical force measured at the supports, total vertical force and the associated line of action during one wave cycle for $h = 2.5$ cm, $T = 2.02$ sec, $H = 17.5$ cm. (a) free surface elevation and wetted length; (b) vertical force; (c) total vertical force and line of action.
- Fig. 4.9 Maximum upward force coefficient $F_p/\rho g b H \ell$ as a function of relative plate clearance h/H and relative plate length ℓ/L . (a) $0.016 < H/L < 0.020$; (b) $0.026 < H/L < 0.030$; (c) $0.035 < H/L < 0.041$.
- Fig. 4.10 Maximum downward force coefficient $F_m/\rho g b H \ell$ as a function of relative plate clearance h/H and relative plate length ℓ/L . (a) $0.016 < H/L < 0.020$; (b) $0.026 < H/L < 0.030$; (c) $0.035 < H/L < 0.041$.
- Fig. 4.11 Non-dimensionalised duration of plate's partial submergence T_c/T as a function of relative plate clearance h/H and relative plate length ℓ/L . (a) $0.016 < H/L < 0.020$; (b) $0.026 < H/L < 0.030$; (c) $0.035 < H/L < 0.041$.
- Fig. 4.12 Non-dimensionalised duration of plate's complete submergence T_s/T as a function of relative plate clearance h/H and relative plate length ℓ/L . (a) $0.016 < H/L < 0.020$; (b) $0.026 < H/L < 0.030$; (c) $0.035 < H/L < 0.041$.
- Fig. 4.13 Non-dimensionalised rise-time T_p/T of peak vertical force as a function of relative plate clearance h/H and relative plate length ℓ/L . (a) $0.016 < H/L < 0.020$; (b) $0.026 < H/L < 0.030$; (c) $0.035 < H/L < 0.041$.
- Fig. 4.14 Non-dimensionalised time of occurrence T_m/T of maximum downward force as a function of relative plate clearance h/H and relative plate length ℓ/L . (a) $0.016 < H/L < 0.020$; (b) $0.026 < H/L < 0.030$; (c) $0.035 < H/L < 0.041$.
- Fig. 4.15 Non-dimensionalised line of action s_p/L of maximum upward force as a function of relative plate clearance h/H and relative plate length ℓ/L . (a) $0.016 < H/L < 0.020$; (b) $0.026 < H/L < 0.030$; (c) $0.035 < H/L < 0.041$.
- Fig. 4.16 Non-dimensionalised line of action s_m/L of maximum downward force as a function of relative plate clearance h/H and relative plate length ℓ/L . (a) $0.016 < H/L < 0.020$; (b) $0.026 < H/L < 0.030$; (c) $0.035 < H/L < 0.041$.
- Fig. 4.17 Non-dimensionalised wetted length λ_p/L corresponding to maximum upward force as a function of relative plate clearance h/H and relative plate length ℓ/L . (a) $0.016 < H/L < 0.020$; (b) $0.026 < H/L < 0.030$; (c) $0.035 < H/L < 0.041$.
- Fig. 4.18 Non-dimensionalised wetted length λ_m/L corresponding to maximum downward force as a function of relative plate clearance h/H and relative plate length ℓ/L . (a) $0.016 < H/L < 0.020$; (b) $0.026 < H/L < 0.030$; (c) $0.035 < H/L < 0.041$.
- Fig. 4.19 Photographs of wave impact. (a) instant of complete submergence; (b) water drainage following the submergence.
- Fig. 4.20 Video images indicating various stages of wave impact during one wave cycle. (a) partial submergence; (b) complete submergence; (c) wave recession; (d) water drainage.

- Fig. 4.21 Variation of normalized free surface elevation and predicted vertical force based on Eq. 2.23 for $H/L = 0.04$, $\ell/L = 0.146$ with two different plate clearances. (a) free surface elevation; (b) vertical force for $h/H = 0$; (c) vertical force for $h/H = 0.15$.
- Fig. 4.22 Variation of normalized free surface elevation and predicted vertical force based on Eq. 2.27 for $H/L = 0.04$, $\ell/L = 0.146$ with two different plate clearances. (a) free surface elevation; (b) vertical force for $h/H = 0$; (c) vertical force for $h/H = 0.15$.
- Fig. 4.23 Comparison of vertical force predicted by analytical models with experimental observation for $h = 0$ cm, $T = 2.02$ sec, $H = 17.5$ cm. (a) free surface elevation and the wetted length; (b) vertical force.
- Fig. 4.24 Comparison of vertical force predicted by analytical models with experimental observation for $h = 0$ cm, $T = 1.68$ sec, $H = 14.2$ cm. (a) free surface elevation and the wetted length; (b) vertical force.
- Fig. 4.25 Comparison of vertical force predicted by analytical models with experimental observation for $h = 1.4$ cm, $T = 2.02$ sec, $H = 17.5$ cm. (a) free surface elevation and the wetted length; (b) vertical force.
- Fig. A1 Free body diagram of the plate indicating the support forces and the line of action of the vertical force.

List of Symbols

b	=	width of the plate
C	=	damping of the measuring system
c	=	wave celerity
c'	=	wave front velocity
C_d	=	drag coefficient
C_s	=	slamming coefficient
D	=	cylinder diameter
d	=	water depth
F	=	vertical force due to wave action on the plate
F_A	=	reaction measured at support A (see Fig. A1)
F_a	=	hydrodynamic force
F_{a1}	=	inertia force
F_{a2}	=	added mass force
F_B	=	reaction measured at support B (see Fig. A1)
F_d	=	drag force
F_m	=	peak downward force
F_o	=	peak force
F_p	=	peak upward force
F_t	=	measured vertical force
g	=	gravitational constant
H	=	wave height
h	=	plate clearance above the still water level
K	=	stiffness
k	=	wave number, $2\pi/L$

k_1	=	stiffness of support A
k_2	=	stiffness of support B
L	=	wave length
ℓ	=	length of the cylinder or plate
M	=	mass of measuring system
m	=	added mass per unit width of the plate
p_m	=	amplitude of the free vibration force trace measured after m cycles
q	=	half wetted length of the plate
s	=	line of action of F
s_m	=	line of action associated with F_m
s_p	=	line of action associated with F_p
T	=	wave period
t	=	time
t_0	=	instant at initial impact
t_1	=	instant at complete submergence
t_2	=	instant at which leading edge of the horizontal plate located at a clearance h just emerges out of wave
t_3	=	instant at which horizontal plate located at a clearance h completely out of water.
T_c	=	duration for plate's partial submergence (= $t_1 - t_0$)
T_d	=	decay-time
T_m	=	time of occurrence associated with F_m
t_m	=	average of times t_1 and t_2
T_r	=	rise-time associated with applied force
T_s	=	duration of plate's complete submergence (= $t_2 - t_1$)
T_t	=	measured rise-time associated with F_p
u	=	displacement of the measuring system
v	=	vertical velocity of the free surface

w	=	plate thickness
x	=	horizontal coordinate in wave direction
\bar{F}	=	vertical force per unit width
\ddot{u}	=	acceleration of the measuring system
\dot{u}	=	velocity of the measuring system
\dot{v}	=	vertical acceleration of the free surface profile
α	=	added mass correction factor
η	=	free surface elevation
η_0	=	free surface elevation at $x = 0$
η_ℓ	=	free surface elevation at $x = \ell$
$\ddot{\eta}$	=	vertical particle acceleration of the free surface profile
$\dot{\eta}$	=	vertical particle velocity of the free surface profile
ℓ	=	plate length
λ	=	wetted length
λ_m	=	wetted length associated with F_m
λ_p	=	wetted length associated with F_p
ρ	=	fluid density
ω	=	wave angular frequency, $2\pi/T$
ω_d	=	damped frequency of the measuring system
ω_n	=	natural frequency of the measuring system
ξ	=	damping ratio

Acknowledgments

The author would like to thank his supervisor Dr. Michael Isaacson for his guidance and encouragement throughout the preparation of this thesis. The author would like to express his gratitude to Kurt Nielson for his help in building the model and other facilities associated with the experimental investigation; to John Wong for his help relating to electronic parts for the experiments; and to Sundar Prasad for his help relating to the experimental setup, computing and the wave generator facilities. Also, Amal Phadke, Neal Whiteside and Henry Kandioh are thanked for their help in running the experiments. The author would also like to thank the Director, National Institute of Oceanography, Goa, India, (Council for Scientific and Industrial Research), for granting a study leave to pursue higher education, and also the Ministry of Human Resources Development, Government of India, for being selected for the Canadian Commonwealth Scholarship Plan. Finally, financial support in the form of a Scholarship from the Canadian Commonwealth Fellowship Plan, Canadian Bureau for International Education, Government of Canada, is gratefully acknowledged.

Chapter 1

Introduction

1.1 General

The design of coastal and offshore structures requires a thorough understanding of environmental loads which are primarily due to waves. Structural elements such as decks, which are located in the splash zone (i.e. at elevations which cause them to be intermittently submerged), may be subjected to impulsive loads that can be several times larger than those experienced by continuously submerged elements. These impulsive forces may give rise to fatigue and to localized damage.

There are various examples of structural damage due to wave impact. For example, Denson and Priest (1971) described the inspection of structural damage due to hurricanes along the Gulf Coast, which revealed that horizontal floors, decks and platforms are susceptible to severe damage by wave action. Da Costa and Scott (1988) reported that a moderate storm on Lake Michigan in 1987 moved partially constructed concrete slabs at the Jones Island East Dock. Another example is the case of the Ekofisk platform whose deck was exposed to severe wave impact (Broughton and Horn, 1987).

Figure 1.1 provides a view of a typical jetty with its deck structure above the mean water level. Clearly, such structures should be designed for local stresses due to wave impact in addition to the design for overall loads. Even so, decks need to be sufficiently high above the water surface in order to avoid unduly severe wave impact. Besides the phenomenon of wave impact on decks, other situations such as seaplane landing, ship bow slamming,

platform bracings situated in the splash zone, and liquid sloshing in tanks also require design with respect to hydrodynamic impact. It is therefore important to have a good understanding of the wave slamming process on the basis of theoretical and/or experimental investigations. Although previous work has contributed to the understanding of the wave impact nature, there is still considerable uncertainty in the estimation of impact loads on structural elements near the water surface. In this context, the present study has been carried out to address the problem of wave loads on a fixed horizontal plate located near the still water level.

1.2 Literature Review

The Morison equation is commonly used to calculate the wave force on fully submerged slender structural members of different cross sections. However, structural members which are located in the splash zone, such as the deck of a wharf, are intermittently submerged and experience a large vertical force which cannot be predicted by the Morison equation. These vertical forces are highly dynamic and characterized by large magnitudes with short duration.

Although, problems relating to water entry and wave impact on flat bottom ships have been the subject of numerous theoretical and experimental studies for many years, wave impact forces on horizontal decks has received attention only since the early sixties. In the following sections, a brief review of available theoretical and experimental investigations relating to water impact and entry problem is presented.

1.2.1 Water Entry Problem

Hydrodynamic impact refers to the early stages of the entry of a body into water. Approaches to describing this have generally been based on potential flow theory for an incompressible fluid with a free surface. The solution of such problems may be related to

the determination of a variable added mass associated with the body as it enters the fluid. In a classical paper, von Kármán (1929) presented a physical picture of the impact of a wedge on a still water surface, intended to represent the impact process for the case of a seaplane landing. On the basis of von Kármán's approach, Wagner (1932) provided a mathematical treatment of forces acting on a seaplane float. In this classical approach, no consideration has been given to the effects of entrapped air or water compressibility. Nevertheless, Wagner's theoretical values show reasonable agreement with experimental results obtained for two-dimensional models (Chuang, 1967).

The above approach is based on potential flow theory and provides an estimate of the impact force on the impacting member during the initial stage of water entry. Beyond this stage, the member also experiences inertia and drag forces. An extensive review of the subject has been given by Szebehely (1966), emphasizing the principles involved in different kinds of wave impact. Also, Faltinsen (1990) has summarized recent developments of the water impact and entry problem.

A number of experimental studies on a flat bottom plate striking normal to a smooth water surface have been reported. The magnitude of the maximum impact pressure is theoretically equal to the acoustic pressure, which is the product of the velocity of sound in the fluid, the fluid density and the velocity of the striking body. The results of drop tests on models with flat bottoms have, however, shown that peak pressures are usually much lower than the acoustic pressure because of the air entrapped between the body and the water surface. Verhagen (1967) developed a theory to predict the impact pressures by considering the influence of the compressed air between the plate and water surface. He also investigated the phenomenon experimentally and showed that the predicted values are in good agreement with the observed values obtained from two-dimensional tests of a body having a completely flat bottom. Recently, Chan *et al.* (1991) emphasized the influence of

trapped air on impulsive pressure and examined the process of wave impact relating to vertical plates on the basis of a simplified one-dimensional model.

In the following sections, the related situation of a horizontal circular cylinder is considered, followed by experimental investigations of wave action on a horizontal plate.

1.2.2 Horizontal Cylinder

The impact force on a cylinder is given by the rate of change of fluid momentum which is a function of the cylinder's added mass that varies with the submergence. From a number of past theoretical and experimental investigations on circular cylindrical horizontal members, the slamming force F_s is considered to be proportional to the square of the wave impact velocity and is expressed as:

$$F_s = (C_s) \left(\frac{1}{2} \rho v^2\right) (D\ell) \quad (1.1)$$

where C_s is a slamming coefficient, ℓ is the cylinder length, D is the cylinder diameter, ρ is the fluid density, and v is water particle velocity normal to the member surface. There has been considerable debate on the choice of a proper value of C_s , typically ranging from π to 2π (e.g. Kaplan and Silbert, 1976, Sarpkaya, 1978, Sarpkaya and Isaacson, 1981, Armand and Cointe, 1987, Greenhow and Li, 1987, Chan and Melville, 1989, Chan, *et al.* 1991, Isaacson and Prasad, 1992). Although the slamming force is associated with the rate of change of momentum during the early stages of impact, extending such a formulation beyond the initial stages gives rise to a number of complications. These are mainly attributed to the water level variations in the vicinity of the partially submerged member and the subsequent onset of drag forces. In addition to the above, the buoyancy force and the inertia force also form significant components of the vertical force on the cylinder. The associated force coefficients also vary with the submergence, member size and flow kinematics. Also, the problem of wave action on a

cylinder may involve splashing and air entrapment, and partial and/or complete submergence.

1.2.3 Horizontal Plate

The following paragraphs give a brief account of previous studies relating to wave action on a horizontal plate.

El Ghamry (1963) carried out an early experimental study on the vertical force due to non-breaking and breaking regular waves slamming on a horizontal plate. He indicated that the vertical force is characterized by an initial peak of considerable magnitude and short duration, followed by a slowly varying force of smaller magnitude extending over the remaining period of submergence. He proposed a theoretical description of the force based on a potential flow past a rigid fixed flat plate, incorporating suitable correction factors relating to the deck length, wave length and water depth.

Furudo and Murita (1966) studied experimentally the total vertical force on a horizontal plate extending seaward from a vertical wall and noted a sharp impulsive force as indicated by El Ghamry, with the average pressure head on the platform ranging from 1 to 8 times the incident wave height.

Wang (1967) carried out experiments on a horizontal pier model subjected to slamming by progressive and standing waves. He derived simple theoretical values for peak pressures, by adapting an approximate analysis based on the fluid momentum principle, and related the peak pressure to the celerity of the wave and the velocity of the fluid element near the wave front. The slowly varying pressure head was simply taken as the pressure in the undeformed wave at the deck elevation.

French (1969) carried out an extensive laboratory study and confirmed the nature of the impact force to be similar to that observed by El Ghamry. He predicted the impact force

magnitude on the basis of a momentum conservation and energy equation. Denson and Priest (1971) carried out a laboratory study to identify the influence of relative wave height, relative plate clearance, relative plate width and relative plate length on the pressure distribution under a thick horizontal plate. Tanimoto and Takahashi (1979) reported on an experimental investigation to obtain the horizontal and vertical forces on a rigid platform due to periodic waves. The uplift pressure was expressed as the sum of a shock pressure component and a static pressure component. They developed an empirical shock pressure term as a function of the contact angle between the undisturbed wave surface and the bottom of the horizontal platform. More recently, Toumazis *et al.* (1989) investigated experimentally wave impact pressures on both horizontal and vertical plates. Pressure measurements in conjunction with observations using video records were adopted to study the impact loading behaviour.

Irajpanah (1983) studied wave uplift pressures on horizontal platforms and presented a finite element method to investigate the hydrodynamic loads on a horizontal platform. Also, Lai and Lee (1989) developed a potential flow model using the finite element method, and predicted the vertical forces of large amplitude waves on docks. They used a Galerkin finite element method and studied the interaction of finite amplitude nonlinear water waves with platforms. Their results compared reasonably well with the experimental results of French (1969).

Kaplan (1992) extended the hydrodynamic theory of ship slamming to study wave action on a deck slab. He proposed the time varying vertical force as a combination of a hydrodynamic impact force and a drag force. The drag force was computed from a constant force coefficient and assumed to act over a complete slamming event. Although he did not compare the predicted vertical force with experimental results, in his re-examination of hydrodynamic impact theory, he briefly assessed the features of time histories of the

predicted force with respect to field data. The time histories of force indicated that the magnitudes were comparable during the initial stages of impact. However, the variation showed a large discontinuity at the instant of complete submergence of the structure.

1.3 Scope of the Present Investigation

The primary aim of the present investigation is to study experimentally hydrodynamic aspects of the vertical force on a fixed rigid horizontal plate. Despite the considerable importance of this problem, a literature review reveals little information regarding the estimation of the slamming force. On the basis of the studies carried out by El Gahmry (1963) and French (1969), an experimental investigation was carried out on an instrumented horizontal plate located above the still water level and subjected to wave action. Vertical reactions at the two plate supports were measured for different combinations of incident wave conditions and plate elevations, and the vertical force and its line of action was computed from the measured support reactions. The results are presented in the form of time series of the force and its line of action. Also, an analysis of the force records is made in order to obtain the peak upward and downward forces, their times of occurrence and their lines of action. Video records of the experiments are studied in order to identify the problems involved in the experimental investigations. Finally, an attempt is also made to predict the slamming force on a theoretical basis.

Chapter 2

Theoretical Development

In this chapter, important parameters influencing the vertical force on a fixed horizontal plate subjected to regular waves are identified and a theoretical description of the force is presented.

2.1 Dimensional Analysis

Dimensional analysis provides an important preliminary step to any experimental investigation and may be used to identify important dimensionless parameters of the problem at hand. Figure 2.1 provides a simplified definition sketch indicating a unidirectional regular progressive wave train in water of constant depth d propagating past a horizontal plate of width b , thickness w and length ℓ located at a distance h above the mean water level. The vertical force on the plate, denoted F , is of interest and is influenced by a number of variables which include the following:

- wave height, H
- wave period, T
- water depth, d
- plate length, ℓ
- plate width, b
- plate thickness, w
- plate elevation, h
- fluid density, ρ

- gravitational constant, g
- fluid viscosity, μ
- time, t

Additional parameters such as surface roughness, surface tension, air and water compressibility, and spray effects may also play significant role but are neglected here.

The width of the plate may be important since it influences the escape of air below the plate as the wave advances. The deck thickness w is assumed to be small enough so that its influence may be neglected. And finally, the effect of the fluid viscosity μ is also neglected.

In view of the above simplifications, the vertical force may be expressed in the form:

$$\bar{F} = f(\rho, g, H, T, d, h, \ell, b, t) \quad (2.1)$$

where \bar{F} is the vertical force per unit width. A dimensional analysis provides

$$\frac{\bar{F}}{\rho g H \ell} = f\left(\frac{h}{H}, \frac{H}{L}, \frac{d}{L}, \frac{\ell}{L}, \frac{b}{\ell}, \frac{t}{T}\right) \quad (2.2)$$

In engineering applications, the maximum force F_o , is of particular interest and is given as:

$$\frac{F_o}{\rho g H b \ell} = f\left(\frac{h}{H}, \frac{H}{L}, \frac{d}{L}, \frac{b}{\ell}, \frac{\ell}{L}\right) \quad (2.3)$$

The parameter h/H defines the relative clearance such that there is no wave contact for $h/H > 0.5$ if waves are assumed to be sinusoidal. H/L is the wave steepness, d/L is a depth parameter, and ℓ/L is a relative length parameter of the plate, analogous to a wave diffraction parameter.

It is illustrative to consider the typical ranges of some of these parameters. Intermittent submergence of the plate occurs for $-0.5 < h/H < 0.5$. The depth parameter d/L should have a negligible influence on the force for deep water conditions corresponding to $d/L > 0.5$. Based on stability considerations, the wave steepness varies up to 0.142 in deep water. Typical wave conditions may include wave periods ranging from 5 to 20 sec so that ℓ/L may span a relatively wide range.

2.2 Vertical Force Formulation

The vertical force on a horizontal member subjected to intermittent submergence in waves is generally taken to be made up of hydrodynamic impact, drag and buoyancy force components. (Although the buoyancy force was omitted in Section 2.1, in typical experiments it may not be negligible compared to the other force components.) Thus, the vertical force expressed as:

$$F(t) = F_a(t) + F_d(t) + F_b(t) \quad (2.4)$$

where $F_a(t)$, $F_d(t)$ and $F_b(t)$ are hydrodynamic impact, drag and buoyancy force components respectively. These components are briefly discussed in the sections to follow. However, it is useful to consider initially the various stages of interaction during a wave cycle.

Stages of Wave Interaction

Consider a wave train interacting with the plate during the course of one cycle. Figure 2.2 shows the various stages of the plate submergence in terms of the positions of water surface relative to the plate, and the corresponding times of occurrence. Figure 2.2(a) shows the instant at which a wave just makes contact with the leading edge of the plate. In Fig. 2.2(b), the wave progresses further, partially wetting the plate. Figure 2.2(c) shows

the stage at which the plate is fully submerged. The plate remains submerged until the downwave free surface reaches the leading edge of the plate. Figure 2.2(d) shows the wave recession stage, during which the leading edge of the plate is exposed. Finally, Fig. 2.2(e) shows the instant of complete detachment of the wave from the rear edge of the plate.

Defining the intersection locations of the downwave and upwave free surfaces as x_1 and x_2 respectively, along the length of the plate, with the origin at the leading edge of the plate, and with the wetted length denoted as $\lambda = x_2 - x_1$, the above sequence for one cycle may be summarized as follows.

- For $t = t_0$: $x_1 = 0$, $x_2 = 0$, $\lambda = 0$
- For $t_0 < t < t_1$: $x_1 = 0$, $0 < x_2 < \ell$, $\lambda = x_2$
- For $t_1 < t < t_2$: $x_1 = 0$, $x_2 = \ell$, $\lambda = \ell$
- For $t_2 < t < t_3$: $0 < x_1 < \ell$, $x_2 = \ell$, $\lambda = \ell - x_1$
- For $t = t_3$: $x_1 = \ell$, $x_2 = \ell$, $\lambda = 0$

In the present study, only the case $\ell/L < 1$ is considered so that there is no more than one region of water contact at any instant.

Hydrodynamic Impact

A simplified hydrodynamic analysis similar to that for a cylinder, can be carried out to provide an approximate formulation for the vertical force on the plate. It is assumed that the fluid is incompressible and inviscid, the flow is irrotational, the body is rigid, and that the surface tension is negligible. Following Kaplan (1992), the force component F_a due to

hydrodynamic impact may be expressed in terms of the rate of change fluid momentum associated with the submerged portion of the plate:

$$F_a = \frac{\partial(mv)}{\partial t} \quad (2.5)$$

where m is the vertical added mass of the submerged portion of the plate, t is time, and v is the vertical velocity of the fluid striking the plate. Equation 2.5 can be expanded to obtain

$$F_a = m \frac{\partial v}{\partial t} + v \frac{\partial m}{\partial t} = m \dot{v} + v \frac{\partial m}{\partial \lambda} \frac{\partial \lambda}{\partial t} \quad (2.6)$$

where λ is the wetted length of the plate and \dot{v} is the vertical acceleration.

The primary difficulty with applying this equation relates to the use of a reliable expression for the added mass, since the flow field around the plate is rather complex. A suitable approach to estimating m is to equate this to the added mass of a fully submerged plate in an infinite fluid. Thus, the required added mass m when submerged plate length is λ is considered to be equal to the added mass of a fully submerged plate length λ . However, because of the uncertainty associated with this equivalence, it is appropriate to introduce an unknown factor α . Thus the expression for added mass m is given by :

$$m = \alpha \rho \lambda b^2 f_1(\lambda/b) \quad (2.7)$$

where α replaces $\pi/4$ in Eq. 2.7 and the function $f_1(\lambda/b)$ is described in Sarpkaya and Isaacson (1981). On the basis of Eq. 2.7, the hydrodynamic impact force F_a given by Eq. 2.6 may be expressed as:

$$F_a = \alpha \rho \lambda b^2 f_1(\lambda/b) \dot{v} + \alpha \rho b^2 v \frac{\partial \lambda}{\partial t} f_2(\lambda/b) \quad (2.8)$$

where an overdot denotes a time derivative, the function $f_2(\lambda/b)$ is given as:

$$f_2(\lambda/b) = f_1(\lambda/b) + (\lambda/b)f_1'(\lambda/b) \quad (2.9)$$

and a prime denotes a derivative with respect to the argument. The first term in Eq. 2.8, denoted F_{a1} , is an inertia force associated with the fluid acceleration, and the second term, denoted F_{a2} , is an added mass force associated with the rate of change of added mass.

It is also possible to formulate the impact force by considering instead the hydrodynamic force, ΔF_a on an element of length Δx and integrating this over the instantaneous wetted length of the plate.

$$\Delta F_a = \frac{\partial(\Delta m v)}{\partial t} \quad (2.10)$$

where Δm is an infinitesimal added mass, given as $\Delta m = [4\rho v b \sqrt{4q^2 - x^2}] \Delta x$ (Lamb, 1932), x is the coordinate measured from the centre of the plate's wetted length, and q is half the wetted length of the plate. By integrating over the wetted length, the total impact force may be obtained as:

$$F_a = \int_{x_1}^{x_2} \Delta F_a dx \quad (2.11)$$

where x_1 and x_2 are the intersection locations of the downwave and upwave limits of the submerged plate length, measured here from the centre of this submerged plate length. An analytical solution of the above integration is intractable, and this approach has not been pursued since it may not lead to increased accuracy because of the various uncertainties in the procedure.

Drag Force

The drag force F_d acting on the submerged portion of the plate is expressed in usual way in terms of a drag coefficient C_d and is given by:

$$F_d = C_d \frac{1}{2} \rho b v |v| \lambda \quad (2.12)$$

where C_d is the drag coefficient. The choice of C_d depends on various factors such as the geometry and shape of the plate, and its orientation relative to the wave propagation direction. The drag coefficient value during the early stages of the impact is unclear, but has been chosen to be equal to 2.0, as for the plate when completely submerged.

Buoyancy Force

Although it is consistent to assume that the plate is very thin, in practice the submerged volume of the plate may not be negligible, so that any comparison with the experimental data should account for the buoyancy force associated with the finite volume of the plate, the stiffeners and the submerged portion of the support system. Thus, the buoyancy force is given as:

$$F_b = \rho g V \quad (2.13)$$

where V is the submerged volume of the plate and submerged portion of the support system. In the present study, F_b is assumed to vary sinusoidally with the time.

2.2.1 Wave Theory and Associated Kinematics

The hydrodynamic impact and drag forces discussed in the previous sections are expressed in terms of the particle velocity and acceleration evaluated at the plate elevation. In the present study, linear wave theory is used to determine the free surface elevation and associated kinematics for application to these expressions.

For a regular progressive wave train, the water surface elevation η is expressed as:

$$\eta = \frac{H}{2} \cos(kx - \omega t) \quad (2.14)$$

where H is the wave height, $k = 2\pi/L$ is the wave number, $\omega = 2\pi/T$ is the wave angular frequency, L is the wave length, and T is the wave period. The wave number and the wave frequency are related by the linear dispersion relationship:

$$\omega = \sqrt{gk \tanh(kd)} \quad (2.15)$$

where d is the still water depth. On the basis of linear wave theory, the associated kinematics are given as

$$v = \frac{\omega H}{2} \frac{\sinh[k(d+z)]}{\sinh(kd)} \sin(kx - \omega t) \quad (2.16)$$

$$\dot{v} = -\frac{\omega^2 H}{2} \frac{\sinh[k(d+z)]}{\sinh(kd)} \cos(kx - \omega t) \quad (2.17)$$

with z measured upwards from still water level. In the present case z is set to the deck elevation h . Several approaches have been proposed to evaluate water particle kinematics near the instantaneous free surface (e.g. Gudmestad and Connor, 1986). The simplest of these is to take $z = 0$, since this is consistent with the accuracy of linear wave theory. Thus by substituting the approximation into Eqs. 2.16 and 2.17 we get

$$v \approx \dot{\eta} = \omega \frac{H}{2} \sin(kx - \omega t) \quad (2.18)$$

$$\dot{v} \approx \ddot{\eta} = -\omega^2 \frac{H}{2} \cos(kx - \omega t) \quad (2.19)$$

The wave kinematics vary along the submerged length of the plate, and are evaluated here at the centre of the instantaneous submerged length of the plate.

2.2.2 Superposition of Force Components

Wetted Length

The wetted length λ and its time variation are important in the formulation of the vertical force indicated by Eq. 2.8. Figure 2.3(a) is a sketch of the free surface elevation at the leading and rear edges of the plate, denoted η_0 and η_ℓ respectively. And Fig. 2.3(b) is a sketch of the wetted length variation for a given wave form and plate clearance. At time t_0 (see also Fig. 2.2(a)), λ is zero and starts to increase as the wave progresses. At time t_1 , the deck is completely submerged and λ reaches the full plate length, $\lambda = \ell$. From t_1 to t_2 (see also Fig. 2.2(c)), the plate remains fully submerged. For $t > t_2$, the wave recedes so that λ decreases; and finally at $t = t_3$, $\lambda = 0$. On the basis of linear theory, the wetted length λ can be obtained by equating the wave surface elevation η to the plate clearance h and solving for λ replacing x as:

$$h = \frac{H}{2} \cos(k\lambda - \omega t) \quad (2.20)$$

Combinations

Following section 2.2 and Eq. 2.4, the force components may be superposed to obtain the time variation of the vertical force:

$$F = F_{a1} + F_{a2} + F_d + F_b \quad (2.21)$$

Also, as discussed in section 2.2.1, the plate clearance h is of the order of wave height H , so that on the basis of linear wave theory the velocity v and acceleration \dot{v} may be taken as $v \approx \dot{\eta}$ and $\dot{v} \approx \ddot{\eta}$. Substituting the expressions for the force components and the above simplification for wave kinematics in Eq. 2.21, we obtain:

$$F = \alpha \rho \lambda b^2 f_1(\lambda/b) \ddot{\eta} + \alpha \rho b^2 \dot{\eta} \frac{\partial \lambda}{\partial t} f_2(\lambda/b) + \frac{1}{2} C_d \rho b \lambda \dot{\eta} |\dot{\eta}| + \rho g V \quad (2.22)$$

The magnitude of $\partial\lambda/\partial t$ may be taken as the wave celerity c when the plate is partially submerged, and zero when it is fully submerged or completely above the water surface. However, this highlights a difficulty with the force formulation that has been proposed, in that the corresponding term falling abruptly to zero as the plate becomes fully submerged because of this abrupt change in $\partial\lambda/\partial t$. In fact, the actual added mass is expected to vary so as to give rise to a more gradual variation of this term. Based on the foregoing, the variation F_{a2} in Eq. 2.8 is modified by replacing $\partial\lambda/\partial t$ with a *velocity* c' which is constant and equal to wave celerity c during partial submergence (i.e. from t_0 to t_1); and then assumed to fall linearly from c at time t_1 to zero at time t_m . This variation is sketched in Fig. 2.3(c) and is introduced simply as a device to avoid the abrupt fall in F_{a2} .

Then Eq. 2.22 may be re-written as

$$F = \alpha \rho \lambda b^2 f_1(\lambda/b) \ddot{\eta} + \alpha \rho b^2 \dot{\eta} c' f_2(\lambda/b) + \frac{1}{2} C_d \rho b \lambda \dot{\eta} |\dot{\eta}| + \rho g V \quad (2.23)$$

where

$$c' = \begin{cases} c & \text{for } t_0 < t < t_1; & (\text{i.e. } \dot{\eta} > 0) \\ c \left[\frac{t_2 + t_1 - 2t}{t_2 - t_1} \right] & \text{for } t_1 < t < \frac{(t_1+t_2)}{2} & (\text{i.e. } \dot{\eta} \leq 0) \\ 0 & \text{otherwise} \end{cases}$$

A possible variation of the added mass force is sketched in Fig. 2.3(d) along with the other three components. The total vertical force predicted resulting from the superposition is shown in Fig. 2.3(e) along with the actual total vertical force.

In applying Eq. 2.23, some attention should be given to the determination of the functions $f_1()$ and $f_2()$. Tabulated values of the added mass for the three-dimensional case of different length to width ratios are given by Sarpkaya and Isaacson (1981) and are reported in Table 2.1. The two-dimensional limits of infinite width or length correspond

respectively to $f_1(\lambda/b) \rightarrow (\lambda/b)$ (so that $m = \alpha \pi \lambda^2 b$) as $(\lambda/b) \rightarrow 0$; and $f_1(\lambda/b) \rightarrow 1$ (so that $m = \alpha \pi \lambda b^2$) as $(\lambda/b) \rightarrow \infty$. A suitable function $f_1()$ is fitted to this data and used in Eq. 2.23. Thus, the function $f_1()$ and $f_2()$ are given by:

$$f_1(\lambda/b) = (\lambda/b) \exp [- 0.53 (\lambda/b)^{0.88}] + 0.1\varepsilon[(\lambda/b) - 2.0] \quad (2.24)$$

$$f_2(\lambda/b) = 2.0 - [0.53 (\lambda/b)^{0.88}] f_1(\lambda/b) + 0.25 \nu [(\lambda/b) - 1.5] \quad (2.25)$$

where

$$\varepsilon = \begin{cases} 0 & \text{for } (\lambda/b) < 2.0 \\ 1 & \text{for } (\lambda/b) \geq 2.0 \end{cases}$$

$$\nu = \begin{cases} 0 & \text{for } (\lambda/b) < 1.5 \\ 1 & \text{for } (\lambda/b) \geq 1.5. \end{cases}$$

Figure 2.4 is a plot indicating the variation of the added mass functions based on the tabulated values of Table 2.1, and those based on Eqs. 2.24 and 2.25.

Due to the complicated flow around the plate and the associated uncertainty relating to the use of Eq. 2.7 for the added mass, a simpler alternative based on the two-dimensional case of infinite width may instead be adopted. The two-dimensional limit $\lambda/b \rightarrow 0$ corresponds to $f_1(\lambda/b) \rightarrow (\lambda/b)$ so that Eq. 2.7 would be replaced by:

$$m = \alpha \rho \lambda^2 b \quad (2.26)$$

This leads to Eq. 2.23 being replaced by:

$$F = \alpha \rho \lambda^2 b \ddot{\eta} + 2\alpha \rho \lambda c' b \dot{\eta} + \frac{1}{2} C_d \rho \lambda b \dot{\eta} |\dot{\eta}| + \rho g V \quad (2.27)$$

It is illustrative to consider the variation of added mass with the plate aspect ratio. Fig. 2.5 indicates such a variation for arbitrary values of α , 1 and 3 for Eq. 2.23 and 0.5 and 0.7 for the simpler added mass model given by Eq. 2.26.

2.3 Dynamic Response of SDOF System

A formulation of the vertical force on a horizontal plate has been presented in the previous section assuming that the plate and the load-cell assembly act as a fixed structure. However, in almost all cases the dynamic response of the structure and its measuring system occur to some extent, and influence the force that is measured, particularly under impulsive loading. An estimation of the effect of this on the measured force is of interest and may be made on the basis of a simple analysis of single degree of freedom (SDOF) system subjected to impact loading (e.g. Isaacson and Prasad, 1993). The plate and load-cell assembly is modelled as a SDOF system with a mass M , stiffness K and damping coefficient C as indicated schematically in Fig. 2.6. The stiffness K is related to the stiffnesses of each of the load-cells placed at two supports. The equation of motion of the system when subjected to a time varying load $F(t)$, is given as:

$$M\ddot{u} + C\dot{u} + Ku = F(t) \quad (2.28)$$

where u , \dot{u} and \ddot{u} are the instantaneous plate displacement, velocity and acceleration respectively. The natural frequency ω_n and the damping ratio ξ of the system are defined as $\omega_n = \sqrt{K/M}$ and $\xi = C/2M\omega_n$. The response $u(t)$ of the system starting from rest is given by:

$$u(t) = \frac{1}{M\omega_d} \int_0^t F(\tau) e^{-\xi\omega_n(t-\tau)} \sin[\omega_d(t-\tau)] d\tau \quad (2.29)$$

where ω_d is the damped natural frequency of the assembly defined as $\omega_d = \omega_n\sqrt{1-\xi^2}$, and τ is a variable of integration.

The force $F(t)$ is the applied vertical force as given in either Eq. 2.23 or Eq. 2.27 and it is composed of force components given in Eq. 2.21. However, the force transmitted $F_t(t)$

to the load-cell (i.e. measured by the load-cell) at the supports is proportional to the stiffness of the load-cell, (with damping neglected) and is given by:

$$F_t(t) = K u(t) \quad (2.30)$$

The SDOF system is now considered to be subjected to an idealized load, $F(t)$ given as a triangular function as indicated in Fig. 2.7. $F(t)$ increases linearly to a peak value of F_0 in a rise-time T_r and then drops linearly to zero in a decay-time T_d . The complete response history of the system can be determined using the Eq. 2.29 for the given triangular pulse load (e.g. Humar, 1990).

Isaacson and Prasad (1993) obtained a closed-form solution for the SDOF system identifying the peak force F_{t0} immediately after the impact and the associated rise time T_t as important parameters, and presented a set of characteristic curves describing these as indicated in Fig. 2.8. In the figure, F_{t0} is the peak measured force, F_0 is the peak applied force, T_m is the rise-time associated with measured force, T_r is the rise-time associated with the applied force, and $T_n = 2\pi/\omega_n$, is the natural period of the system. The influence of dynamic characteristics on the peak measured force F_{t0} and T_t can readily be estimated from the figure.

Chapter 3

Experimental Investigation

3.1 Introduction

As mentioned earlier, objectives of the present investigation are to study the hydrodynamics of the impact process and to relate the important parameters of the loading to those that govern the process. To this end, a series of experiments was carried out at the Hydraulics Laboratory of the Civil Engineering Department, University of British Columbia, and this chapter gives a detailed account of the experimental investigation.

3.2 The Plate

An important aspect of the force measurement relates to the requirement of providing an accurate measurement of the external force acting on the plate, without including any extraneous effects due to the dynamic response of the test setup. Because of this requirement, the plate and load-cell assembly should have a high natural frequency in comparison to dominant loading frequencies. There are two principal modes of vibration which may affect the force measurement; one corresponding to a first mode beam vibration and the other to the whole assembly vibrating as a lumped mass supported by the load-cells. Because of this, the beam should be as stiff as possible, the overall mass supported by the load-cells should be minimized, and the load-cell should be sufficiently stiff.

Bearing these considerations in mind, a plate model was designed to be stiff enough to approximate a rigid body, and at the same time to be as thin as possible so as to simulate a

thin plate. Photographs of the test assembly are shown in Fig. 3.1, and a sketch of the experimental set-up is provided in Fig. 3.2. The plate assembly was designed as a pinned beam supported at two points and with a large overhang on the upwave side so as to minimize the interference of the load-cells and plate supports during the initial submergence. The plate is constructed of acrylic, and is 20 cm wide, 60 cm long and 6.25 mm thick. Two aluminum angles are fixed above the plate to increase its rigidity. A small gap between the plate and the angles allows overtopped water to drain freely. Pinned supports are made of two bearings attached to the inner face of the angle. Aluminum shafts through these bearings connect the load-cell and support rod to the stiffener angles. These supports are at 30.0 cm and 54.5 cm away from the leading edge of the plate. The supporting rods are threaded and are fixed by nuts to a longitudinal steel box section 5 cm high x 7.5 cm wide. The box section is aligned in such a way that its longitudinal centre-line coincides with that of the flume. It is bolted to steel cross-channels which rested on the top of the flume side-wall and was clamped to the flume walls. The level of the plate was adjusted by lengthening or shortening the part of the rods between the supporting longitudinal channel and the load-cell. By this arrangement, vertical forces were measured by the load-cells at two supports. Since the plate is very thin, and the front end is beveled, the horizontal wave force on the plate during wave impact is neglected.

3.3 Wave Flume and Generator

A sketch of the Hydraulics Laboratory wave flume is shown in Figure 3.3. The wave flume measures 20 m long x 0.6 m wide x 0.75 m deep. An artificial beach is located at one end to reduce wave reflection. Waves are generated by a single paddle wave actuator located at the upwave end. The generator is controlled by a DEC VAXstation-3200 minicomputer using the GEDAP software package developed by the National Research Council, Canada, (NRC). The generator is capable of producing wave heights up to 30 cm

and wave periods as low as 0.5 sec. In the present study, regular waves of heights ranging from 3.0 to 17.5 cm and periods ranging from 0.8 to 2.0 sec. were used. During each of these tests, water depth was maintained at 0.55 m.

3.4 Control and Data Acquisition

The GEDAP general purpose software package was used extensively during all stages of the experimental investigation. This software package is available for the analysis and management of laboratory data, including real-time experimental control and data-acquisition functions. GEDAP is a fully-integrated, modular system which is linked together by a common data file structure. GEDAP maintains a standard data file format so that any GEDAP program is able to process data generated by any other GEDAP program. This package also includes an extensive set of data analysis programs so that most laboratory projects can be handled with little or no project-specific programming. An attractive feature is the fully-integrated interactive graphics capability, such that results can be conveniently examined at any stage of the data analysis process. It also includes an extensive collection of utility packages, which consist of a data manipulation routine, a frequency domain analysis routine, and statistical and time-domain analysis routines. In particular, the program RTC_SIG generates the control signal necessary to drive the wave generator, and the routine RTC_DAS reads the data acquisition unit channels and stores the information in GEDAP binary format compatible with other GEDAP utility programs.

3.5 Measurements

The water surface elevation and the associated vertical force were required to be measured for each test. The vertical forces at two supports were measured using load-cells. The selection of the load-cells is based primarily on considerations of sensitivity, load range and stiffness requirements. Two axial 'S' type load-cells (Interface SSM 500) have been used

in the present study. These work on the principle of flexure of the central limb of an 'S' sensed by precision strain gage circuitry. Each load-cell has a load capacity of 500 lb (2.2 kN) and an axial stiffness of 4.9 kN/mm, with a sensitivity of $15 \mu\text{V/N}$ for an excitation of 10 V. The output voltage of the load-cells are amplified by a Pacific Instruments Model 8255 Transducer Condition Amplifier. An amplification of 1000 was found to be adequate to obtain a reasonably good output to noise ratio. A low-pass filter with a cut-off frequency of 1 kHz was also used. This amplified filtered signal was transmitted to an analog-to-digital converter. Based on the Nyquist criterion, a sampling rate of 2.5 kHz was selected.

Capacitance type 'bow string' probes were used to measure the water surface elevation. Each probe is made up of a taut loop of wire on a light metal 'C' frame and has a linearity better than 98.5% and a resolution better than 1 mm.

3.6 Experimental Procedures

The experiments were carried out in two parts. In the first part, waves were generated with the plate absent, and water surface elevation measurements were carried out using probes placed at two locations ($x = 0 \text{ cm}$) and ($x = 60 \text{ cm}$) along the centre-line of the plate. Due to a limitation of the RTC_DAS package, a sampling rate of 2.5 kHz was used for both force as well as water surface elevation data measurements. Previous tests have indicated that the repeatability of a particular wave train over separate experiments is very good (Isaacson & Prasad, 1993), so that the surface elevation with the plate absent and the forces on the plate were measured in separate stages. In the second stage, the wave probes were removed and the plate assembly was installed in the flume. Waves corresponding to the same stored wave signals were repeated and the vertical forces on the plate were recorded at a sampling rate of 2.5 kHz. A video record was also obtained for each experiment. Experiments were carried out for five different elevations of plate from 0 to 25 mm, in

combination with three wave steepness values and four wave periods. A constant water depth of 0.55 m was maintained during the experiment. Table 3.1 lists the different incident wave conditions used in the investigation.

During the second part of this investigation, video records were obtained using a normal speed camcorder. When the force data sampling was initiated, a switch was also triggered to light up the light emitting diode at the same time instant so as to synchronize the time base of the film with that of vertical force and the free surface elevation records.

The video records were used to study the impact process qualitatively and thereby to access the effects of the assumptions made, and in particular to assess the importance of wave profile deformation, air entrapment, wave overtopping effects, and water curtaining problems due to drainage between each event of wave impact.

3.7 Dynamic Characteristics of the Assembly

After calibrating the load-cells for static loads, free vibration tests of the plate were conducted both in air as well as for a fully submerged condition. In both cases, a step load was applied to the plate assembly by the sudden release of a load carried by a thin steel single stranded wire. This was achieved by cutting-off the wire using an acetylene torch. The free vibration traces were recorded for both the load-cells A and B indicated in Fig. 3.2. The recorded force time histories and the corresponding spectral densities for the plate in air and fully submerged condition are shown in Fig. 3.5 and 3.6 respectively. Figure 3.5 indicates that for vibrations in air the plate response has widely distributed frequencies with a predominant frequency of approximately 125 Hz for both load-cells. It is informative to study the initial stages of an impact event just after releasing the step load. Consider the free vibration trace for the load-cell A as shown in Fig. 3.5(a). The first peak is observed to occur 5 msec after the step load release, indicating the transient response

ability of the assembly. The high frequency component then disappears and lower vibration amplitudes with a frequency of approximately 62.5 Hz become dominant, and ultimately the load-cell stops vibrating after 0.6 sec since the release of the step load. The damping ratio can be evaluated from the above trace using the following relation:

$$\xi = \sqrt{\frac{D_f^2}{D_f^2 + 4 \pi^2 n^2}} \quad (3.1)$$

where $D_f = \ln[p_m/p_{m+n}]$, and p_m and p_{m+n} are the amplitudes of the free vibration force trace measured after n and $(m+n)$ cycles respectively. The average damping ratio was found to be 2.7% in air. Similar features were found from the analysis of the free vibration trace for load-cell B.

Apart from free vibration tests in air, the plate and load-cell assembly were also tested for free vibrations under a fully submerged situation so as to obtain similar characteristics for step load releases (Fig. 3.6(a)). For both load-cells A and B, the traces are more or less smooth and indicate a single dominant oscillation frequency. The first peak is observed at 10 msec and the system comes to rest 1.0 sec after the release of the load. The average damping ratio for this submerged condition was found to be 5.3%. Figure 3.6(b) shows the variance spectral density of the free vibration trace. It indicates that the natural frequency for the submerged condition reduces to approximately 25 Hz.

As explained in Section 2.3, Fig. 2.8 may be used to estimate the influence of the system characteristics on the measured force and associated rise-time. From the preliminary experimental results, the minimum rise-time was found to be not less than 100 msec. And with the natural period of the system taken to be equal to 1/125 sec, there appears to be no noticeable amplification in the peak value of the measured force and the rise-time. The natural period of the system is taken to be the one that corresponds to the

tests conducted in air since the preliminary tests indicated that the impact occurs just before complete submergence of the plate.

3.8 Data Processing

The first step in data analysis involves filtering the measured data to remove noise in the records. One of the causes of noise may be due to electromagnetic frequency at 60 Hz. Another would be due to the system response itself, as discussed in sections 3.2 and 3.7. On the amplifier, a low-pass filter was used with a cut-off frequency of 1000 Hz. The force data from two the load-cells were first plotted to observe the noise present in the records. The GEDAP filtering program FILTW was used to filter the data. Several levels of cut-off frequency ranging from 500 to as low as 5 Hz were used to examine the effect on the peak force. Cut-off frequencies below 10 Hz show considerable smoothing of the force peak and loss of information, and it was decided to set the cut-off frequency at 15 Hz. As an illustration of the low-pass filter that was adopted, Fig. 3.7 shows corresponding unfiltered and filtered force records.

A static analysis was applied to obtain the vertical force and its line of action in the manner indicated in Appendix A. Figure A1 is a sketch of free body diagram of the plate represented as pinned rigid beam. From this analysis, the total vertical force and its line of action were obtained and are illustrated in Fig. 3.8 for the case of unfiltered signals and filtered signals.

In a similar way, the wave records were filtered and resampled at 10 Hz since such a high sampling rate is unnecessary for a slowly varying signal. The GEDAP routines, FILTW and RESAMPLE2 were used to filter and resample the wave records. Once the vertical force from the filtered records are available along with the resampled wave profile, the remaining analysis was carried out as explained below. It was decided to study only one slamming event for each test and therefore only one slamming cycle is selected from a

4 sec record as shown in Fig. 3.9. The instant of slamming t_0 is determined from the measured water surface elevation η_0 and the known plate clearance. This method was found to be consistent and reliable for all the experimental results. The wave kinematics were evaluated half way along the instantaneous wetted length measured from the leading edge of the plate, as mentioned in the Section 2.2.1. The buoyancy force was evaluated based on the displaced volume of the water by the plate and load-cell assembly as discussed in Section 2.2, and is assumed to vary sinusoidally for the duration of submergence with the peak buoyancy force occurring at $t = t_m$. Various other parameters such as peak upward and downward forces, their lines of action, times of occurrence and associated wetted lengths were then determined. The vertical force was predicted based on the linear wave theory for different wave conditions tested and a comparison of the measured and observed force was carried out. A flow chart of the procedure is given in Fig. 3.10.

Chapter 4

Results and Discussion

The results of the experimental and analytical investigation are presented and discussed in this chapter. The first part primarily describes the results from the tests with regular non-breaking waves of different heights and periods, and different plate elevations. The important parameters thereby estimated correspond to the maximum upward force, the associated point of application, the rise-time, and the corresponding value of the wetted length. Similar quantities relating to maximum downward force are also presented. A brief qualitative analysis of the video records included is also presented, with a focus on the physical process involved and the related departure of the theory in predicting the vertical force is discussed.

The application of the two analytical models (Eqs. 2.23 and 2.27) for estimating the vertical force is discussed, and associated discrepancies are identified. Finally, a correction factor for the added mass associated with each of these model is introduced, and its range for different incident wave conditions is presented.

A total of 69 tests were carried out, corresponding to 5 plate elevations, 5 wave periods, and 3 wave steepness. (Some of the 75 combinations of these three do not give rise to immersion of the plate.) The plate elevations ranged from $h = 0$ to $h = 2.5$ cm; wave periods ranged from 0.8 to 2.0 sec; and the wave heights for each wave period were selected to correspond to steepness $H/L \approx 0.02, 0.03, \text{ and } 0.04$, such that the wave heights are in the range of 3 to 17 cm.

4.1 Vertical Force

Figures 4.1 to 4.8 show the time histories of the vertical forces measured at two support locations F_A and F_B , the total vertical force F , and the corresponding water surface elevations η_0 and η_ℓ , at the leading and rear edges of the plate. The figures correspond to eight different test conditions characterized by changes in wave steepness and plate clearance. In these figures, t is the time measured from an arbitrary origin. As an aid to interpreting results, these figures include horizontal and vertical lines indicating the plate elevation and the corresponding instants of impact and complete submergence. On this basis, the variation of wetted length $\lambda(t)$ is also obtained.

Figures 4.1, 4.2 and 4.3 correspond to a plate clearance $h = 0.8$ cm and waves with $T \approx 1.70$ sec and $H = 14.2, 10.5$ and 6.8 cm respectively. As a wave advances past the plate, the force increases quite gradually from the instant of water contact, exhibits a fairly sharp maximum, and then varies more gradually over the remainder of the cycle, passing through a noticeable minimum during the later stages of the event. The noticeable maximum downward (i.e. negative) force which is present during the later portion of the wave cycle is due to a suction associated with the water surface receding below the plate, together with the weight of some overtopped water remaining above the plate.

Similarly, Figs. 4.4 and 4.5 correspond to a plate clearance $h = 1.4$ cm and waves with $T \approx 1.70$ sec and $H = 14.2$ cm and $H = 10.5$ cm respectively. These figures indicate a sharper rise in force than for the case $h = 0.8$ cm. Finally, Figs. 4.6, 4.7 and 4.8 correspond to different clearances, $h = 0, 1.4$ and 2.5 cm respectively, with the same wave condition $T = 2.02$ sec and $H = 17.5$ cm.

It is useful to study the slamming process with respect to the free surface elevation η . As mentioned already, horizontal lines in Figs. 4.1(a) - 4.8(a) indicate the plate elevation, and the vertical lines indicate the instants of initial wave contact, complete submergence, the

onset of wave recession and complete wave recession. The time between the two lower vertical lines indicate the duration over which a wave is in contact with the plate. Extending these line to the force time histories $F(t)$, the observed instant of impact agrees reasonably well with the instant at which the wetted length λ starts rising from zero. It may be noticed that the total force F before and after these points is non-zero even though the plate is entirely in air. This may be attributed to the overtopped water draining from the top of the plate. It can be observed that the water drains out completely for the wave of period $T = 2.02$ sec, so that then the force F is nearly zero as indicated in the Fig. 4.6(c). The time between the upper two vertical lines indicate the duration for which the plate is completely submerged. The intersection of two wave profiles η_0 and η_ℓ shows the symmetric wave profile with respect to support A (mid span location) along the plate length for that instant. The total force F is positive indicating that the plate experiences an upward force which exceeds the weight of the water above the plate.

Another interesting feature included in Figs. 4.1 - 4.8 relates to the time histories of the line of action, $s(t)$. The sharp changes in s are associated with $F(t)$ passing through zero. The force's line of action initially moves away from the leading edge of the plate as expected, but does not span the whole wave cycle. It moves abruptly from the leading edge to the rear edge just after the occurrence of the symmetric wave profile along the length. And during the wave recession era, $s(t)$ again commences at the leading edge and travels smoothly up to the mid span approximately.

The noticeable negative (i.e. downward) force, which is present during the later portion of the wave cycle, is due to a suction associated with the water surface receding below the plate, together with the weight of some water remaining above the plate. The negative force seems to start just before the wave surface leaves the plate's leading edge i.e. just

before time t_2 . As the wave recession progresses, the force F reaches a negative maximum just before time t_3 . After time t_3 , the plate is in air and the force F drops gradually to zero.

4.2 Vertical Force and Incident Waves

Results relating to the force parameters have been grouped according to the dimensional analysis indicated earlier and are listed in Table 4.1. These include the maximum upward force F_p , its time of occurrence T_p , its point of application s_p , and the corresponding wetted length λ_p . The table also includes the maximum downward force F_m , its time of occurrence T_m , and point of application s_m as well as the wetted length λ_m . The variations of these values are studied as functions of relative clearance h/H , for various values of wave steepness H/L and relative plate length ℓ/L .

Maximum Force

Figure 4.9 indicates the variation of the peak upward force coefficient $F_p/\rho g H b \ell$ as a function of relative clearance h/H for various values of the relative plate length ℓ/L and for various ranges of wave steepness. As the relative clearance h/H approaches 0.5 the force coefficient $F_p/\rho g H b \ell$ approaches zero. Also, the force coefficient increases as the relative plate length ℓ/L increases. Although, there is no significant change in the force coefficient for the range of wave steepness used in the tests ($H/L \approx 0.016 \sim 0.041$), it may be seen that the trend of the which shows $F_p/\rho g H b \ell$ to decrease linearly with h/H is no longer observed for the case of steeper waves.

Figure 4.10 indicates similar plots for the peak downward force coefficient $F_m/\rho g H b \ell$. Figures 4.10(a), 4.10(b) and 4.10(c) indicate no systematic relationship, although $F_m/\rho g H b \ell$ apparently remains constant for any change in h/H .

Duration of Submergence

Figure 4.11 is a plot of a dimensionless duration of partial submergence, T_c/T where $T_c = t_1 - t_0$. This parameter is important since it indicates the time required for a wave to completely submerge the plate at a known elevation above the mean water level, and consequently influences the occurrence of the peak upward force predicted by the analytical models presented. The figure shows a fairly constant value of T_c/T for increasing relative plate clearance h/H . As the steepness decreases, (Figs. 4.11(a) - 4.11(c)), T_c/T decreases for higher values of h/H .

Similarly, Fig. 4.12 is plot of a dimensionless duration relating to complete submergence T_s/T , where $T_s = t_2 - t_1$. This parameter indicates the duration for which the plate remains submerged and influences the span of gradual variation of the added mass force F_{a2} . As expected, an increasing relative clearance h/H leads to a decreasing value of T_s/T .

Times of Occurrence

Figure 4.13 shows the relative rise-time T_p/T associated with the peak upward force, and Fig. 4.14 shows corresponding results relating to T_m/T . Figure 4.13 exhibits a fair degree of scatter so that there are no particularly noticeable trend in these results. However, there is some tendency for T_p/T to decrease with increasing h/H . On the other hand Fig. 4.14 shows a fairly clear trend for T_m/T to decrease with increasing h/H and with decreasing ℓ/L . The scatter in the rise-times may be attributed to factors such as air-entrapment, spray and splash effects at the instant of impact, plate surface roughness and structural vibration.

Line of Action

Figure 4.15 shows the non-dimensionalised line of action of the peak upward force s_p/L plotted against the relative clearance h/H for various values of relative plate length and

wave steepness. There is considerable scatter in the results once more such that the relative plate length ℓ/L and wave steepness H/L appear to have no significant influence on s_p/L , except that s_p/L increases with an increasing h/H .

Figure 4.16 indicates corresponding results for s_m/L . In this case, it is interesting to note that for all ranges of steepness tested, there seems to be a linear trend between s_m/L and h/H .

Wetted Length

In Fig. 4.17, the dimensionless wetted length λ_p/L associated with the peak upward force is plotted as a function of relative clearance h/H , with H/L and ℓ/L as parameters. It is observed that for lower value of the ℓ/L , the λ_p seems to reduce as h/H increases. Corresponding results for λ_m/L are shown in Fig. 4.18 and indicate no particular correlation.

From the above, it can be seen that in general as h/H increases all impact parameters decrease. The effect of steepness is not noticeable, possibly because of the small range considered in the tests.

4.3 Video Records

In order to complement the results presented in the previous section, a qualitative study of the impact process of the flow past the plate has also been made on the basis of the video records.

Figure 4.19 shows photographs indicating the wave flow past the plate associated with a distortion in the shape of the wave profile. Figure 4.19(a) was taken at the instant of complete submergence and shows some air entrapment at the rear end as the plate

completely submerges, and Figure 4.19(b) was taken just after the wave passes the plate and shows the overtopped water draining from the plate.

The video records have been examined in order to assess further the interaction process, and Fig. 20 shows several frames corresponding to various stages of slamming process. In Fig. 4.20(a), the wave profile deforms considerably during the initial penetration of the plate below the water surface. The wave progresses over the plate without too much further disturbance to its profile until the plate is completely submerged [see Fig. 4.20(b)]. Figures 4.20(c) and 4.20(d) show successive views during the recession stage, during which water drains from the plate including some disturbance to the wave profile. Air entrainment between the plate and the water surface during this stage is noticeable.

The irregularities highlighted above in conjunction with uncontrollable parameters such as the plate roughness, plate orientation, and structural vibrations, influence the force measured and contribute to the scatter observed in the force results.

4.4 Force Predictions

In the present section, a comparison of the predictions of the two analytical models of the vertical force given by Eq. 2.23 and Eq. 2.27 with the experimental measurements is presented and discussed.

The steps involved in the computational aspects of the analytical models are as follows. Eq. 2.23 is evaluated from the instant of initial contact until the instant of complete submergence. This is followed by a computation of the force during complete submergence. Finally, Eq. 2.23 is evaluated for the period of wave recession. Parameters relating to this formulation, which are computed at each time step include the wetted length λ and the wave kinematics $\dot{\eta}$ and $\ddot{\eta}$. λ is obtained by evaluating Eq. 2.20, and $\dot{\eta}$ and $\ddot{\eta}$ are determined at a point half way along the instantaneous wetted length λ on the basis of

Eqs. 2.18 and 2.19. A similar procedure is adopted for the simpler analytical model given by Eq. 2.27.

Figures 4.21 and 4.22 show the variation of the dimensionless vertical force $F/\rho gbH\ell$ over one wave cycle for $H/L = 0.04$; $\ell/L = 0.146$ and for 2 two plate clearances, $h/H = 0$ and 0.15 , and compare the predictions of the analytical models given by Eqs. 2.23 and 2.27. In evaluating these equations a range of suitable α values ranging from 1 to 3 for Eq. 2.23 and 0.5 to 0.7 for Eq. 2.27 were assumed. From these figures it can be observed that a noticeable difference of the force predicted by two models occur in the partially submerged stage, with the model based on Eq. 2.23 indicating a faster rise than Eq. 2.27. This is due to the different assumptions made in added mass variations with respect to submergence [see also Fig. 2.5].

It is also of interest to consider the suitability of the analytical model in predicting the vertical force variation, and a comparison of the force predicted on the basis of Eqs. 2.23 and 2.27 with a measured force record is made in following paragraphs. The added mass constant α is selected so as to match the measured and predicted maximum forces.

Figure 4.23 provides a comparison of the measured and predicted force time histories for the case $h = 0$ cm, $T = 2.02$ sec and $H = 17.5$ cm. The predicted force based on Eq. 2.23 rises to a peak much earlier and drops to negative values faster than the observed force. On the other hand, the force predicted on the basis of Eq. 2.27 reaches a maximum during the partial submergence with a rise-time almost equal to the measured force and it seems to follow the measured force reasonably well until the maximum force is reached.

Figure 4.24 compares the predicted and measured force for incident waves with $T = 1.68$ sec, and $H = 14.2$ cm with the plate located at $h = 0$ cm. In this case, the rise-time of the predicted force based on Eq. 2.27 seems to be much smaller and significantly

deviates from the observed force. However, prediction based on Eq. 2.23 seems to deviate more than that by Eq. 2.27.

Figure 4.25 is similar plot for the incident wave with $T = 2.02$ sec, $H = 17.5$ cm with $h = 1.4$ cm. For the case of Eq. 2.27, although the predicted peak occurs slightly later than that for the measured force, it follows the observed force reasonably well. The prediction based on Eq. 2.23 does not show any improvement compared to that based on Eq. 2.27.

Form all the three figures, it is observed that the predicted forces deviate significantly from the observed force during the stage of complete submergence followed by wave recession.

As mentioned earlier, the factor α of Eqs. 2.23 and 2.27 has been evaluated by matching the measured and predicted maximum upward force. The results for a selected number of tests are listed in Table 4.2. These correspond to 9 tests with $h = 0$, two tests with $h = 1.4$ cm and one test with $h = 2.5$ cm. For all the 12 selected tests, the factor α is in the range of 1.2 to 3.1 on the basis of Eq. 2.23, and is in the range of 0.5 to 0.7 on the basis of Eq. 2.27. Thus, α based on Eq. 2.27 is approximately equal to $\pi/4$, which corresponds to the theoretical value of a plate in an infinite flow situation, so that there is no requirement of any reduction factor. On the other hand, the values of α based on Eq. 2.23 seem to exhibit considerable scatter.

Chapter 5

Conclusions and Recommendations

The primary objective of this study was to examine experimentally the vertical force due to regular non-breaking waves interacting with a fixed horizontal plate located near the still water level. Force time histories were analyzed to obtain peak upward and downward forces, their times of occurrence, their lines of action and the associated wetted length of the plate. Also, the free surface elevation at the leading and rear edges of the plate were recorded for different wave conditions with the plate absent. Two analytical models based on a varying added mass of the submerged portion of the plate together with a drag and buoyancy forces were used to predict the force on the plate, and a comparison of these predictions with the experimental results was made.

The dependence of the various characteristics of the maximum and minimum forces on the relative plate clearance h/H , wave steepness H/L and relative plate length ℓ/L have been examined and are indicated. Even though there is a considerable degree of scatter in the results, some general conclusions may be made. The maximum upward force decreases with increasing relative clearance of the plate h/H . And the peak upward force is higher for larger value of relative plate length ℓ/L . In the present study the wave steepness H/L was in the range of 0.016 to 0.041 and is observed not to influence the peak upward force noticeably. The maximum downward force seems to remain constant for increasing relative clearance h/H . However, it shows similar variation as that of the peak upward force for changes in relative plate length ℓ/L and in wave steepness H/L . The rise-time associated with the peak upward force shows considerable scatter. However, it is observed that there is some tendency for T_p/T to decrease with increasing h/H . On the

other hand, the dimensionless time of occurrence T_m/T showed a decreasing trend for increasing values of plate clearance. Also, for higher relative lengths, ℓ/L , a higher T_m/T was observed. For relative line of action, associated with both the F_p and F_m indicated increasing trend for steeper waves and remained constant for less steep waves. Summarily, the analysis indicated that the peak forces F_p and F_m and associated times of occurrence decrease some what linearly with the increasing plate clearance.

The maximum upward force and associated rise-time can be predicted reasonably well on the basis of the simpler hydrodynamic model given by Eq. 2.27, with the factor α ranging from 0.5 to 0.7. However, the predicted force deviates significantly from the measured force after the occurrence of the peak upward force. This indicates the need for a clearer understanding of the wave interaction with the plate during complete submergence and recession stages.

Several avenues of further study may be suggested. Improvements may be made to analytical / numerical models to predict the vertical force; and experiments relating to irregular and breaking waves also need to be carried out.

References

Armand J. L., and R. Cointe, (1987), "Hydrodynamic impact analysis of a cylinder," *J. Offshore Mechanics and Arctic Engineering*, ASME, Vol. 109, pp. 237 - 243.

Broughton, P., and E. Horn, (1987), "Ekofisk platform 2/4C: re-analysis due to subsidence," *Proc. Institution of Civil Engineers*, Part 1, Vol. 82, pp. 949 - 979.

Chan, E. S., and W. K. Melville, (1989), "Plunging wave forces on surface-piercing structures," *J. Offshore Mechanics and Arctic Engineering*, ASME, Vol. 111, pp. 93-130.

Chan, E. S., H. F. Cheong, and K. Y. H. Gin, (1991), "Wave impact loads on horizontal structures in the splash zone," *Proc. 1st International Offshore and Polar Engineering Conference*, Vol. 3, pp. 203 - 209

Chuang, S. L., (1967), "Experiments on slamming of wedge-shaped bodies with variable dead rise angle," *J. Ship Research*, SNAME, Vol. 11, No. 4, pp. 190-198.

De Costa, S. L., and J. L. Scott, (1988), "Wave impact forces on the Jones Island east dock, Milwaukee, Wisconsin," *Oceans*, IEEE, pp. 1231-1238.

Denson, K. H., and M. S. Priest, (1971), "Wave pressure on the underside of a horizontal platform," *Proc. Offshore Technology Conference*, Houston, Texas, Paper No. OTC 1385, Vol. 1, pp. 555 - 570.

El Ghamry, O. A., (1963), "Wave forces on a dock," Report no. HEL-9-1, Inst. of Engg. Research, Hydraulic Engg. Lab., *University of California*, Berkeley, California.

Faltinsen O., (1990), "Sea loads on ships and offshore structures," Cambridge Ocean Technology Series, Cambridge University Press, Cambridge, UK.

French, J. A., (1969), "Wave uplift pressures on horizontal platforms," Report no. KH-R-19, Division of Engineering and Applied Science, California Institute of Technology, Pasadena, California.

Furudoi, T., and A. Murota, (1966), "Wave induced uplift forces acting on quay-aprons," *Technology Reports of Osaka University*, Vol. 16, No. 734, pp. 605 - 616.

Greenhow, M., and Y. Li, (1987), "Added mass for circular cylinders near or penetrating fluid boundaries - review extension, and application to water-entry, -exit, and slamming," *Ocean Engineering*, Vol. 14, No. 4, pp. 325 - 348.

Gudmestad, O. T., and J. J. Connor, (1986), "Engineering approximation to nonlinear deep water waves," *Applied Ocean Research*, Vol. 8, No. 2, pp. 76 - 88.

Humar, J. L., (1990), "Dynamics of structures," *Prentice Hall*, Englewood, New Jersey.

Irajpanah, K., (1983), "Wave uplift force on horizontal platform," Ph. D. Thesis, Univ. of Southern California, Los Angeles, California.

- Isaacson, M., and S. Prasad, (1992), "Wave slamming on a horizontal circular cylinder," *Proc. Civil Engineering in the Oceans V*, ASCE, College Station, Texas, pp. 652 - 666.
- Isaacson, M., and S. Prasad, (1993), "Wave slamming on a horizontal circular cylinder," *Proc. 3rd International Offshore and Polar Engineering Conference*, Singapore, Vol. 3, pp. 274-281.
- Kaplan, P., and N. Silbert, (1976), "Impact on platform horizontal members in the splash zone," *Proc. Offshore Technology Conference*, Houston, Texas, Paper No. OTC 2498, Vol. 1, pp. 749 - 758.
- Kaplan, P., (1992), "Wave impact forces on offshore structures: re-examination and new interpretations," *Proc. Offshore Technology Conference*, Houston, Texas, Paper No. OTC 6814, Vol. 1, pp. 79-88.
- Lai, C. P., and J. J. Lee, (1989), "Interaction of finite amplitude waves with platforms or docks," *J. Waterways, Port, Coastal and Ocean Engineering*, ASCE, Vol. 115, No. 1, pp. 19-39.
- Lamb, H., (1932), "Hydrodynamics," 6th edition, Dover Publications, Inc., New York, N. Y.
- Sarpkaya, T., (1978), "Wave impact loads on cylinders," *Proc. Offshore Technology Conference*, Houston, Texas, Paper No. OTC 3065, pp. 169-176.
- Sarpkaya, T., and M. Isaacson, (1981), "Mechanics of wave forces on offshore structures," Van Nostrand Reinhold, New York, N.Y.
- Szebehely, V. G., and M. K. Ochi, (1966), "Hydrodynamic impact and water entry," *Applied Mechanics Survey*, ed. H. N. Abramson, *et al.*, Spartan Books, MacMillan & Co. Ltd., pp. 951-957.
- Tanimoto, K., and S. Takahashi, (1979), "Wave forces on a horizontal platform," *Proc. 5th International Ocean Development Conference*, Tokyo, Japan, Vol. D1, pp. 29 - 38.
- Toumazis, A. D., W. K. Shih, and K. A. Anastasiou, (1989), "Wave impact loading on horizontal and vertical plates," *Proc. 23rd Congress, International Association of Hydraulic Research*, Ottawa, Canada, Vol. C, pp. 209 - 216.
- Verhagen, J. H. G., (1967), "The impact of flat plate on a water surface," *J. Ship Research*, SNAME, Vol. 11, No. 4, pp. 211-223.
- von Kármán, T., (1929), "The impact on seaplane floats during landing," *National Advisory Committee for Aeronautics*, Technical Note No. 321.
- Wagner, H., (1932), "Landing of Seaplanes," *National Advisory Committee for Aeronautics*, Technical Note No. 622.
- Wang, H., (1967), "Estimating wave pressures on a horizontal pier," *Naval Civil Engineering Laboratory*, Port Heneme, California, Technical Report No. R-546.

Appendix A

Static Analysis

The load-cells placed at the two supports measure the support reactions due to the wave action on the plate. The plate can be assumed to be analogous to a simply supported beam with an over-hang from its supports and can be analyzed by the simple principles of statics in order to provide the unknown vertical force along with its line of action at any instant from the recorded reactions at the two supports. The plate is assumed to be thin enough for any horizontal force to be neglected, and no measurement of the horizontal force has been carried out.

Referring to the Fig. A1, let $F_A(t)$ and $F_B(t)$ be the support reactions recorded at any time t , $F(t)$ the unknown force acting on the plate and $s(t)$ its line of action measured from the leading edge of the plate. $F(t)$ can be obtained by summing the support reactions $F_A(t)$ and $F_B(t)$.

$$F(t) = F_A(t) + F_B(t) \quad (\text{A-1})$$

The line of action $s(t)$ can be obtained by taking moments of the forces acting on the plate about the plate's leading edge. This gives

$$s(t) = \frac{0.30 F_A(t) + 0.545 F_B(t)}{F(t)} \quad (\text{A-2})$$

where $s(t)$ in m.

Table 2.1 Added mass constant for a thin rectangular plate.
(Sarpkaya and Isaacson, 1981).

b/λ	β
1.00	0.579
1.25	0.642
1.59	0.704
2.00	0.757
2.50	0.801
4.00	0.872
5.00	0.897
8.00	0.934
10.00	0.947
∞	1.000

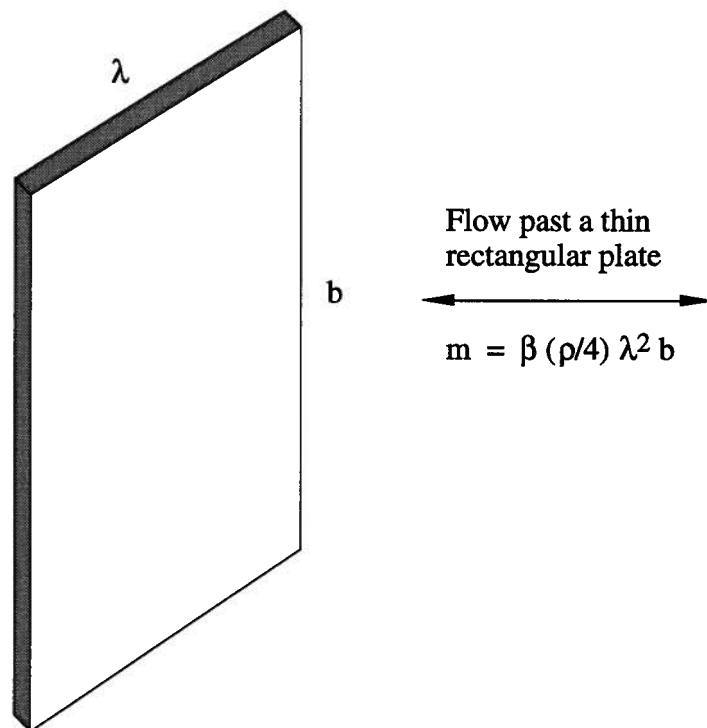


Table 3.1 Wave parameters used in the experiments.

Set no.	Wave period T (s)	Wave height h (m)	Wave steepness H/L	Wave celerity c (m/s)
1.1	1.08	0.062	0.035	1.640
1.2	1.38	0.101	0.039	1.877
1.3	1.68	0.142	0.042	2.012
1.4	2.02	0.175	0.041	2.113
2.1	1.12	0.048	0.026	1.648
2.2	1.38	0.075	0.029	1.874
2.3	1.70	0.105	0.030	2.059
2.4	2.02	0.128	0.030	2.112
3.1	1.12	0.030	0.016	1.674
3.2	1.40	0.050	0.019	1.880
3.3	1.70	0.068	0.020	2.000
3.4	1.96	0.081	0.020	2.066

Table 4.1 Summary of test conditions and principal results.

h = 0 cm																
Run#	T (s)	H (m)	H/L	h/H	$\frac{\ell}{L}$	$\frac{\rho g H \ell}{(N)}$	$\frac{F_p}{\rho g H \ell}$	$\frac{F_m}{\rho g H \ell}$	$\frac{T_c}{T}$	$\frac{T_s}{T}$	$\frac{T_p}{T}$	$\frac{T_m}{T}$	$\frac{s_p}{L}$	$\frac{s_m}{L}$	$\frac{\lambda_p}{L}$	$\frac{\lambda_m}{L}$
2	1.08	0.06	0.04	0.00	0.34	72.8	0.32	-0.14	0.33	0.17	0.25	0.70	0.17	0.16	0.27	0.12
3	1.38	0.10	0.04	0.00	0.23	119.0	0.24	-0.21	0.23	0.27	0.12	0.64	0.10	0.14	0.09	0.20
4	1.68	0.14	0.04	0.00	0.18	167.7	0.25	-0.16	0.17	0.34	0.21	0.52	0.10	0.09	0.18	0.14
5	2.02	0.18	0.04	0.00	0.14	205.7	0.27	-0.15	0.14	0.37	0.14	0.51	0.07	0.08	0.14	0.00
7	1.12	0.05	0.03	0.00	0.32	56.5	0.36	-0.13	0.32	0.18	0.24	0.71	0.17	0.18	0.25	0.10
8	1.38	0.08	0.03	0.00	0.23	88.5	0.26	-0.23	0.24	0.27	0.13	0.64	0.09	0.14	0.13	0.09
9	1.70	0.11	0.03	0.00	0.17	123.1	0.27	-0.19	0.17	0.33	0.22	0.55	0.09	0.09	0.17	0.12
10	2.02	0.13	0.03	0.00	0.14	150.9	0.32	-0.17	0.14	0.36	0.14	0.54	0.07	0.08	0.14	0.10
12	1.12	0.03	0.02	0.00	0.32	35.1	0.41	-0.14	0.32	0.18	0.30	0.70	0.17	0.14	0.31	0.12
13	1.40	0.05	0.02	0.00	0.23	59.0	0.26	-0.23	0.23	0.28	0.31	0.65	0.11	0.13	0.23	0.08
14	1.70	0.07	0.02	0.00	0.17	80.3	0.31	-0.21	0.17	0.33	0.25	0.57	0.09	0.09	0.18	0.08
15	1.96	0.08	0.02	0.00	0.15	94.8	0.34	-0.19	0.15	0.35	0.16	0.57	0.07	0.08	0.15	0.08
h = 0.8 cm																
Run#	T (s)	H (m)	H/L	h/H	$\frac{\ell}{L}$	$\frac{\rho g H \ell}{(N)}$	$\frac{F_p}{\rho g H \ell}$	$\frac{F_m}{\rho g H \ell}$	$\frac{T_c}{T}$	$\frac{T_s}{T}$	$\frac{T_p}{T}$	$\frac{T_m}{T}$	$\frac{s_p}{L}$	$\frac{s_m}{L}$	$\frac{\lambda_p}{L}$	$\frac{\lambda_m}{L}$
17	1.08	0.06	0.04	0.13	0.34	72.8	0.24	-0.14	0.344	0.34	0.08	0.66	0.20	0.18	0.26	0.06
18	1.38	0.10	0.04	0.08	0.23	119.0	0.19	-0.22	0.232	0.23	0.22	0.60	0.12	0.14	0.15	0.18
19	1.68	0.14	0.04	0.06	0.18	167.7	0.23	-0.18	0.171	0.17	0.29	0.54	0.09	0.11	0.18	0.09
20	2.02	0.18	0.04	0.05	0.14	205.7	0.24	-0.17	0.144	0.14	0.33	0.48	0.07	0.08	0.14	0.00
22	1.12	0.05	0.03	0.17	0.32	56.5	0.24	-0.14	0.321	0.32	0.08	0.59	0.17	0.16	0.18	0.10
23	1.38	0.08	0.03	0.11	0.23	88.5	0.19	-0.20	0.225	0.22	0.20	0.60	0.11	0.14	0.19	0.05
24	1.70	0.11	0.03	0.08	0.17	123.1	0.24	-0.20	0.176	0.18	0.29	0.54	0.09	0.10	0.17	0.08
25	2.02	0.13	0.03	0.06	0.14	150.9	0.29	-0.19	0.139	0.14	0.32	0.50	0.07	0.08	0.12	0.08
27	1.12	0.03	0.02	0.27	0.32	35.1	0.24	-0.18	0.33	0.33	-	0.57	0.17	0.16	0.19	0.08
28	1.40	0.05	0.02	0.16	0.23	59.0	0.21	-0.16	0.221	0.22	0.17	0.59	0.09	0.13	0.12	0.04
29	1.70	0.07	0.02	0.12	0.17	80.3	0.25	-0.19	0.165	0.16	0.26	0.52	0.09	0.09	0.18	0.05
30	1.96	0.08	0.02	0.10	0.15	94.8	0.30	-0.23	0.143	0.14	0.30	0.53	0.08	0.09	0.15	0.04

Table 4.1 (contd.) Summary of test conditions and principal results.

h = 1.4 cm														
Run#	T (s)	H (m)	H/L	h/H	$\frac{\ell}{L}$	pgHb ℓ (N)	$\frac{F_p}{\text{pgHb}\ell}$	$\frac{F_m}{\text{pgHb}\ell}$	$\frac{T_c}{T}$	$\frac{T_s}{T}$	$\frac{T_p}{T}$	$\frac{T_m}{T}$	$\frac{\lambda_p}{L}$	$\frac{\lambda_m}{L}$
32	1.08	0.06	0.04	0.23	0.34	72.8	0.20	-0.11	0.33	0.02	0.16	0.60	0.17	0.06
33	1.38	0.10	0.04	0.14	0.23	119.0	0.19	-0.18	0.22	0.18	0.19	0.57	0.12	0.16
34	1.68	0.14	0.04	0.10	0.18	167.7	0.25	-0.17	0.18	0.26	0.15	0.52	0.09	0.11
35	2.02	0.18	0.04	0.08	0.14	205.7	0.24	-0.17	0.14	0.31	0.11	0.46	0.07	0.00
37	1.12	0.05	0.03	0.29	0.32	56.5	0.19	-0.12	0.29	-	0.15	0.54	0.18	0.09
38	1.38	0.08	0.03	0.19	0.23	88.5	0.15	-0.16	0.22	0.09	0.30	0.51	0.14	0.10
39	1.70	0.11	0.03	0.13	0.17	123.1	0.24	-0.18	0.18	0.24	0.15	0.49	0.08	0.09
40	2.02	0.13	0.03	0.11	0.14	150.9	0.24	-0.19	0.14	0.30	0.12	0.49	0.07	0.08
42	1.40	0.05	0.02	0.28	0.23	59.0	0.13	-0.13	0.23	0.09	0.28	0.52	0.13	0.00
43	1.70	0.07	0.02	0.21	0.17	80.3	0.21	-0.15	0.17	0.19	0.12	0.48	0.08	0.07
44	1.96	0.08	0.02	0.17	0.15	94.8	0.23	-0.21	0.15	0.24	0.13	0.50	0.08	0.04
h = 1.8 cm														
Run#	T (s)	H (m)	H/L	h/H	$\frac{\ell}{L}$	pgHb ℓ (N)	$\frac{F_p}{\text{pgHb}\ell}$	$\frac{F_m}{\text{pgHb}\ell}$	$\frac{T_c}{T}$	$\frac{T_s}{T}$	$\frac{T_p}{T}$	$\frac{T_m}{T}$	$\frac{\lambda_p}{L}$	$\frac{\lambda_m}{L}$
46	1.08	0.06	0.04	0.29	0.34	72.8	0.18	-0.09	0.31	-	0.15	0.58	0.19	0.03
47	1.38	0.10	0.04	0.18	0.23	119.0	0.15	-0.17	0.23	0.15	0.21	0.55	0.12	0.16
49	2.02	0.18	0.04	0.10	0.14	205.7	0.21	-0.17	0.13	0.30	0.11	0.46	0.07	0.00
51	1.12	0.05	0.03	0.38	0.32	56.5	0.10	-0.12	0.23	-	0.12	0.43	0.19	0.11
52	1.38	0.08	0.03	0.24	0.23	88.5	0.14	-0.14	0.25	0.09	0.23	0.50	0.13	0.08
53	1.70	0.11	0.03	0.17	0.17	123.1	0.24	-0.16	0.16	0.23	0.15	0.48	0.09	0.07
54	2.02	0.13	0.03	0.14	0.14	150.9	0.22	-0.20	0.12	0.27	0.07	0.47	0.05	0.08
56	1.40	0.05	0.02	0.36	0.23	59.0	0.09	-0.13	0.24	0.01	0.26	0.45	0.18	-
57	1.70	0.07	0.02	0.26	0.17	80.3	0.21	-0.13	0.18	0.16	0.12	0.43	0.09	0.06
58	1.96	0.08	0.02	0.22	0.15	94.8	0.20	-0.19	0.15	0.21	0.05	0.44	0.05	0.05

Table 4.1 (contd.) Summary of test conditions and principal results.

h = 2.5 cm																
Run#	T (s)	H (m)	$\frac{H}{L}$	$\frac{h}{H}$	$\frac{\ell}{L}$	$\rho g H \ell$ (N)	$\frac{F_p}{\rho g H \ell}$	$\frac{F_m}{\rho g H \ell}$	$\frac{T_c}{T}$	$\frac{T_s}{T}$	$\frac{T_p}{T}$	$\frac{T_m}{T}$	$\frac{s_p}{L}$	$\frac{s_m}{L}$	$\frac{\lambda_p}{L}$	$\frac{\lambda_m}{L}$
60	1.08	0.06	0.04	0.40	0.34	72.8	0.07	-0.08	0.20	-	0.02	0.39	-	0.06	0.17	0.00
61	1.38	0.10	0.04	0.25	0.23	119.0	0.18	-0.14	0.22	0.10	0.22	0.47	0.16	0.15	0.14	0.19
62	1.68	0.14	0.04	0.18	0.18	167.7	0.28	-0.15	0.17	0.23	0.15	0.46	0.16	0.10	0.10	0.10
63	2.02	0.18	0.04	0.14	0.14	205.7	0.20	-0.17	0.13	0.28	0.05	0.45	0.11	0.04	0.09	0.00
66	1.38	0.08	0.03	0.33	0.23	88.5	0.15	-0.12	0.23	0.04	0.25	0.46	0.23	0.17	0.13	0.06
67	1.70	0.11	0.03	0.24	0.17	123.1	0.21	-0.13	0.18	0.16	0.14	0.44	0.13	0.09	0.09	0.08
68	2.02	0.13	0.03	0.20	0.14	150.9	0.20	-0.19	0.13	0.25	0.06	0.44	0.05	0.04	0.08	0.07
69	1.96	0.08	0.02	0.31	0.15	94.8	0.16	-0.14	0.15	0.15	0.05	0.41	0.02	0.05	0.08	0.05

Table 4.2 Computed values of the factor α in selected tests.

Run No.	Wave period T (s)	Wave height H (m)	F _p (N)	α (Eq. 2.23)	α (Eq. 2.27)
h = 0.0 cm					
3	1.38	0.101	28.20	1.225	0.55
8	1.38	0.075	22.92	1.750	0.61
13	1.40	0.050	15.22	1.600	0.63
4	1.68	0.142	42.09	2.050	0.49
9	1.70	0.105	32.99	2.200	0.53
14	1.70	0.068	24.89	2.500	0.61
5	2.02	0.175	54.92	2.500	0.48
10	2.02	0.128	47.83	3.050	0.61
15	1.96	0.081	32.61	3.100	0.69
h = 1.4 cm					
35	2.02	0.175	48.54	2.400	0.53
34	1.68	0.142	41.59	2.350	0.68
h = 2.5 cm					
63	2.02	0.175	41.55	2.200	0.57



Fig. 1.1 Photographs of typical jetty facilities, Jericho beach, Vancouver.

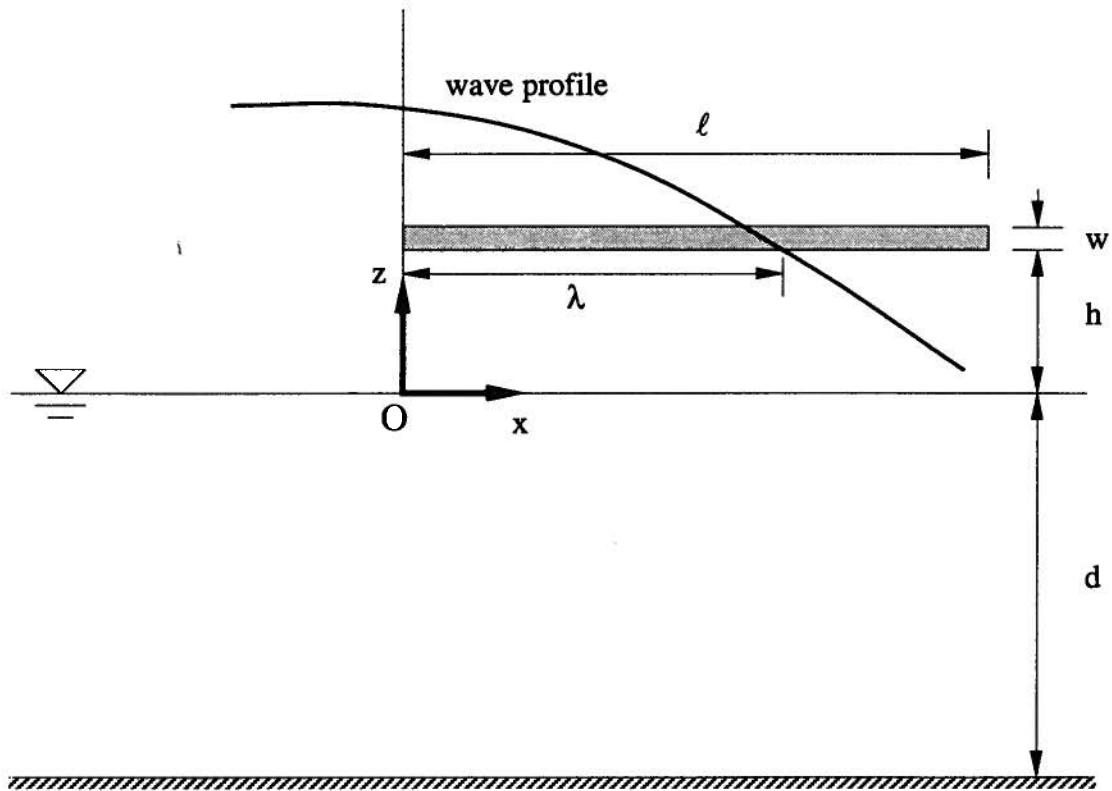


Fig. 2.1 Definition sketch.

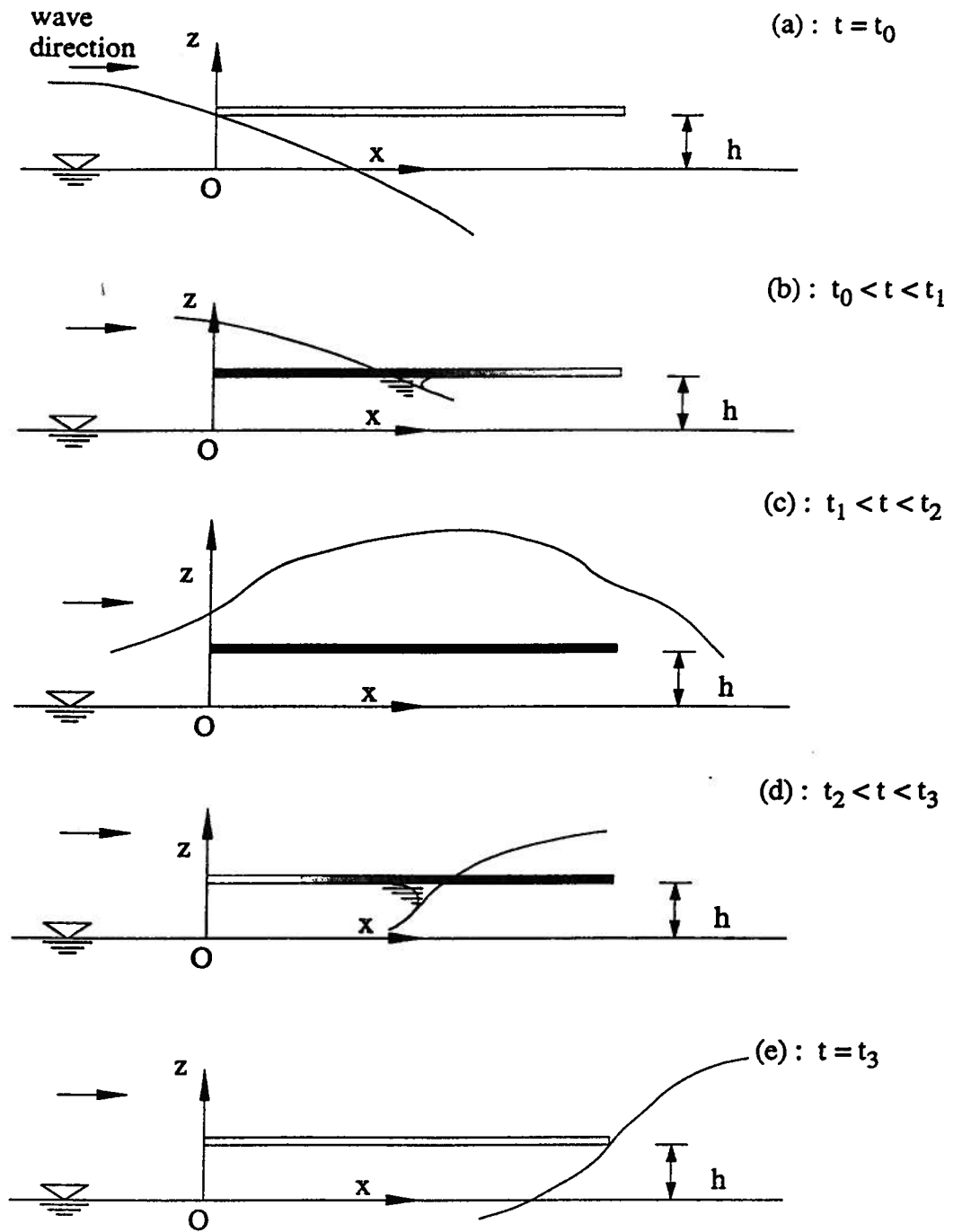


Fig. 2.2 Stages of wave propagation past a horizontal plate. (a) initial contact, $t = t_0$; (b) submergence of upwave portion of plate, $t_0 < t < t_1$; (c) complete submergence of plate, $t_1 < t < t_2$; (d) submergence of downwave portion of plate, $t_2 < t < t_3$; (e) wave detaching from plate, $t = t_3$.

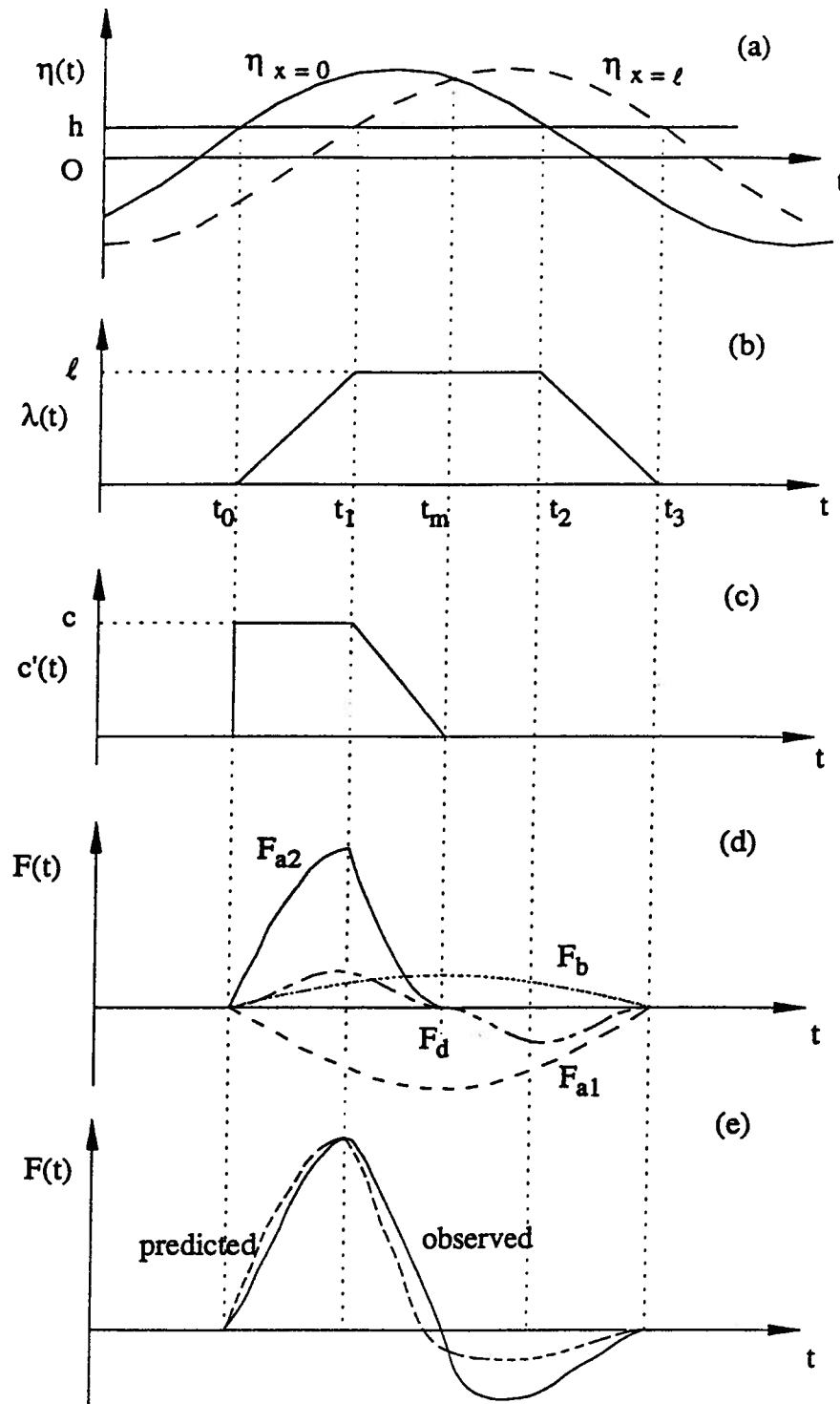


Fig. 2.3 Sketch of ideal force components variation over a wave cycle. (a) free surface elevation; (b) wetted length λ ; (c) proposed variation of $\partial\lambda/\partial t$ as a velocity c' ; (d) force components: inertia force, F_{a1} ; added mass force, F_{a2} ; drag force, F_d ; buoyancy force, F_b ; (d) total vertical force: actual force, predicted force.

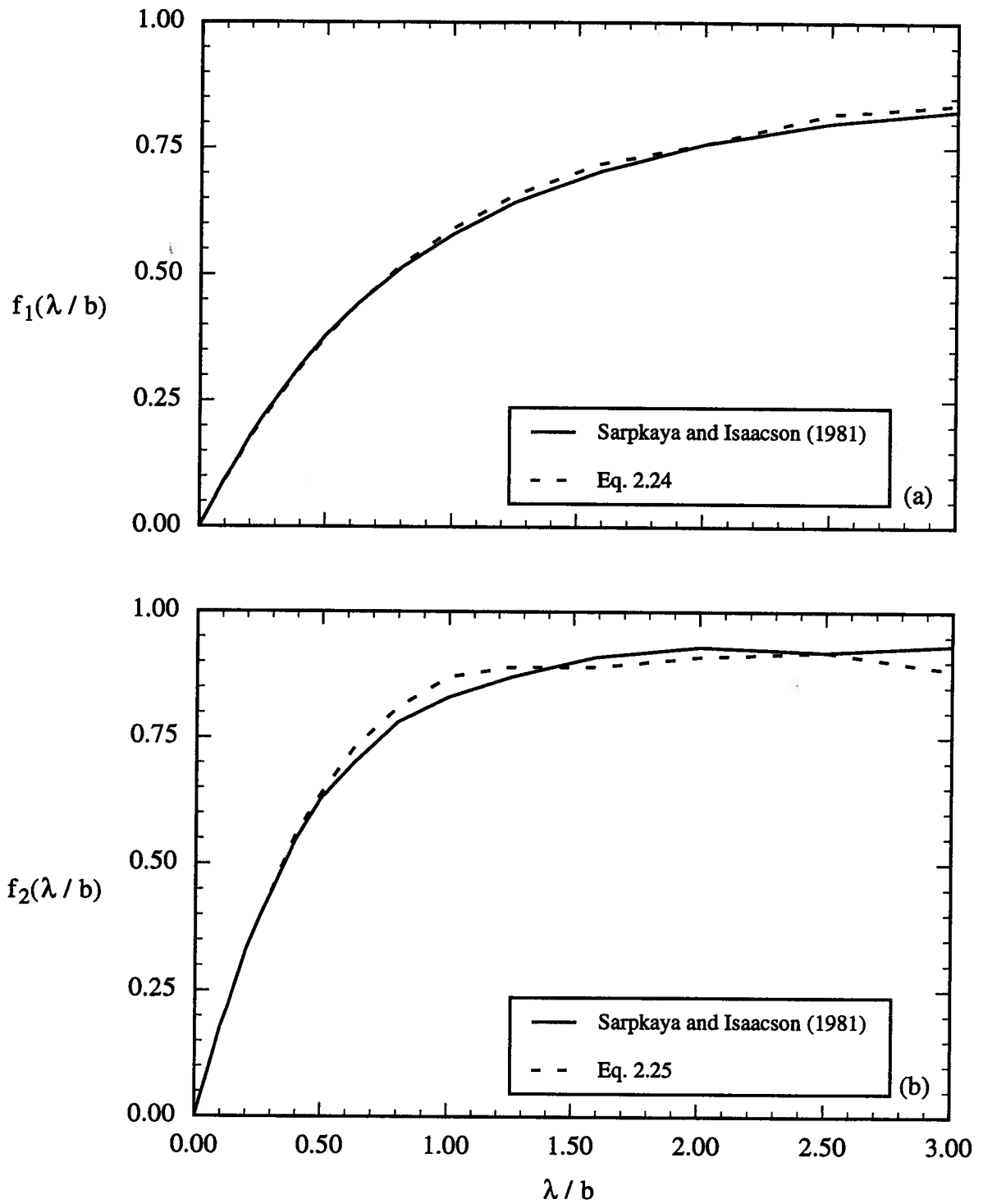


Fig. 2.4 Variation of added mass functions with plate aspect ratio λ/b . (a) $f_1(\lambda/b)$; (b) $f_2(\lambda/b)$.

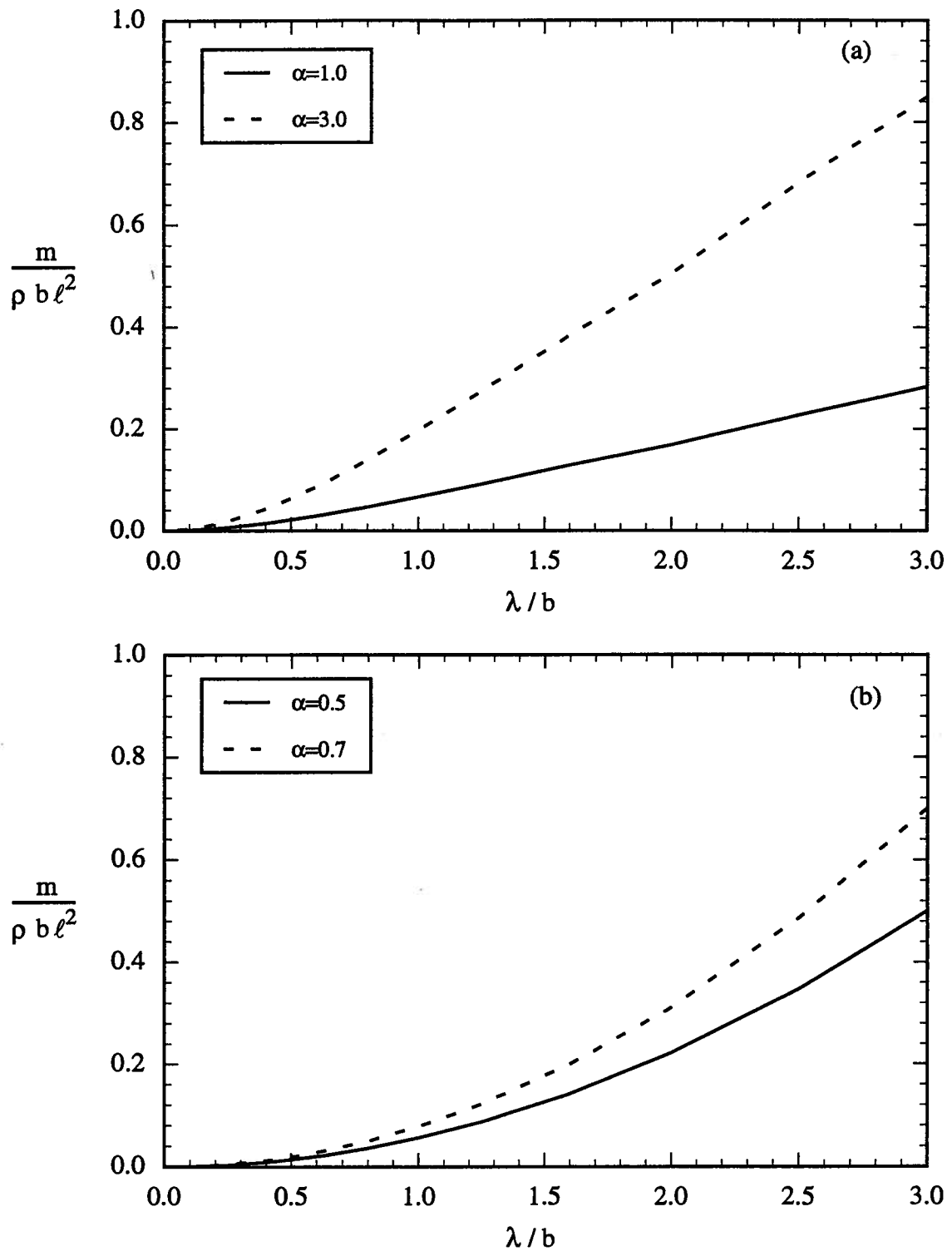


Fig. 2.5 Variation of dimensionless added mass with plate aspect ratio λ/b . (a) Eq. 2.7; (b) Eq. 2.26.

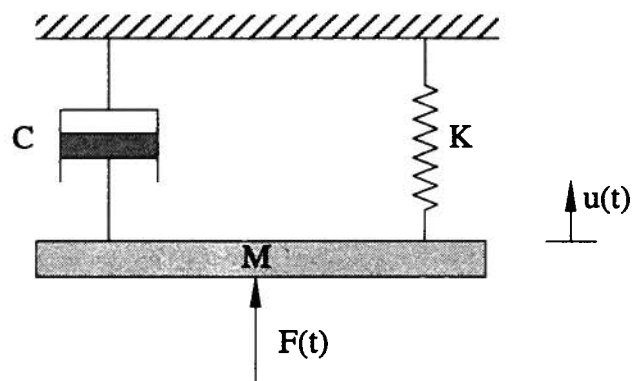


Fig. 2.6 Definition sketch of a single degree of freedom (SDOF) system.

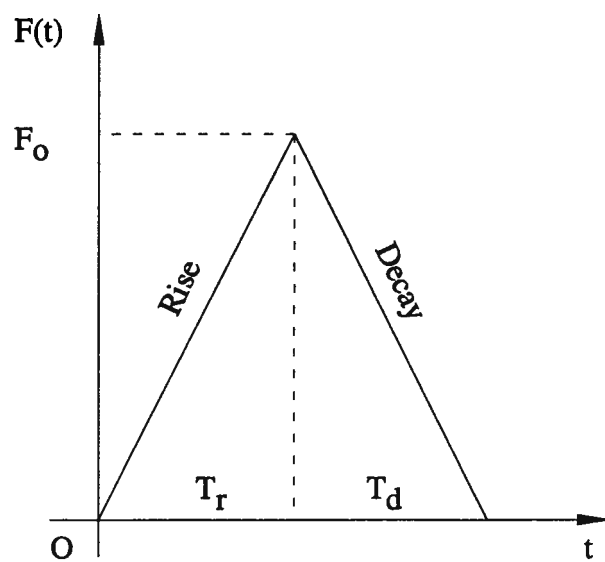


Fig. 2.7 Sketch of an idealized force as a triangular pulse.

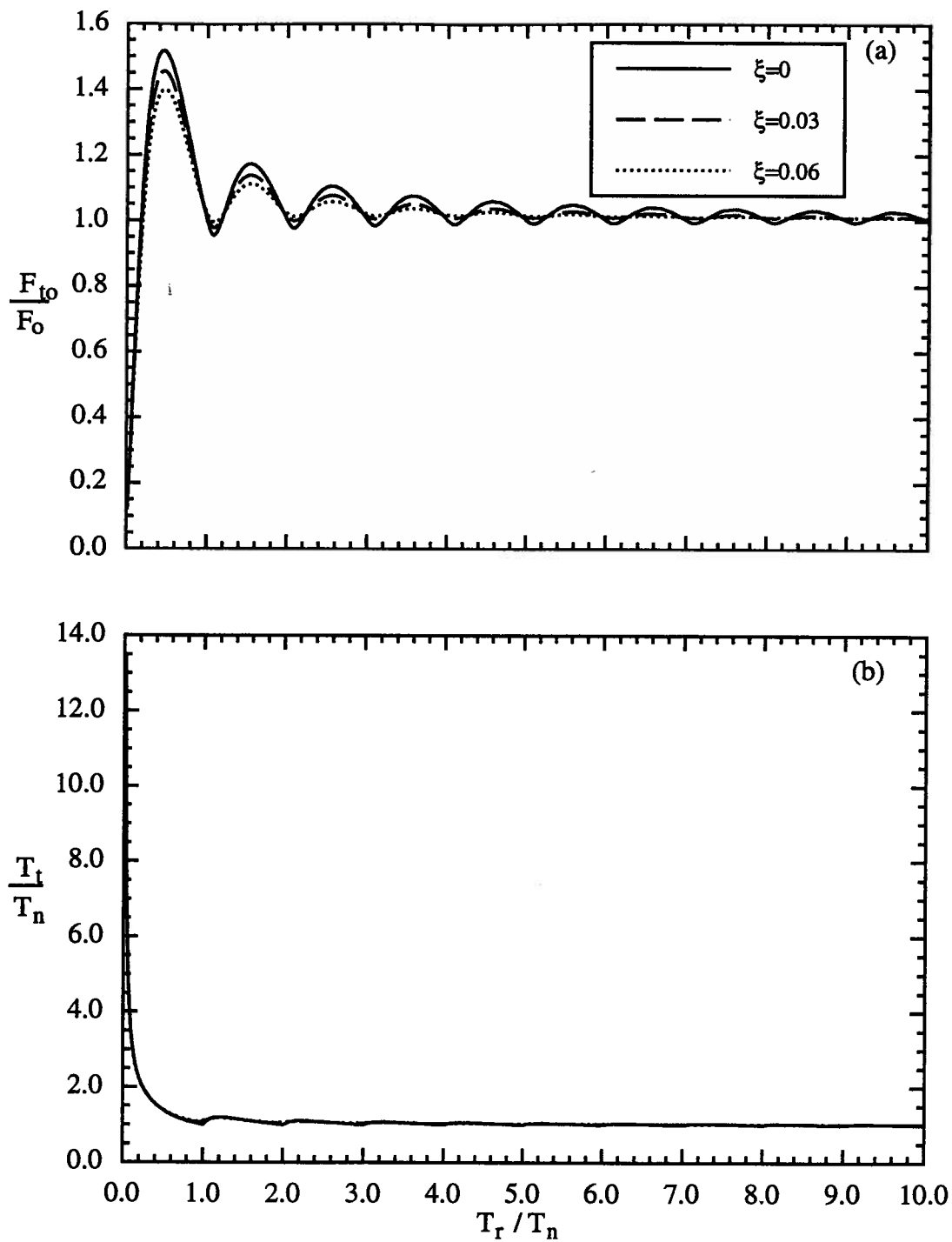


Fig. 2.8 Dynamic amplification factor and relative rise-time as a function of T_r/T_n for applied impulsive force with $T_d/T_r = 1$. (Isaacson and Prasad, 1993).

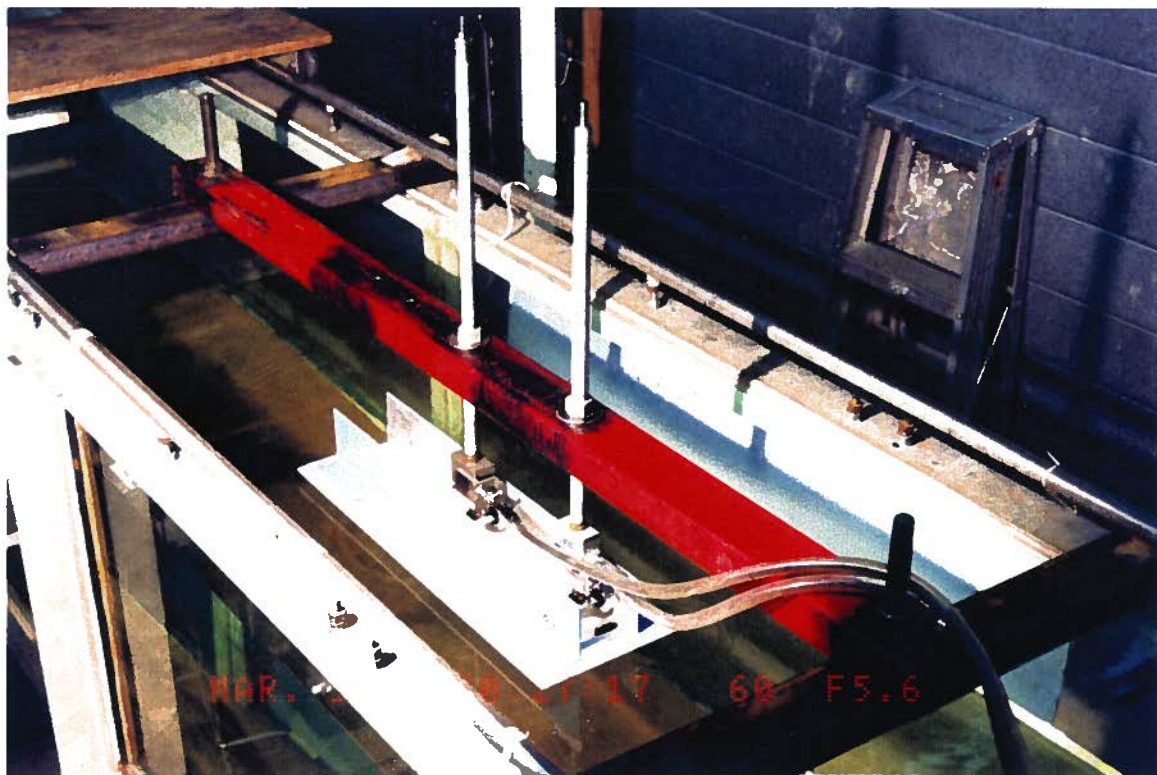
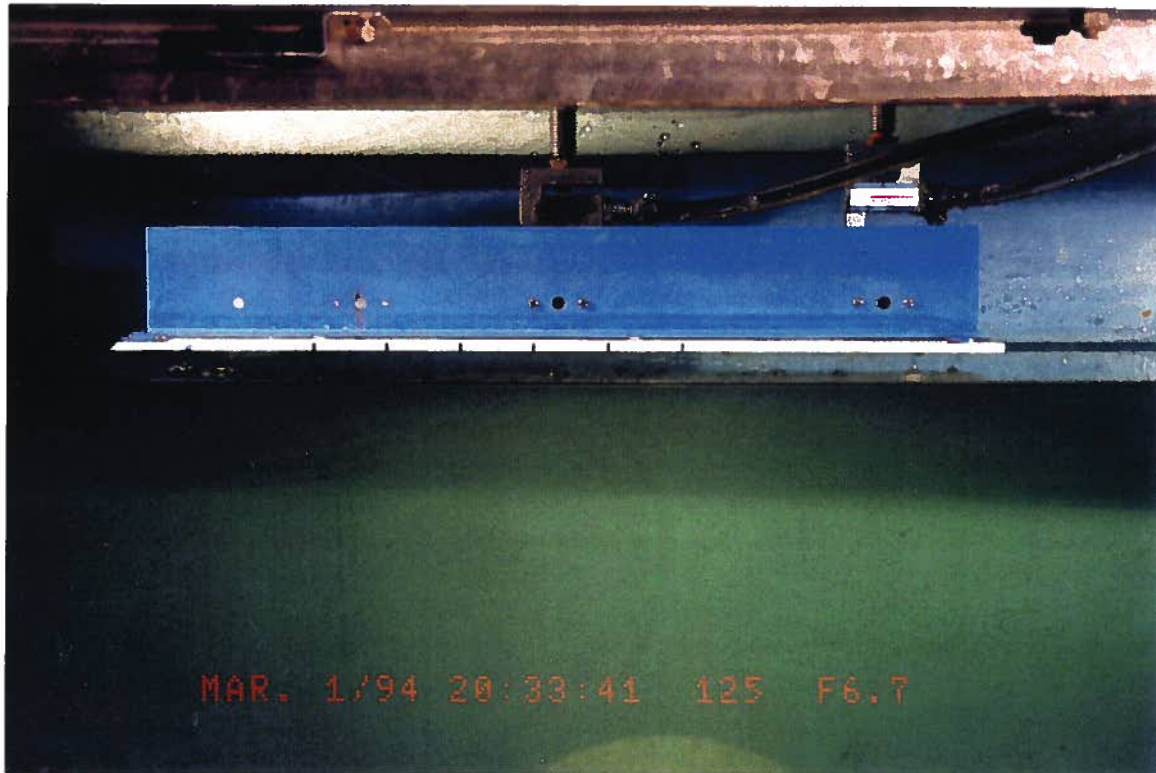


Fig. 3.1 Photographs of the plate assembly. (a) side view; (b) top view indicating the details of supports and load-cell arrangements.

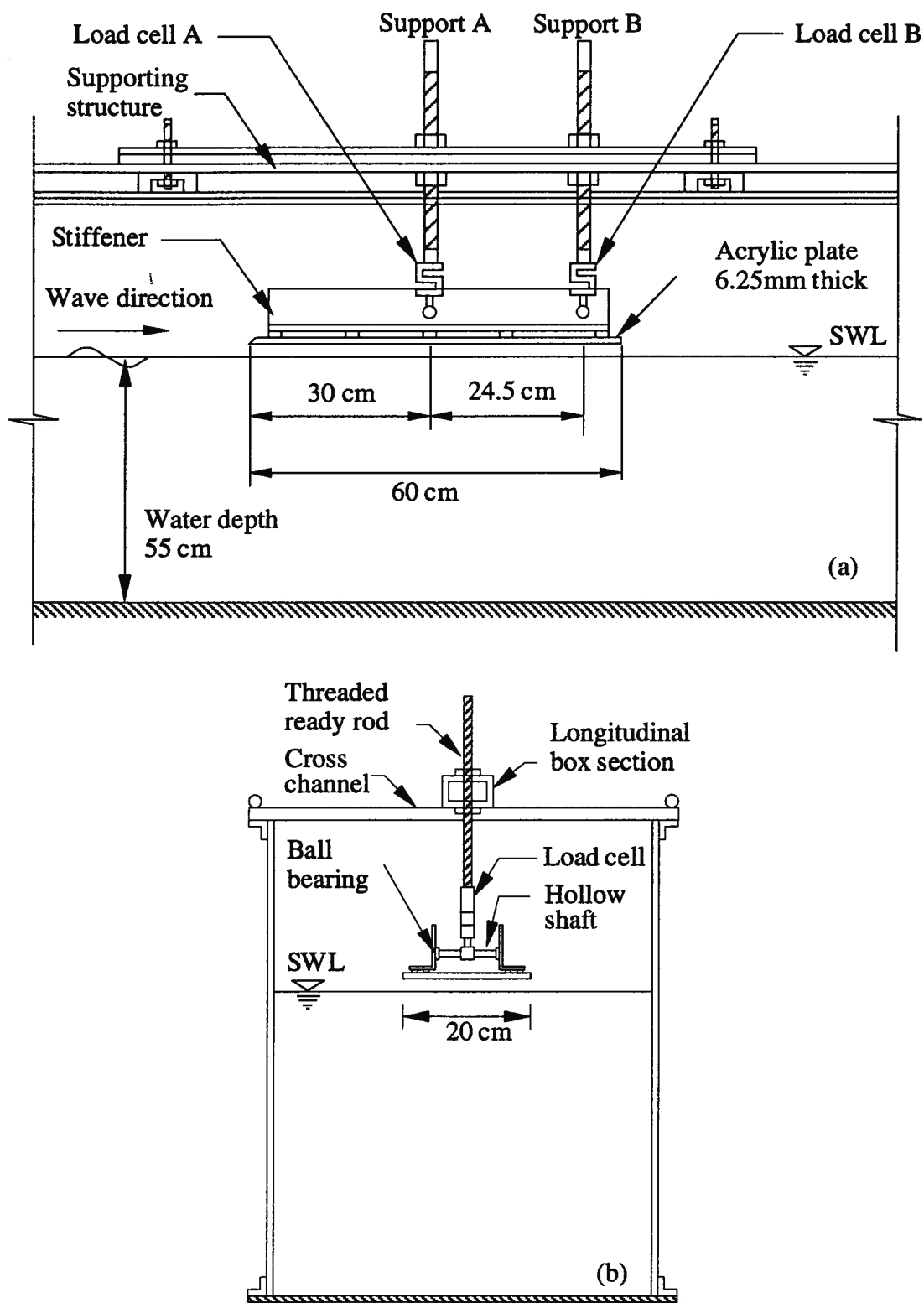


Fig. 3.2 Experimental setup showing the details of the plate and load-cell arrangement.
(a) elevation; (b) cross-section.

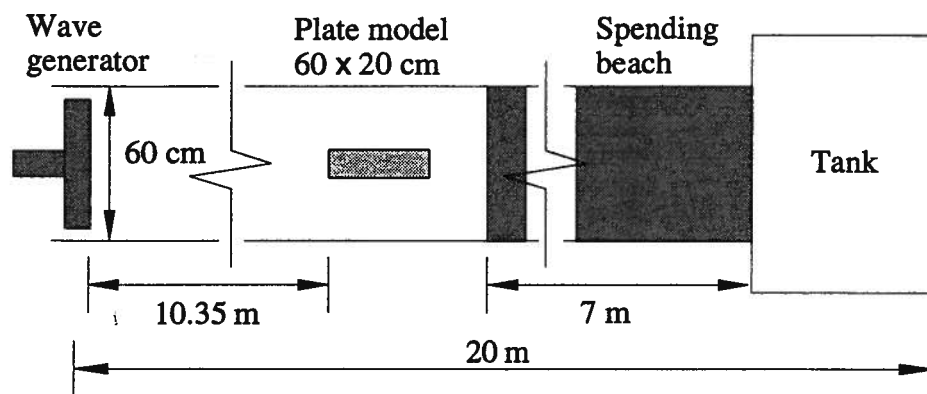


Fig. 3.3 Sketch showing the wave flume and the test location.

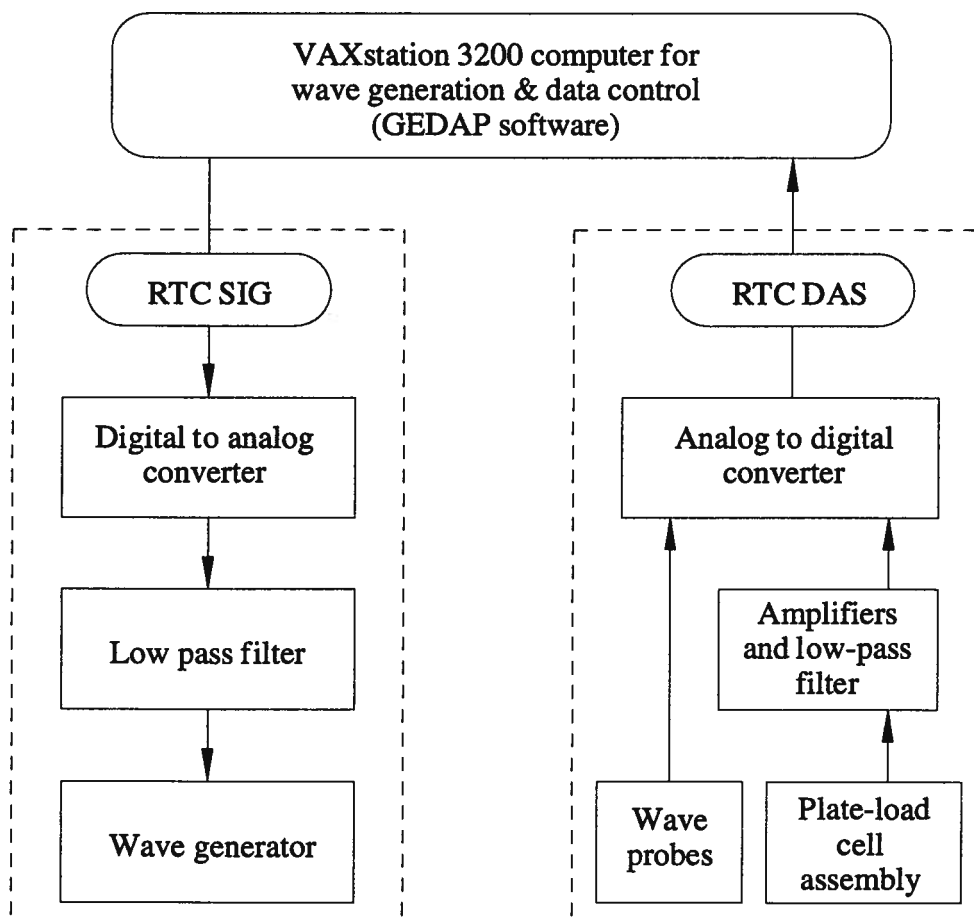


Fig. 3.4 Flow chart indicating the wave generation and the data control setup.

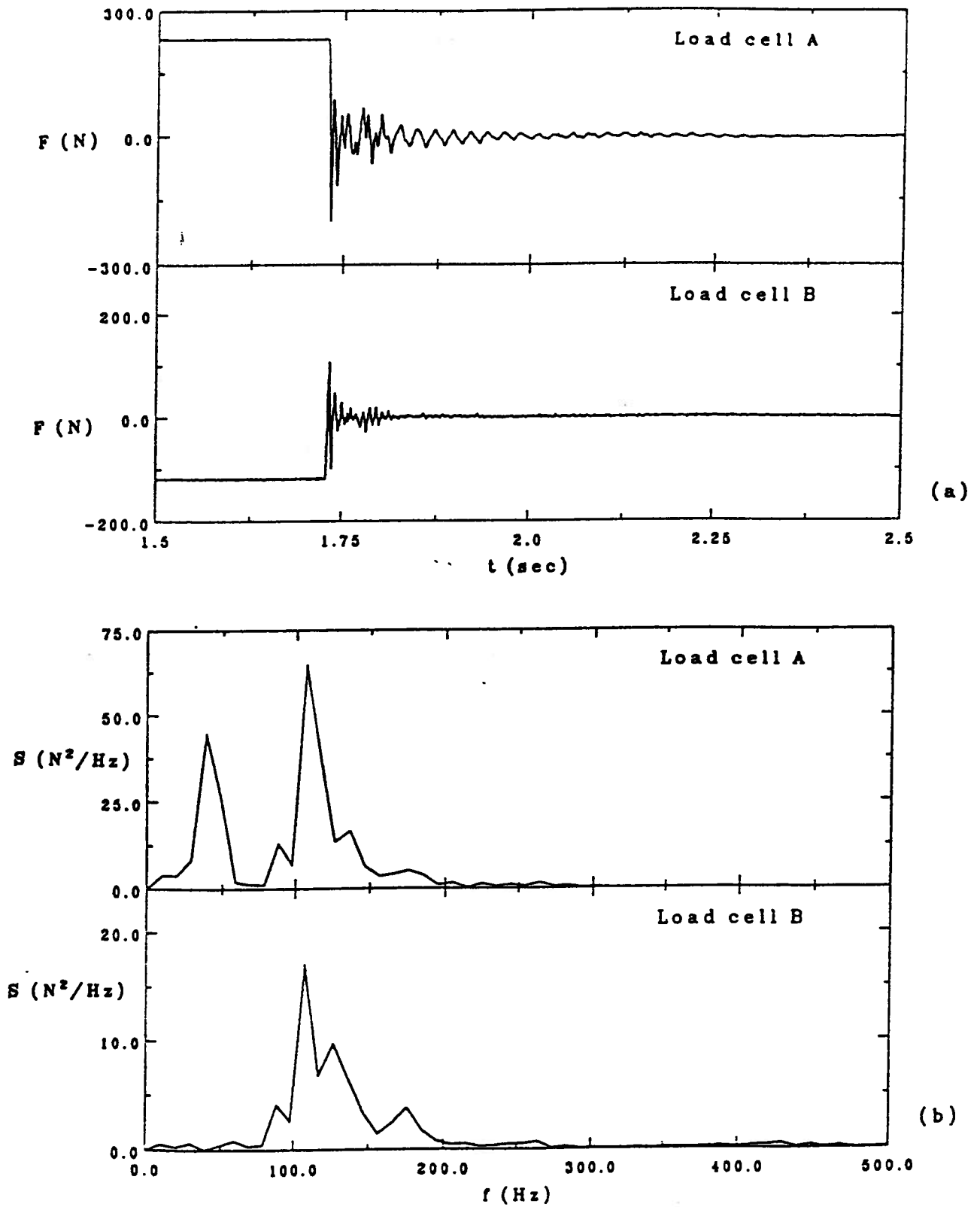


Fig. 3.5 Response of load-cells A and B to a step load of 117.7 N (12 kg) tested in air. (a) time history; (b) spectral density.

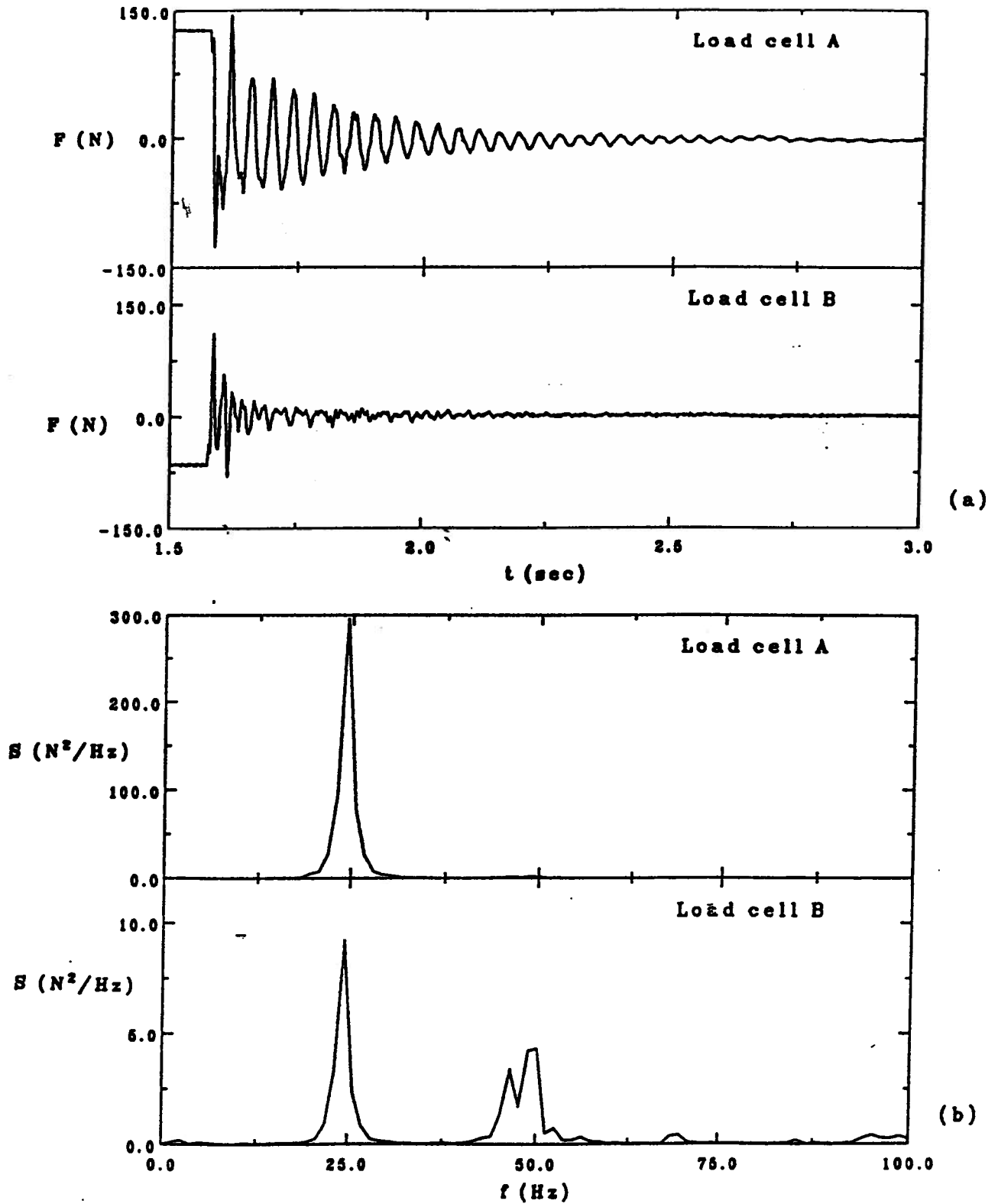


Fig. 3.6 Response of load-cells A and B to a step load of 58.9 N (6 kg) tested for a submerged condition. (a) time history; (b) spectral density.

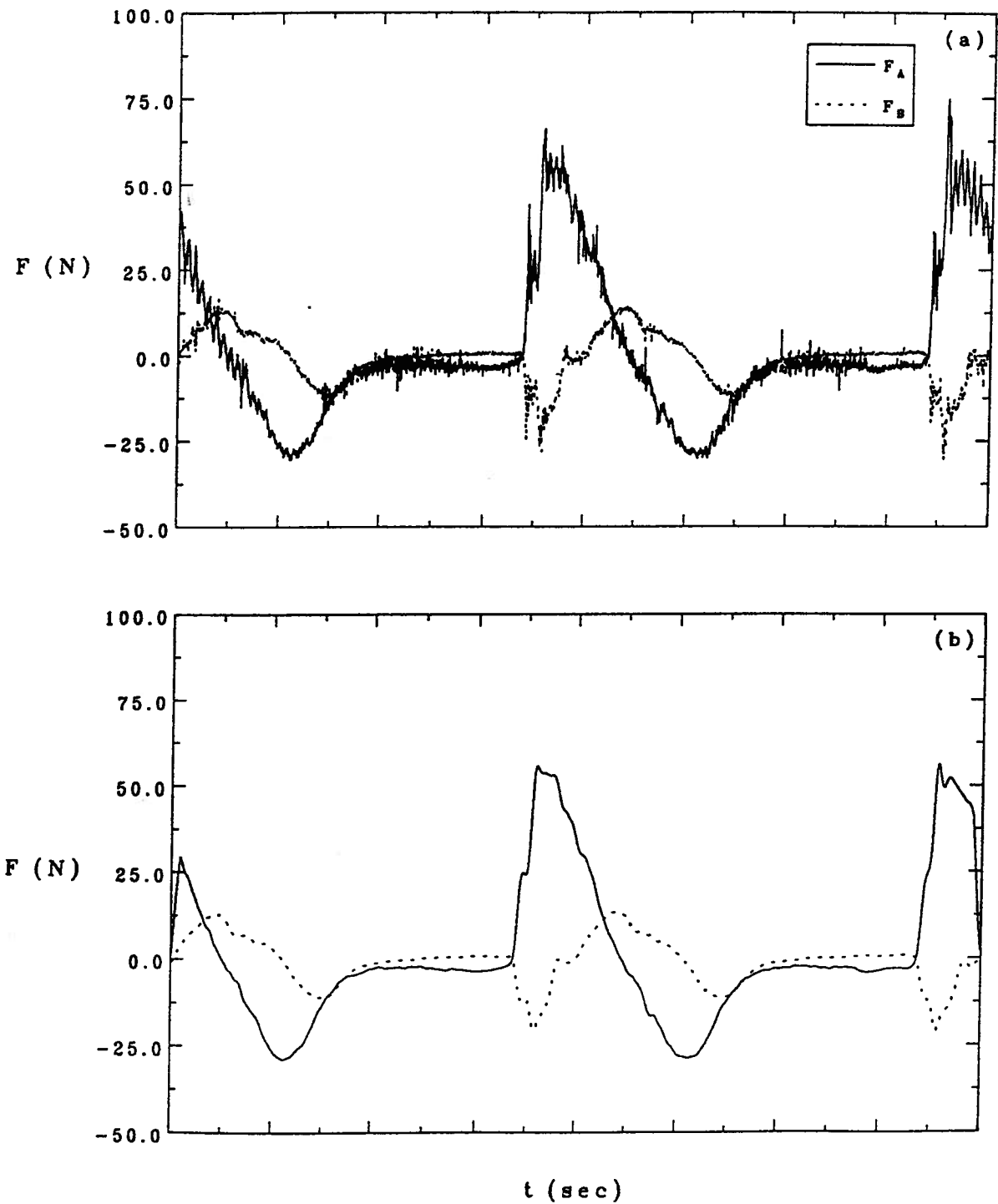


Fig. 3.7 Time histories of the measured vertical force showing the effect of filtering ($h = 1.4$ cm, $T = 2.02$ sec, $H = 17.5$ cm). (a) unfiltered force signal; (b) filtered force signal at 15 Hz cut-off.

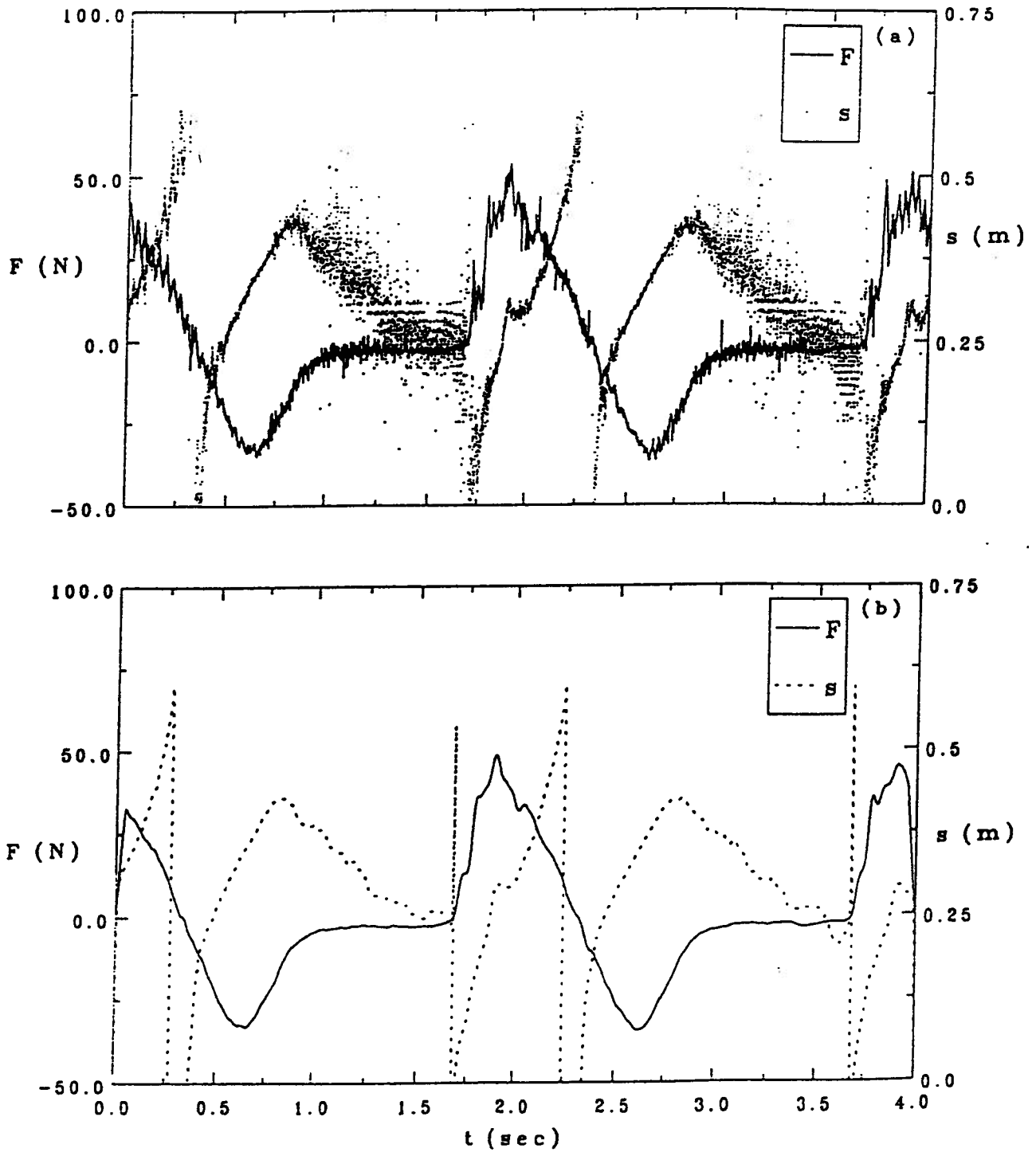


Fig. 3.8 Time histories of total vertical force and its line of action showing the effect of filtering ($h = 1.4$ cm, $T = 2.02$ sec, $H = 17.5$ cm). (a) unfiltered force (b) filtered force with 15 Hz cut-off.

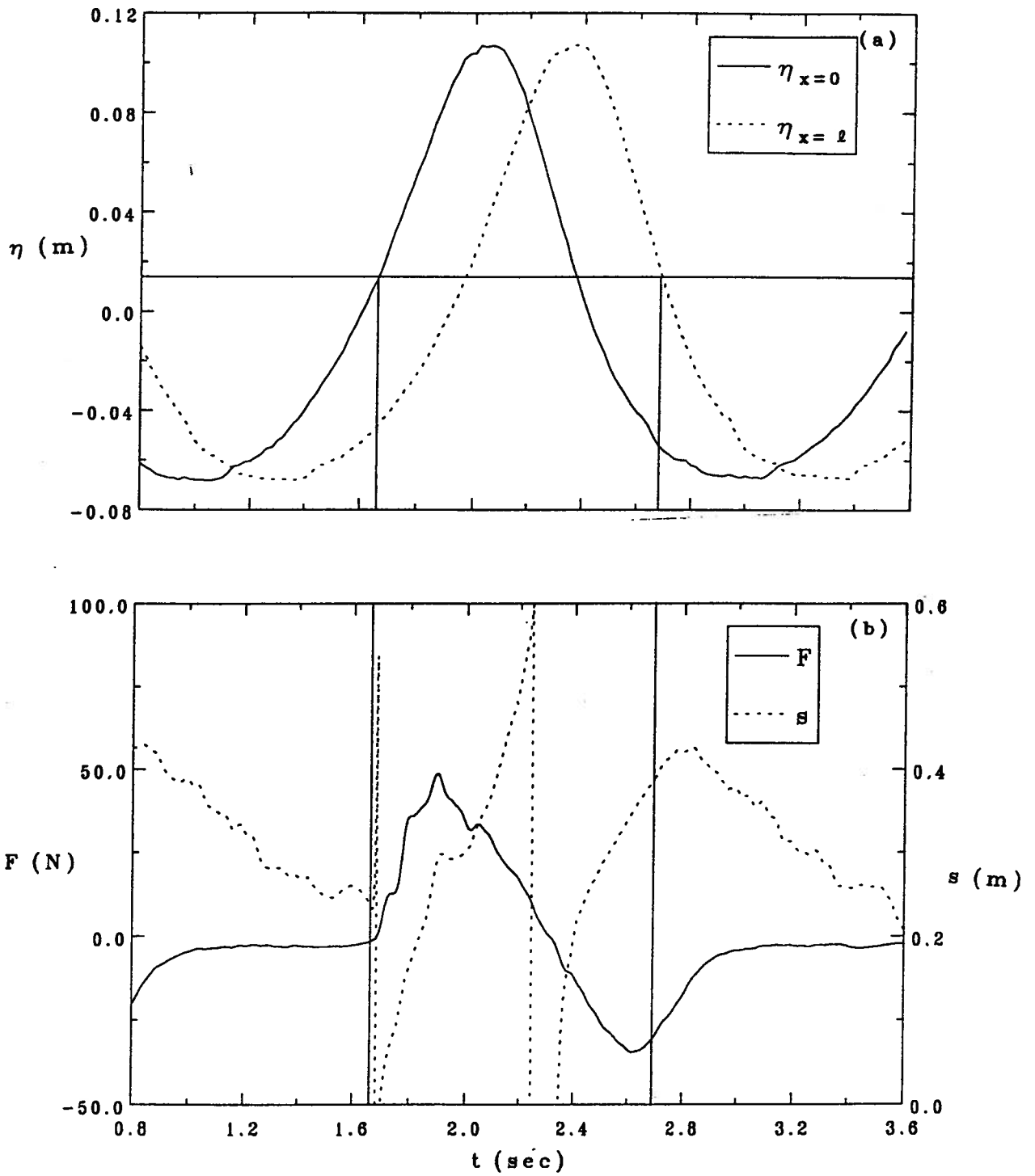


Fig. 3.9 Time histories of (a) free surface elevation; (b) vertical force and its line of action. ($h = 1.4$ cm, $T = 2.02$ sec, $H = 17.5$ cm).

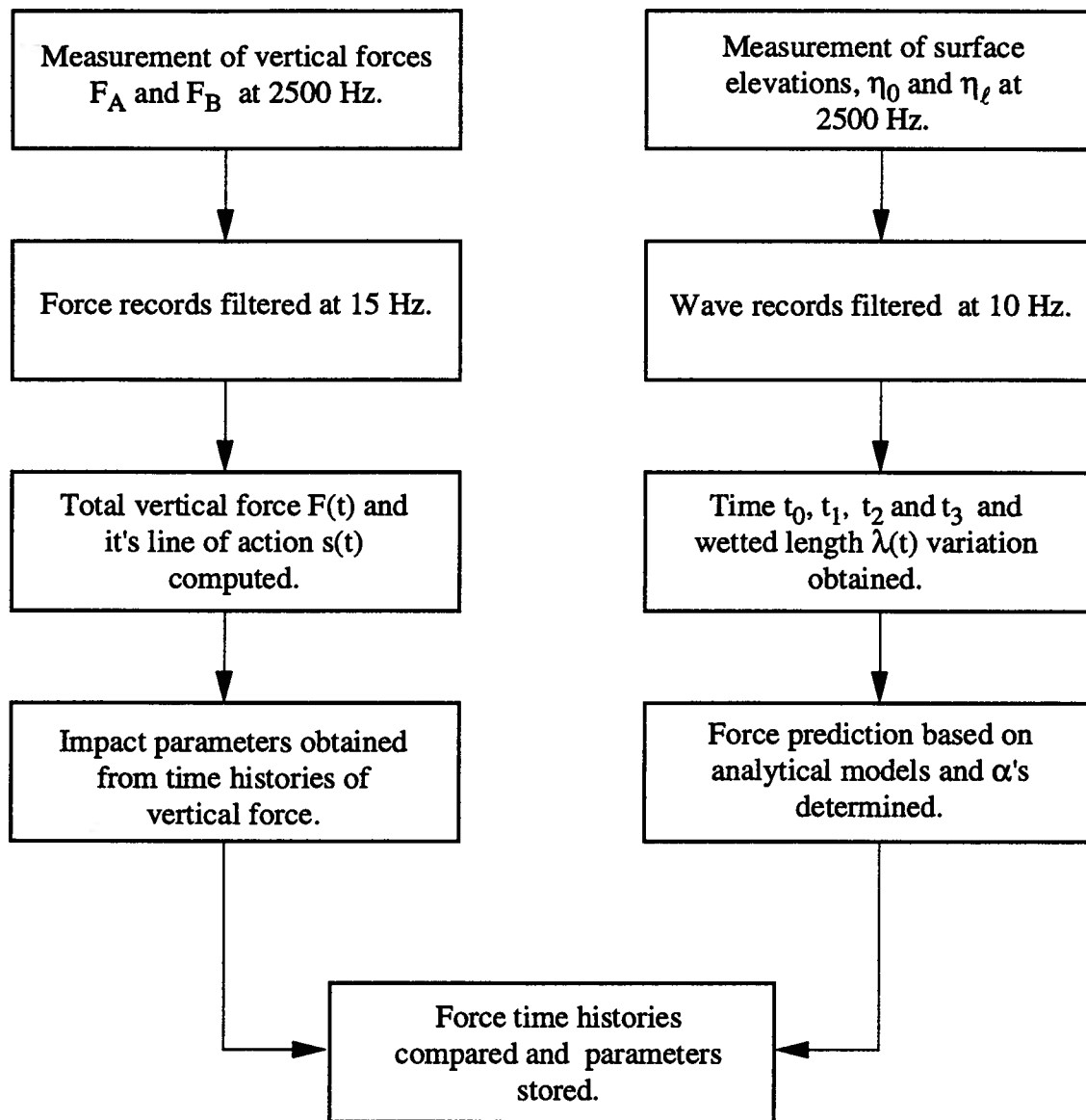


Fig. 3.10 Flow chart indicating the sequence of analysis of the measured force and wave elevation time histories.

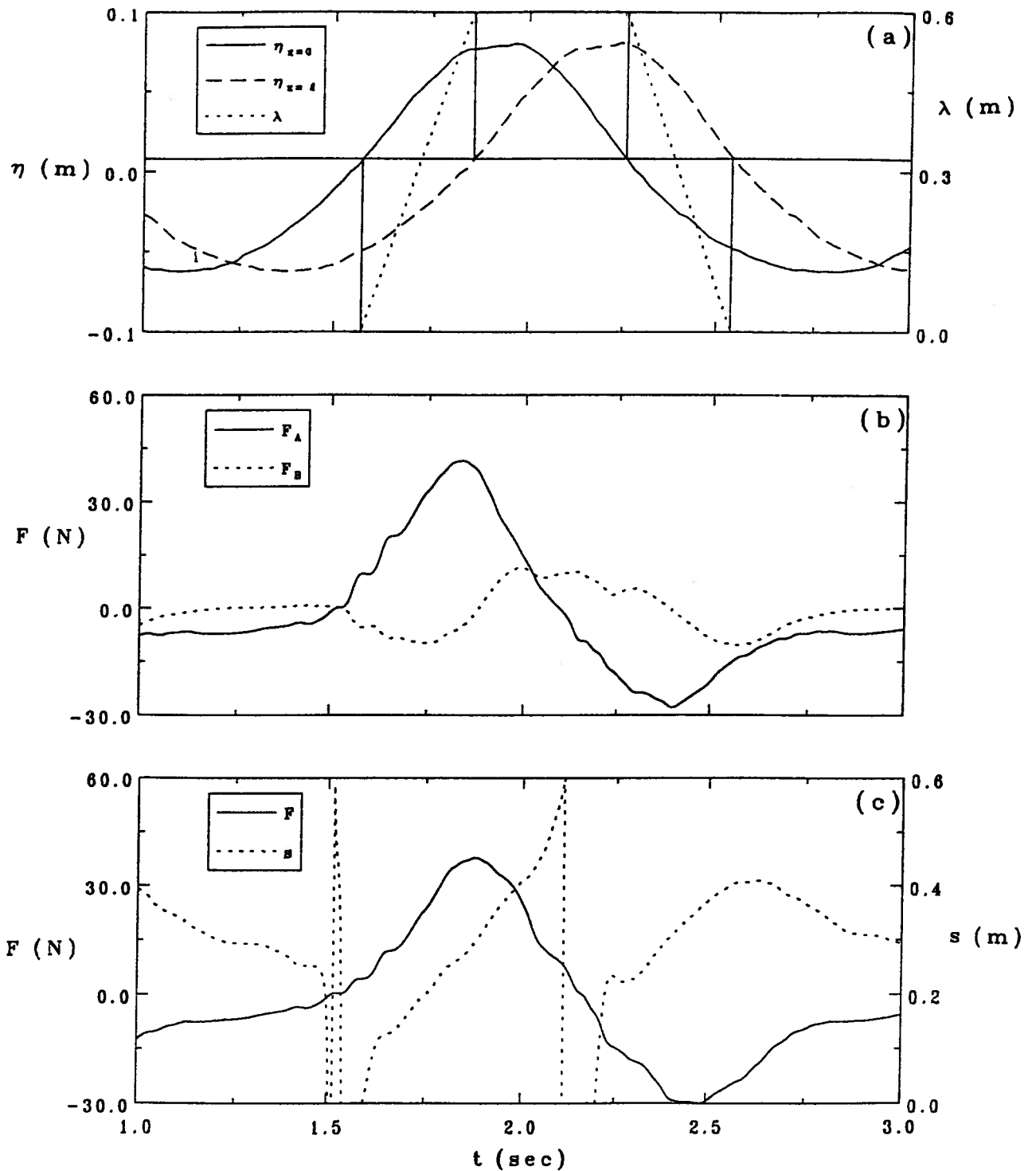


Fig. 4.1 Time histories of free surface elevation, wetted length, vertical force measured at the supports, total vertical force and the associated line of action during one wave cycle for $h = 0.8$ cm, $T = 1.68$ sec, $H = 14.2$ cm. (a) free surface elevation and wetted length; (b) vertical force; (c) total vertical force and line of action.

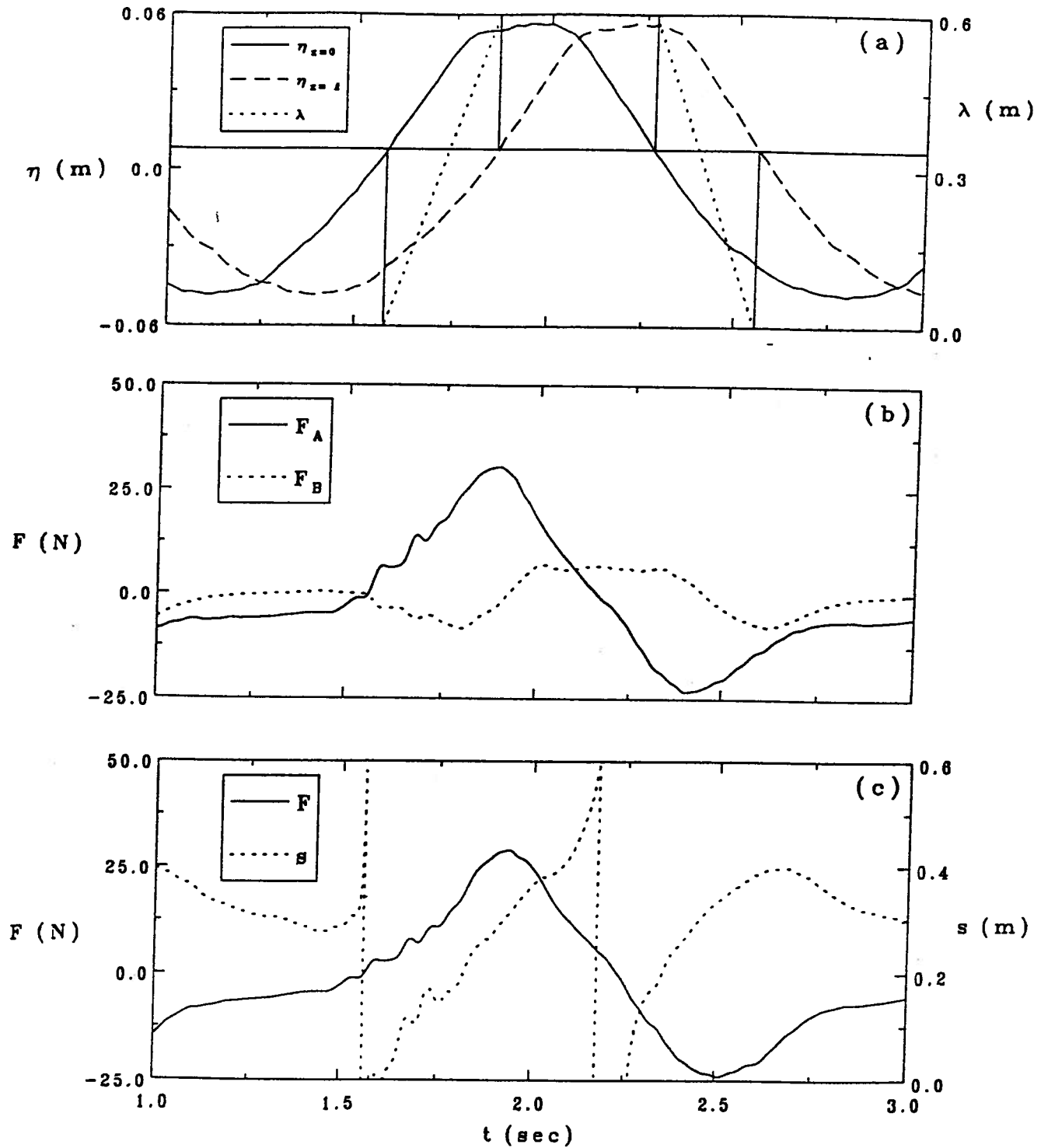


Fig. 4.2 Time histories of free surface elevation, wetted length, vertical force measured at the supports, total vertical force and the associated line of action during one wave cycle for $h = 0.8$ cm, $T = 1.70$ sec, $H = 10.5$ cm. (a) free surface elevation and wetted length; (b) vertical force; (c) total vertical force and line of action.

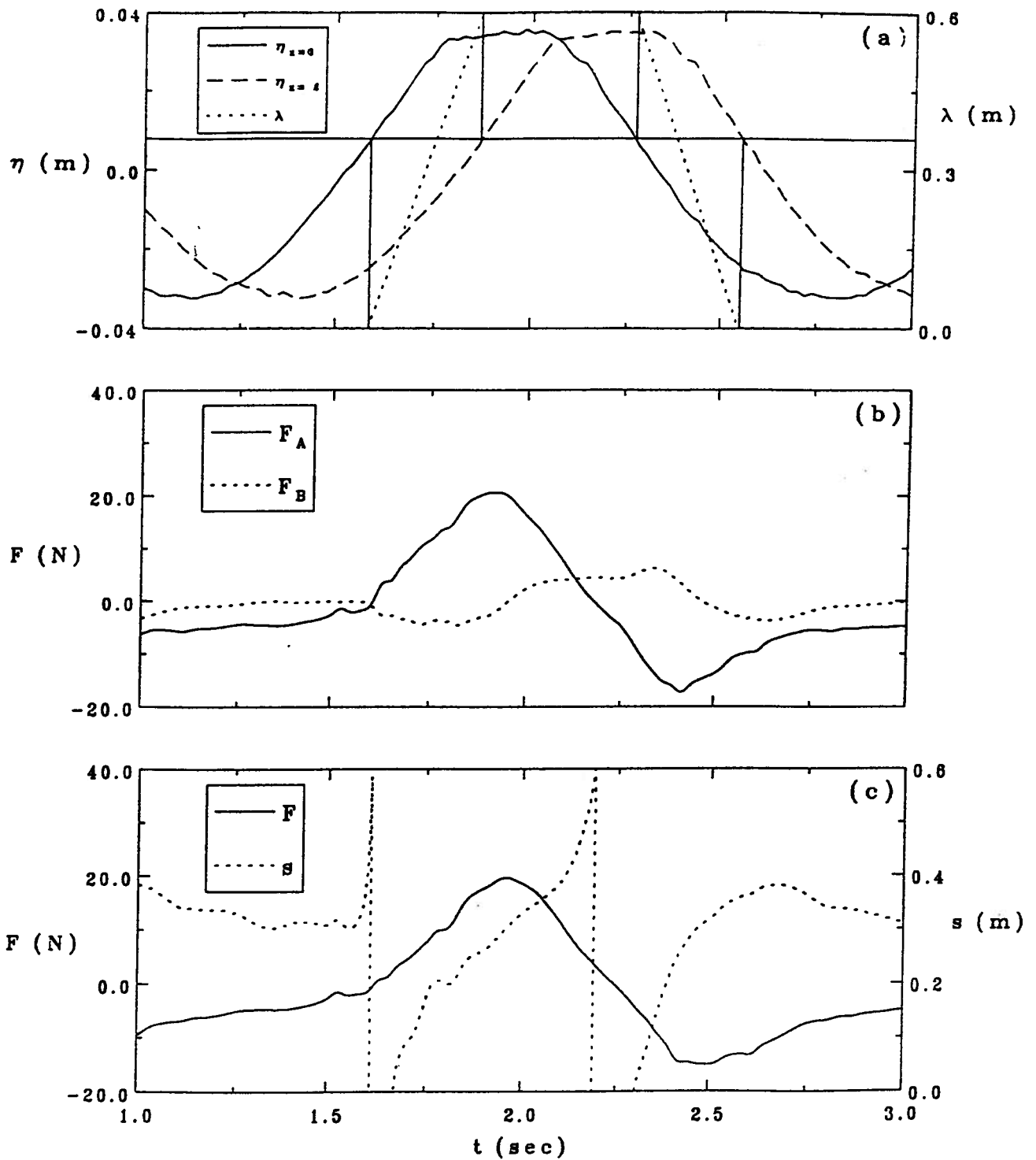


Fig. 4.3 Time histories of free surface elevation, wetted length, vertical force measured at the supports, total vertical force and the associated line of action during one wave cycle for $h = 0.8$ cm, $T = 1.70$ sec, $H = 6.80$ cm. (a) free surface elevation and wetted length; (b) vertical force; (c) total vertical force and line of action.

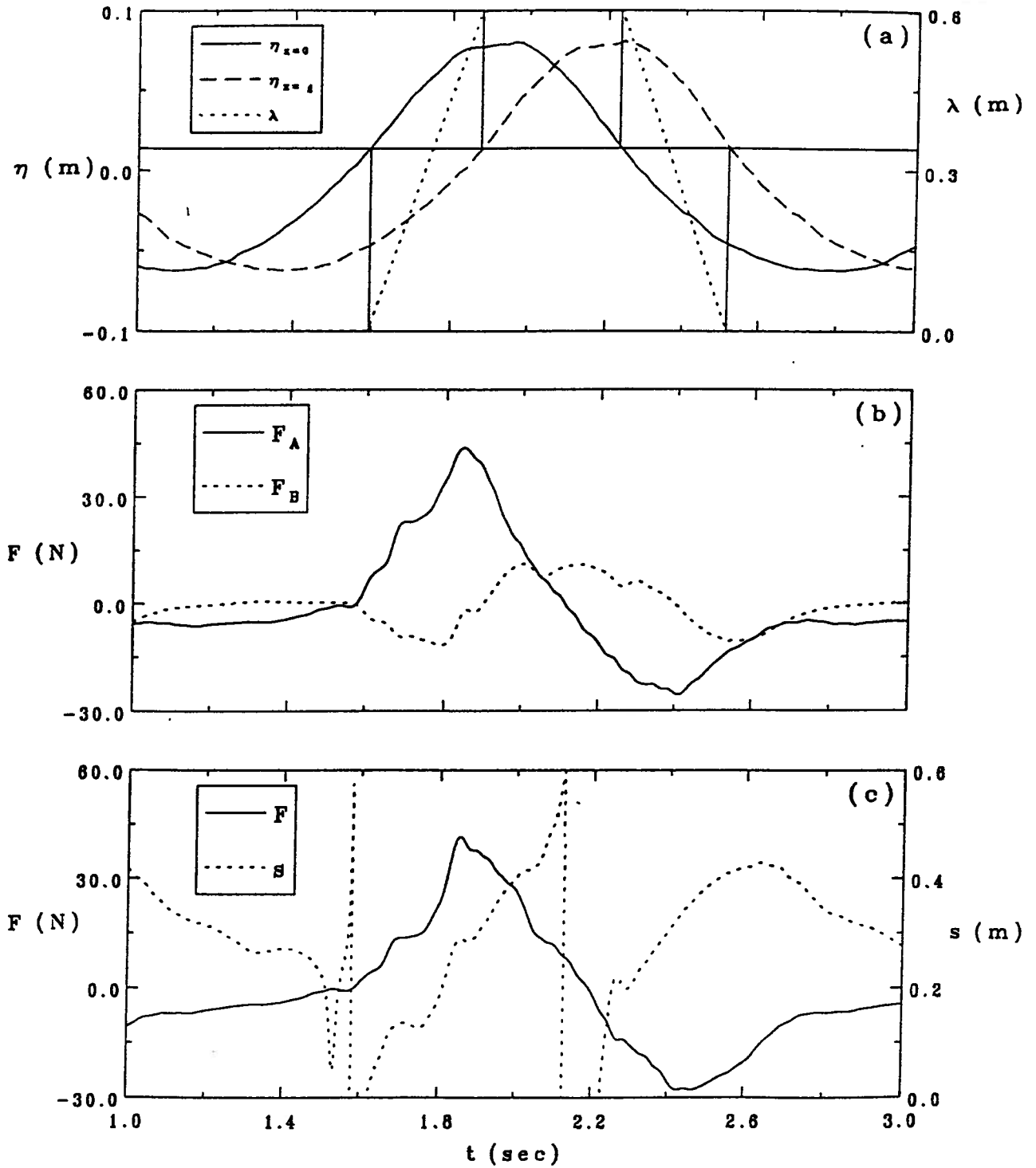


Fig. 4.4 Time histories of free surface elevation, wetted length, vertical force measured at the supports, total vertical force and the associated line of action during one wave cycle for $h = 1.4$ cm, $T = 1.68$ sec, $H = 14.2$ cm. (a) free surface elevation and wetted length; (b) vertical force; (c) total vertical force and line of action.

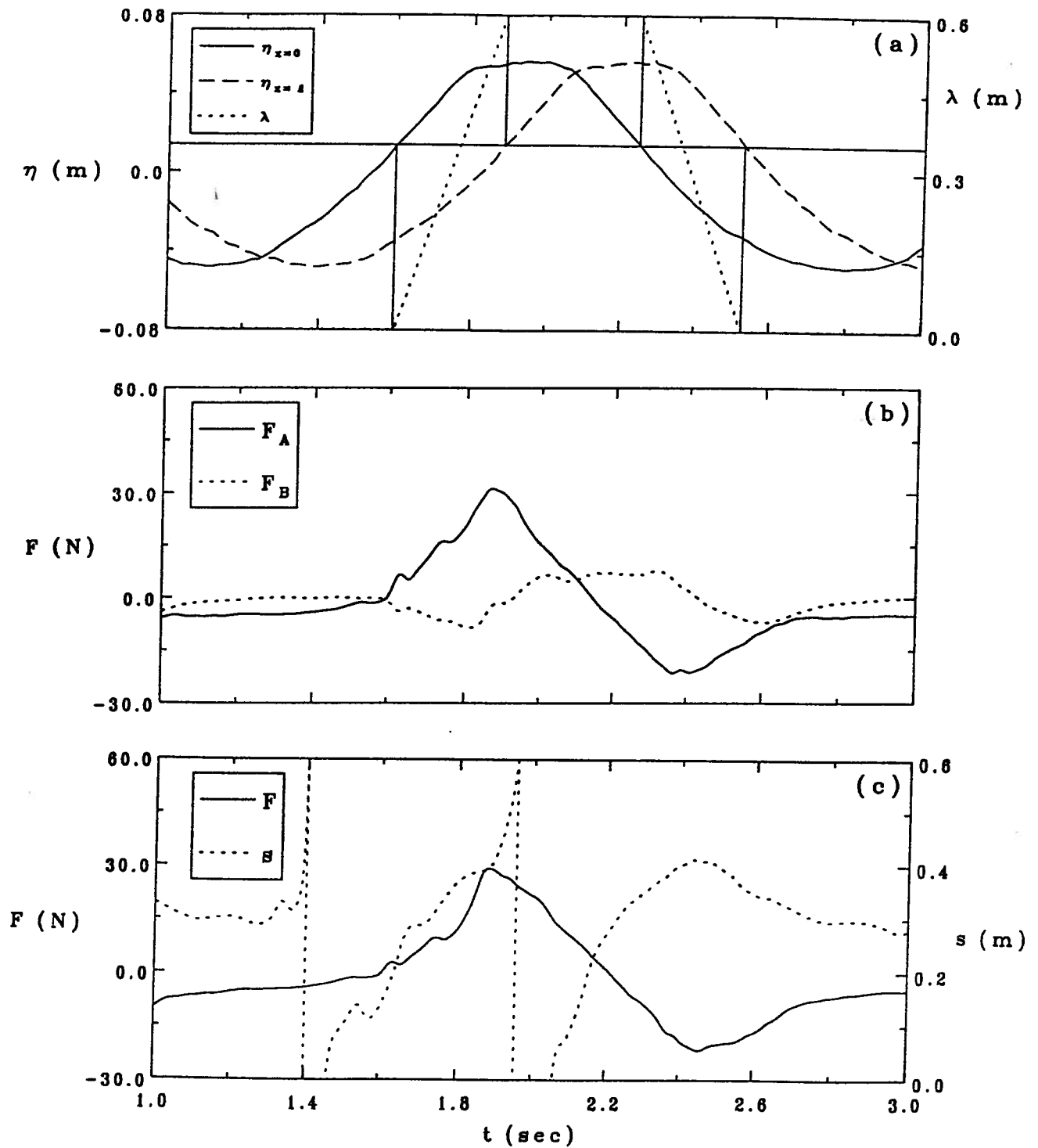


Fig. 4.5 Time histories of free surface elevation, wetted length, vertical force measured at the supports, total vertical force and the associated line of action during one wave cycle for $h = 1.4$ cm, $T = 1.68$ sec, $H = 10.5$ cm. (a) free surface elevation and wetted length; (b) vertical force; (c) total vertical force and line of action.

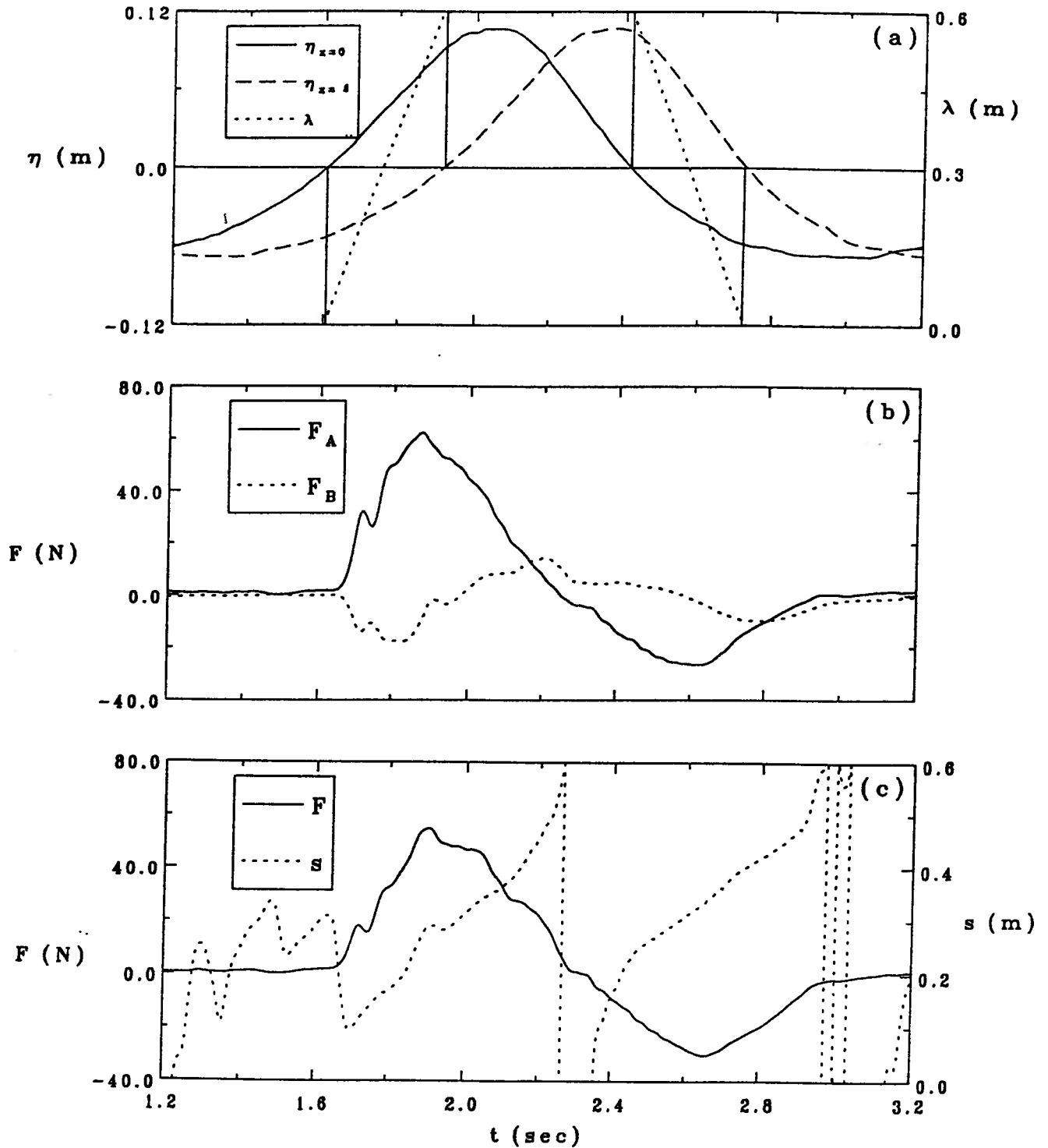


Fig. 4.6 Time histories of free surface elevation, wetted length, vertical force measured at the supports, total vertical force and the associated line of action during one wave cycle for $h = 0$ cm, $T = 2.02$ sec, $H = 17.5$ cm. (a) free surface elevation and wetted length; (b) vertical force; (c) total vertical force and line of action.

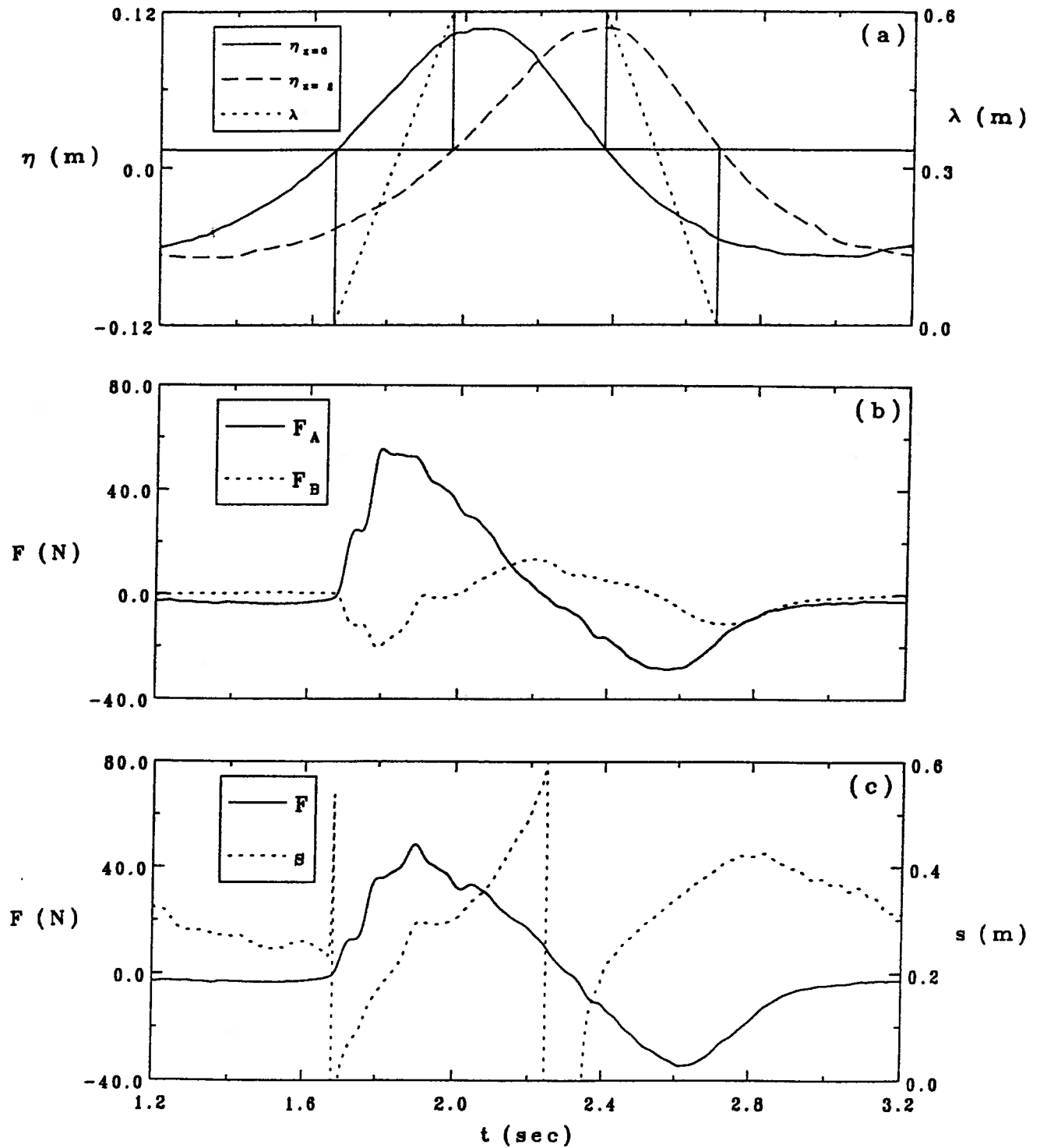


Fig. 4.7 Time histories of free surface elevation, wetted length, vertical force measured at the supports, total vertical force and the associated line of action during one wave cycle for $h = 1.4$ cm, $T = 2.02$ sec, $H = 17.5$ cm. (a) free surface elevation and wetted length; (b) vertical force; (c) total vertical force and line of action.

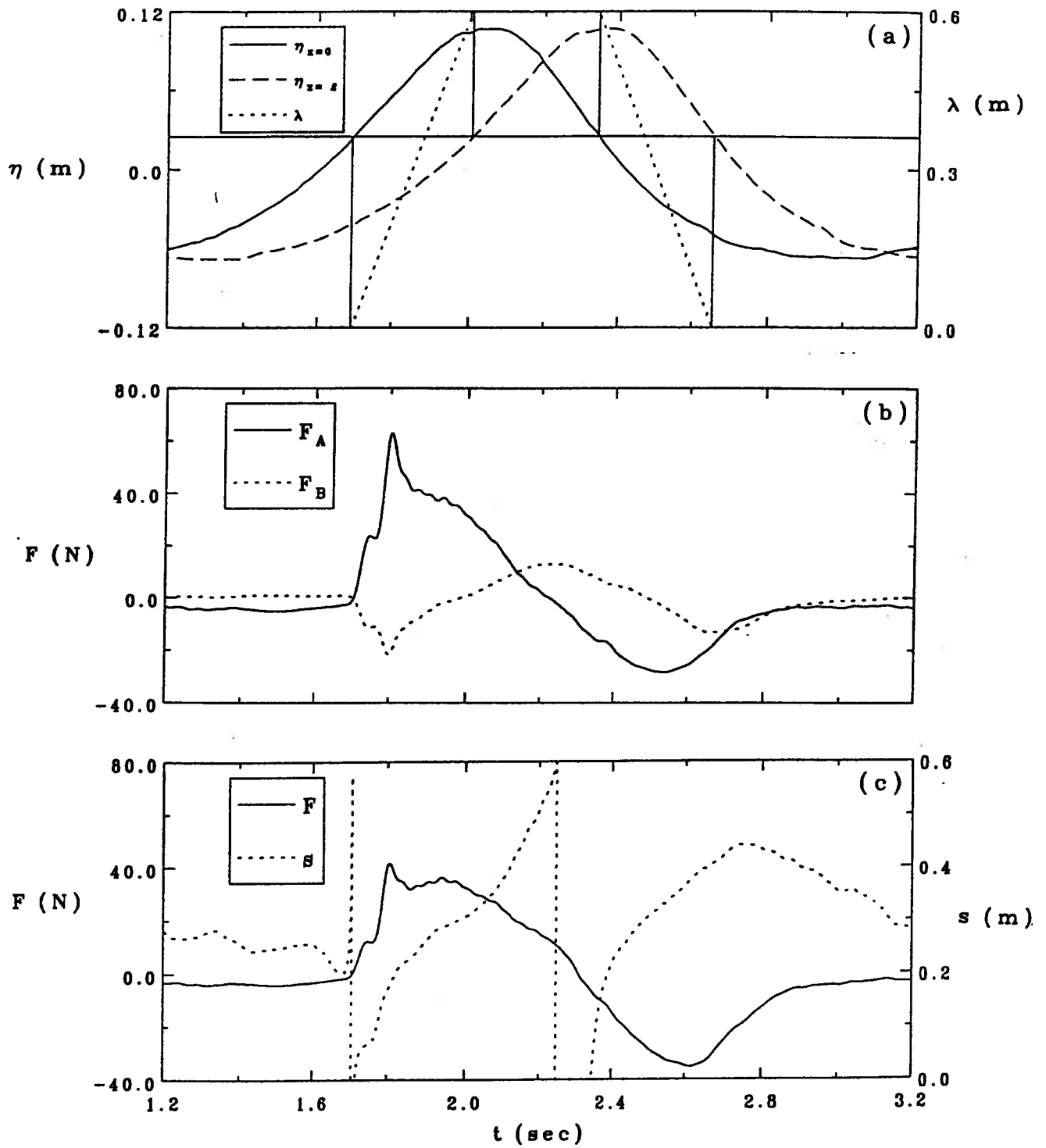


Fig. 4.8 Time histories of free surface elevation, wetted length, vertical force measured at the supports, total vertical force and the associated line of action during one wave cycle for $h = 2.5$ cm, $T = 2.02$ sec, $H = 17.5$ cm. (a) free surface elevation and wetted length; (b) vertical force; (c) total vertical force and line of action.

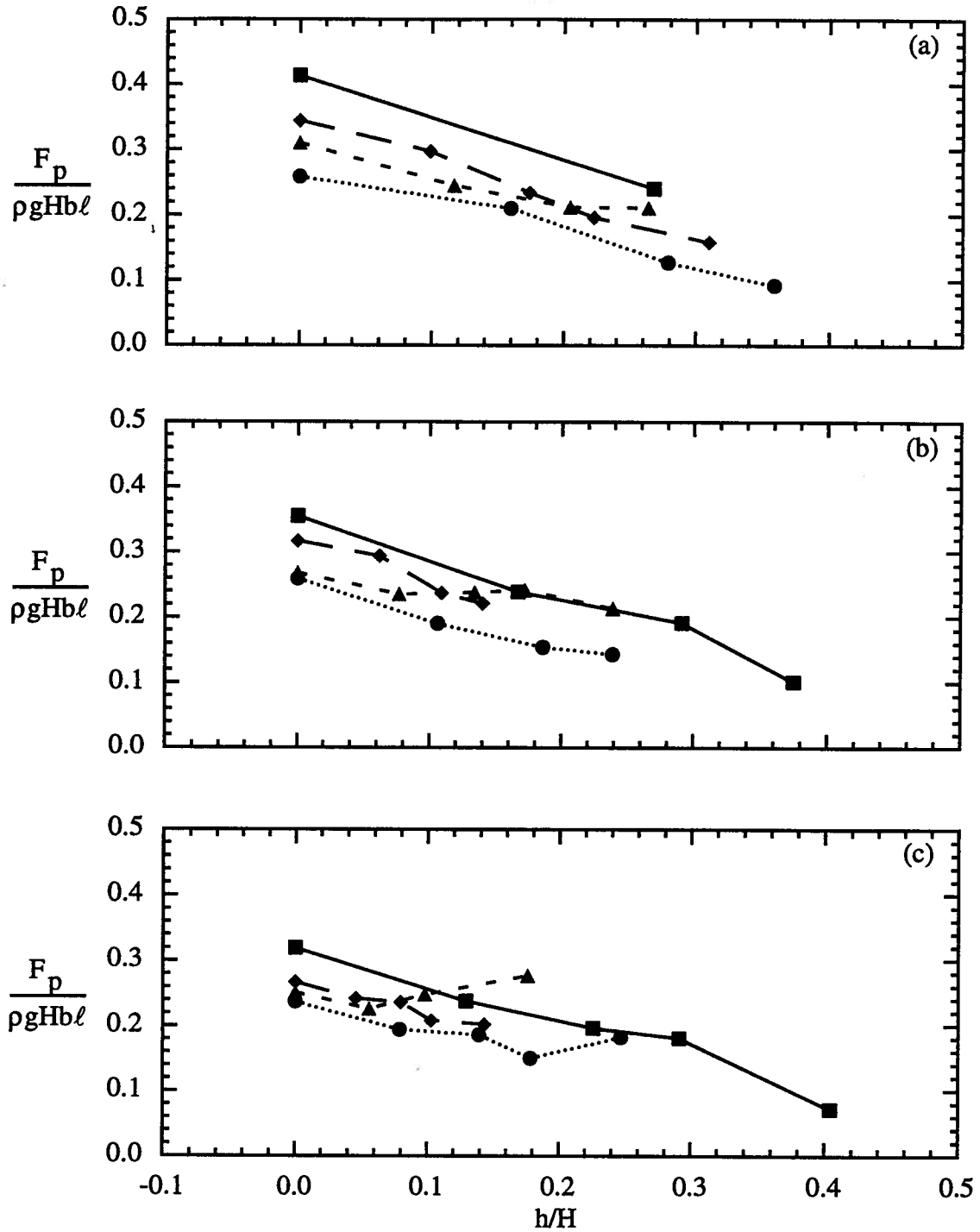


Fig. 4.9 Maximum upward force coefficient $F_p/\rho g b H l$ as a function of relative plate clearance h/H and relative plate length l/L . (a) $0.016 < H/L < 0.020$; (b) $0.026 < H/L < 0.030$; (c) $0.035 < H/L < 0.041$.

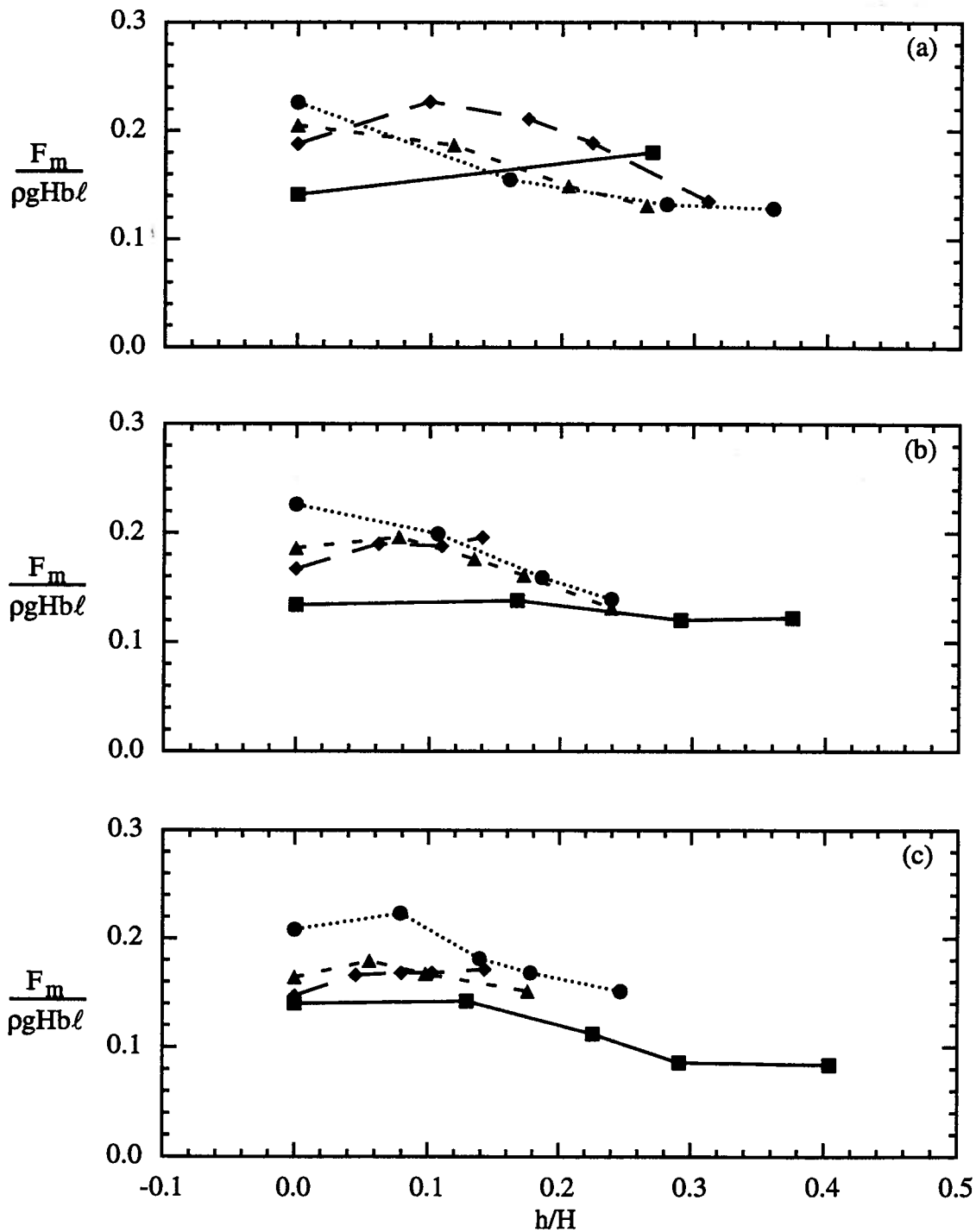


Fig. 4.10 Maximum downward force coefficient $F_m/\rho g b H l$ as a function of relative plate clearance h/H and relative plate length l/L . (a) $0.016 < H/L < 0.020$; (b) $0.026 < H/L < 0.030$; (c) $0.035 < H/L < 0.041$.

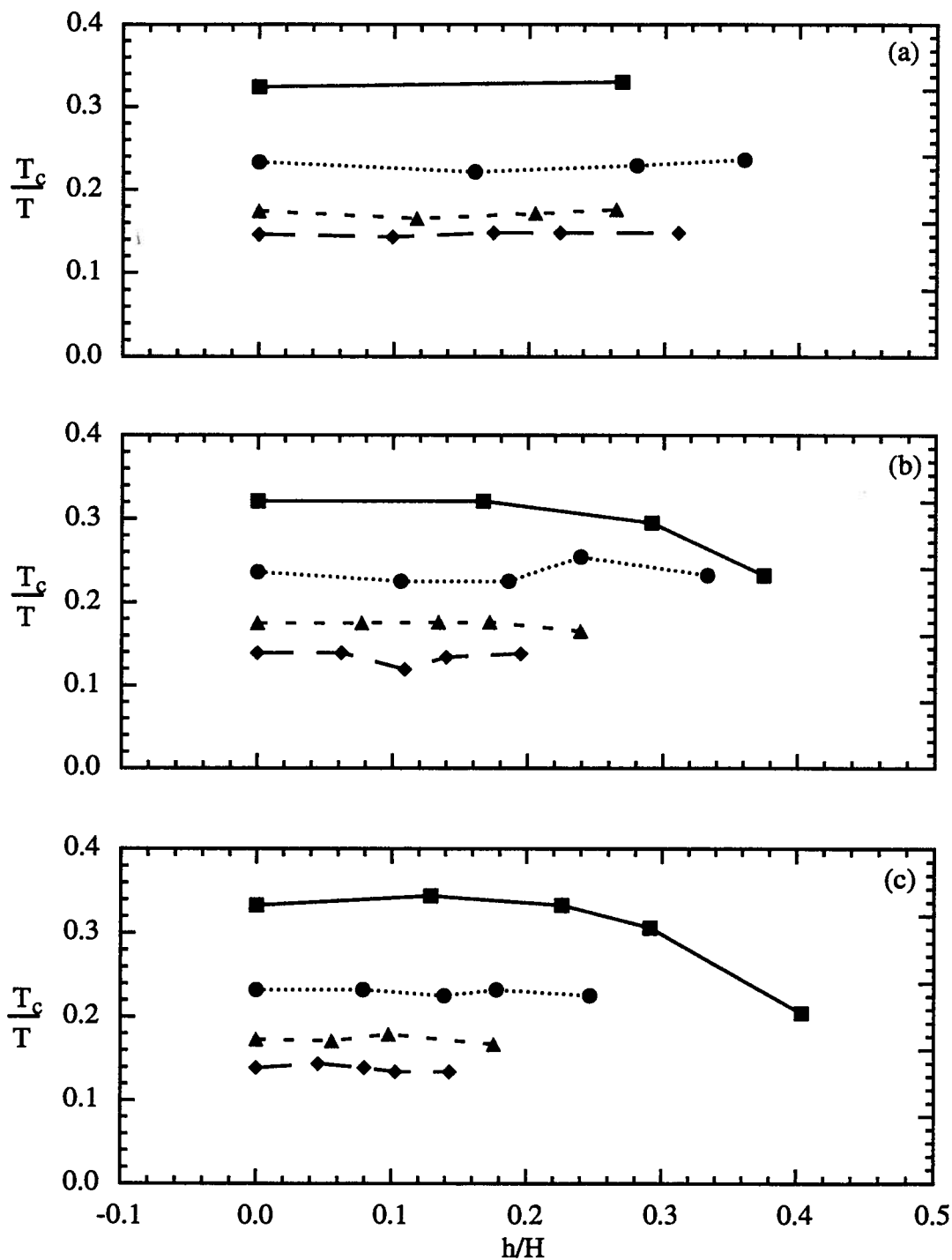


Fig. 4.11 Non-dimensionalised duration of plate's partial submergence T_c/T as a function of relative plate clearance h/H and relative plate length ℓ/L . (a) $0.016 < H/L < 0.020$; (b) $0.026 < H/L < 0.030$; (c) $0.035 < H/L < 0.041$.

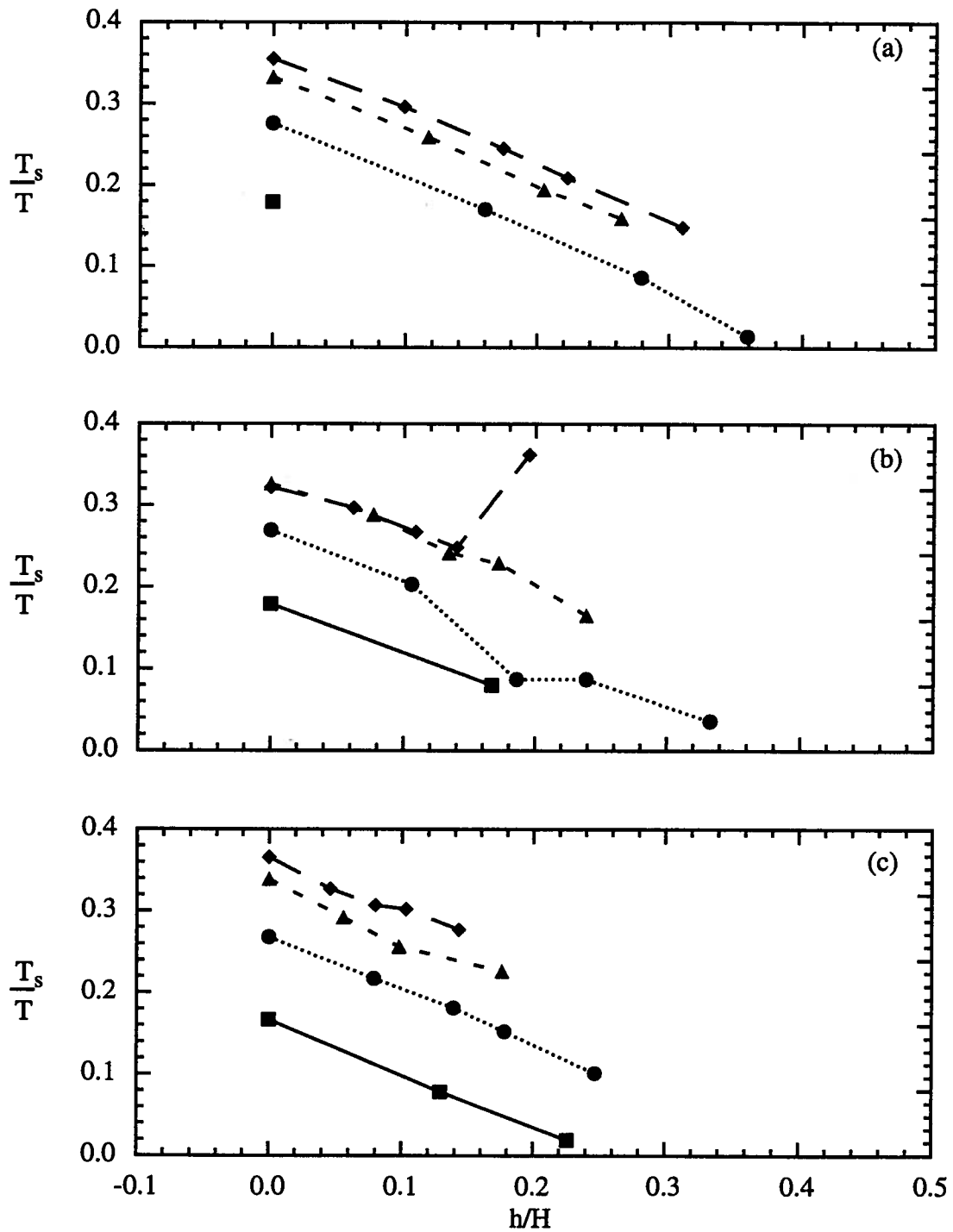


Fig. 4.12 Non-dimensionalised duration of plate's complete submergence T_s/T as a function of relative plate clearance h/H and relative plate length ℓ/L . (a) $0.016 < H/L < 0.020$; (b) $0.026 < H/L < 0.030$; (c) $0.035 < H/L < 0.041$.

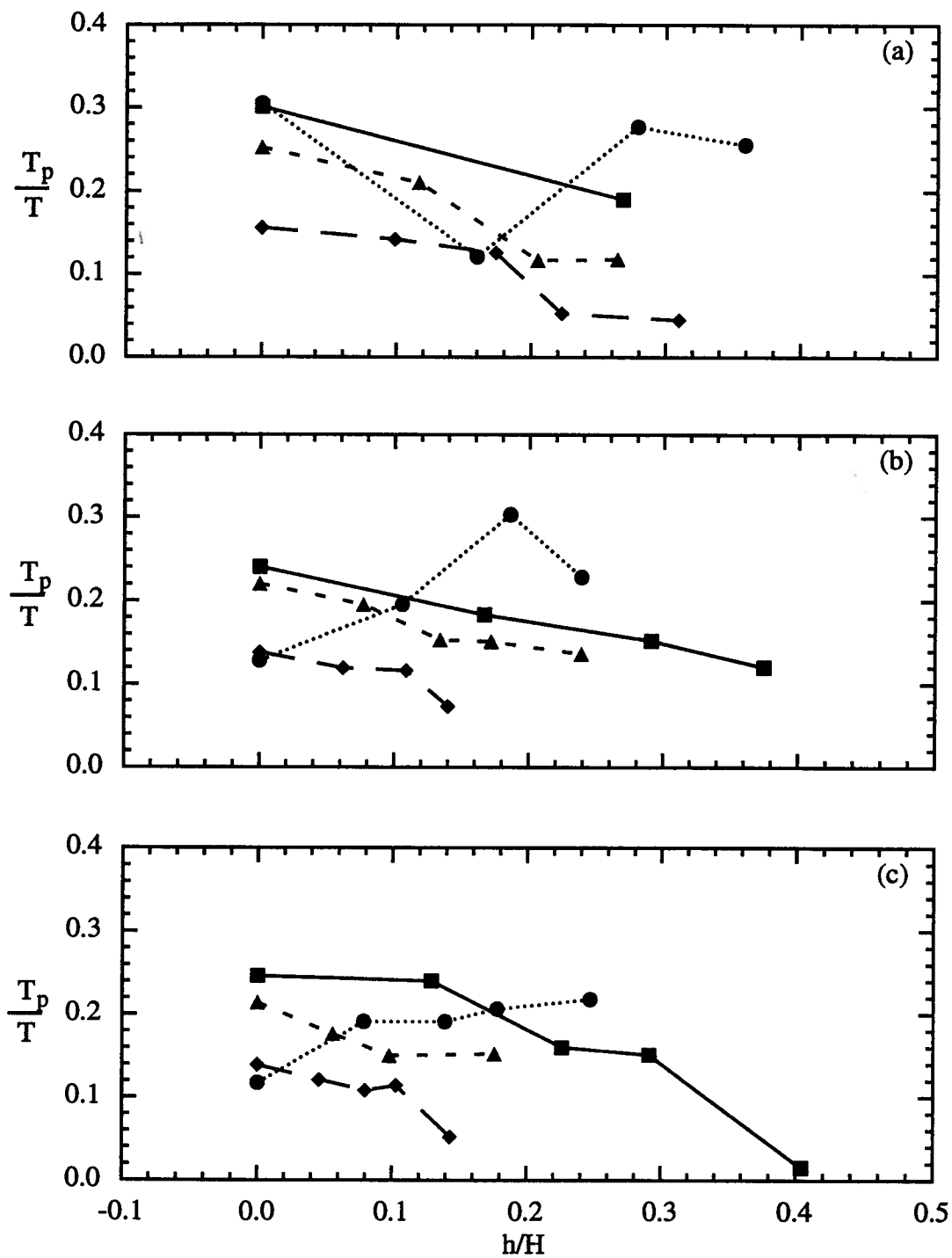


Fig. 4.13 Non-dimensionalised rise-time T_p/T of peak vertical force as a function of relative plate clearance h/H and relative plate length l/L . (a) $0.016 < H/L < 0.020$; (b) $0.026 < H/L < 0.030$; (c) $0.035 < H/L < 0.041$.

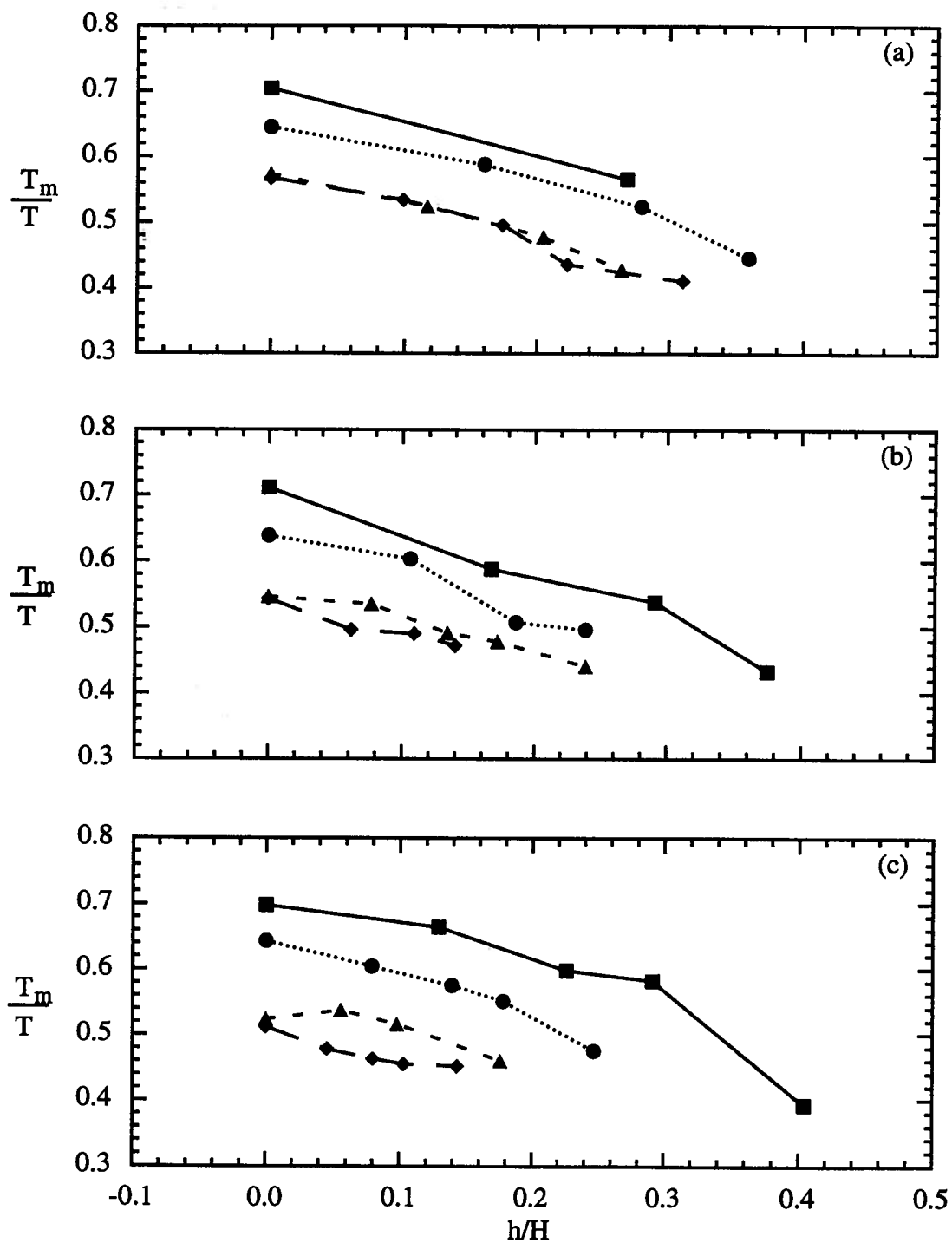


Fig. 4.14 Non-dimensionalised time of occurrence T_m/T of maximum downward force as a function of relative plate clearance h/H and relative plate length ℓ/L . (a) $0.016 < H/L < 0.020$; (b) $0.026 < H/L < 0.030$; (c) $0.035 < H/L < 0.041$.

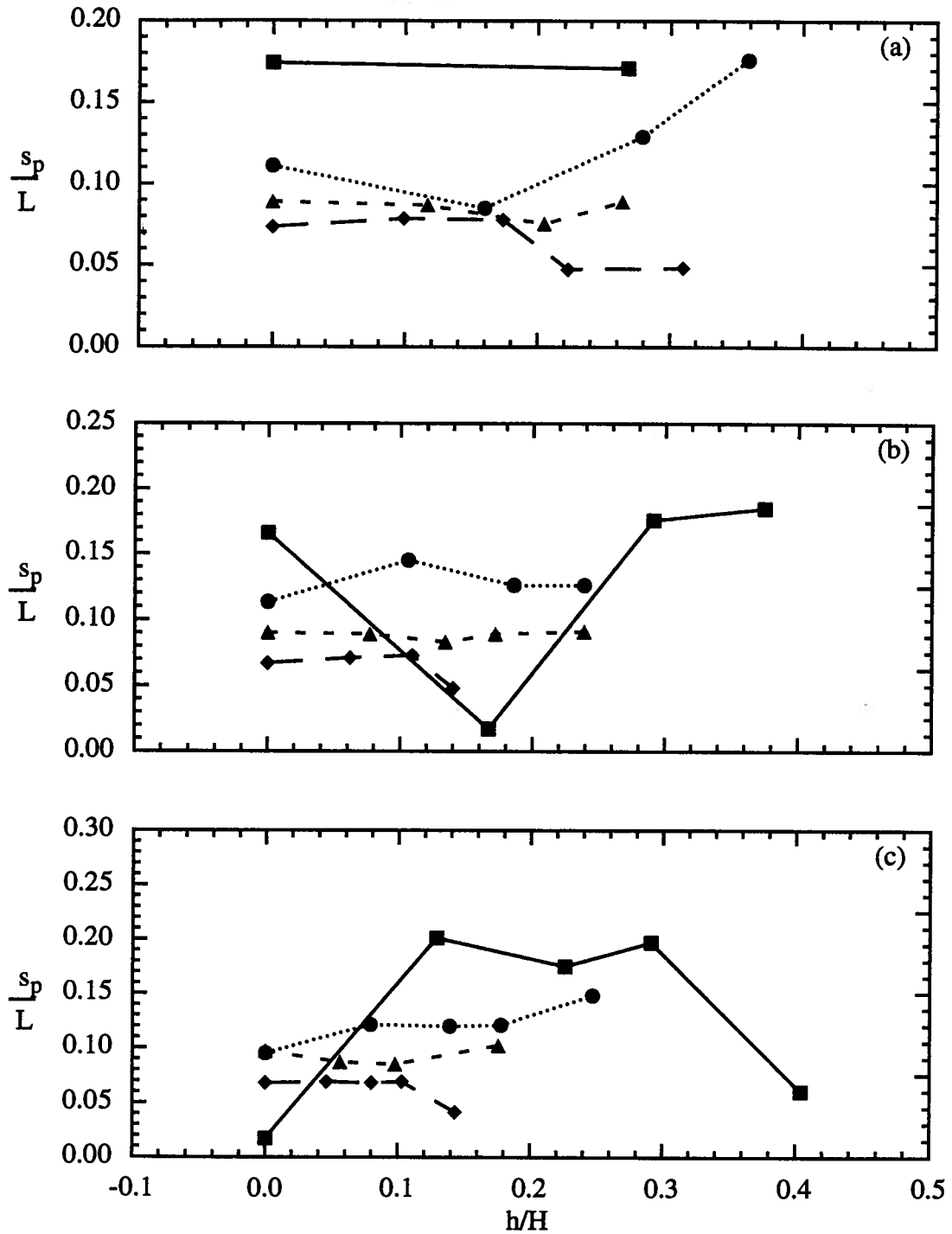


Fig. 4.15 Non-dimensionalised line of action s_p/L of maximum upward force as a function of relative plate clearance h/H and relative plate length l/L . (a) $0.016 < H/L < 0.020$; (b) $0.026 < H/L < 0.030$; (c) $0.035 < H/L < 0.041$.

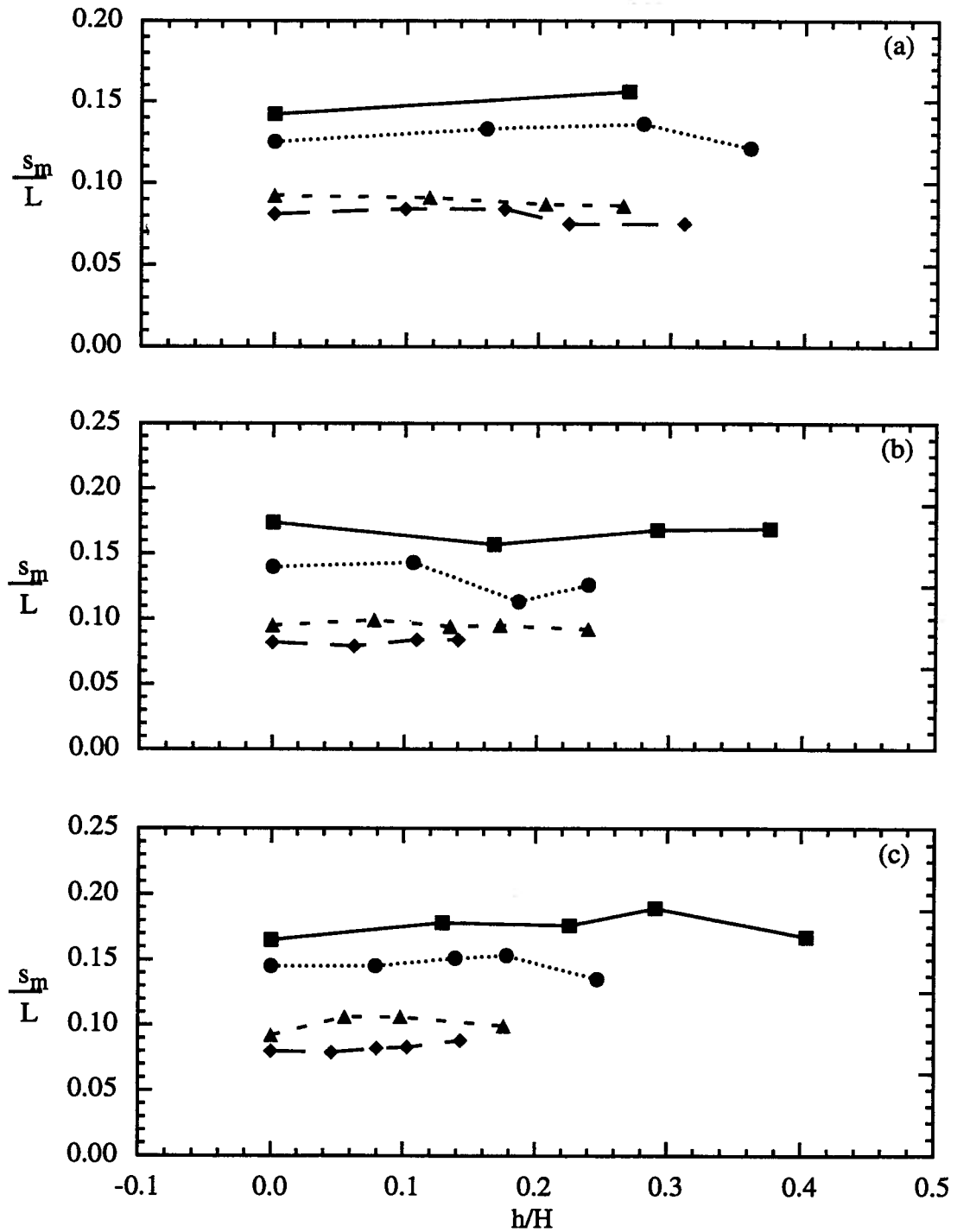


Fig. 4.16 Non-dimensionalised line of action s_m/L of maximum downward force as a function of relative plate clearance h/H and relative plate length ℓ/L . (a) $0.016 < H/L < 0.020$; (b) $0.026 < H/L < 0.030$; (c) $0.035 < H/L < 0.041$.

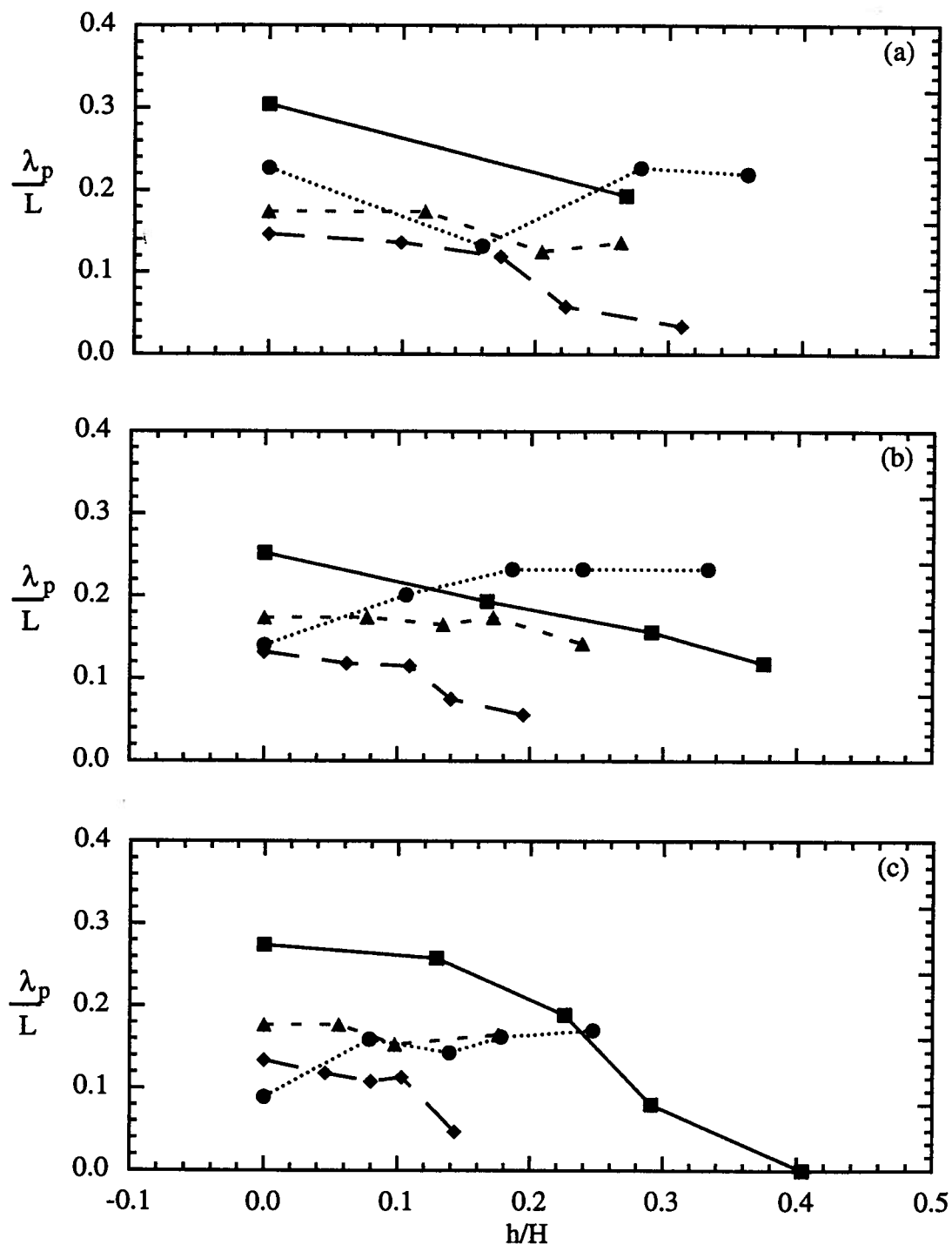


Fig. 4.17 Non-dimensionalised wetted length λ_p/L corresponding to maximum upward force as a function of relative plate clearance h/H and relative plate length l/L . (a) $0.016 < H/L < 0.020$; (b) $0.026 < H/L < 0.030$; (c) $0.035 < H/L < 0.041$.

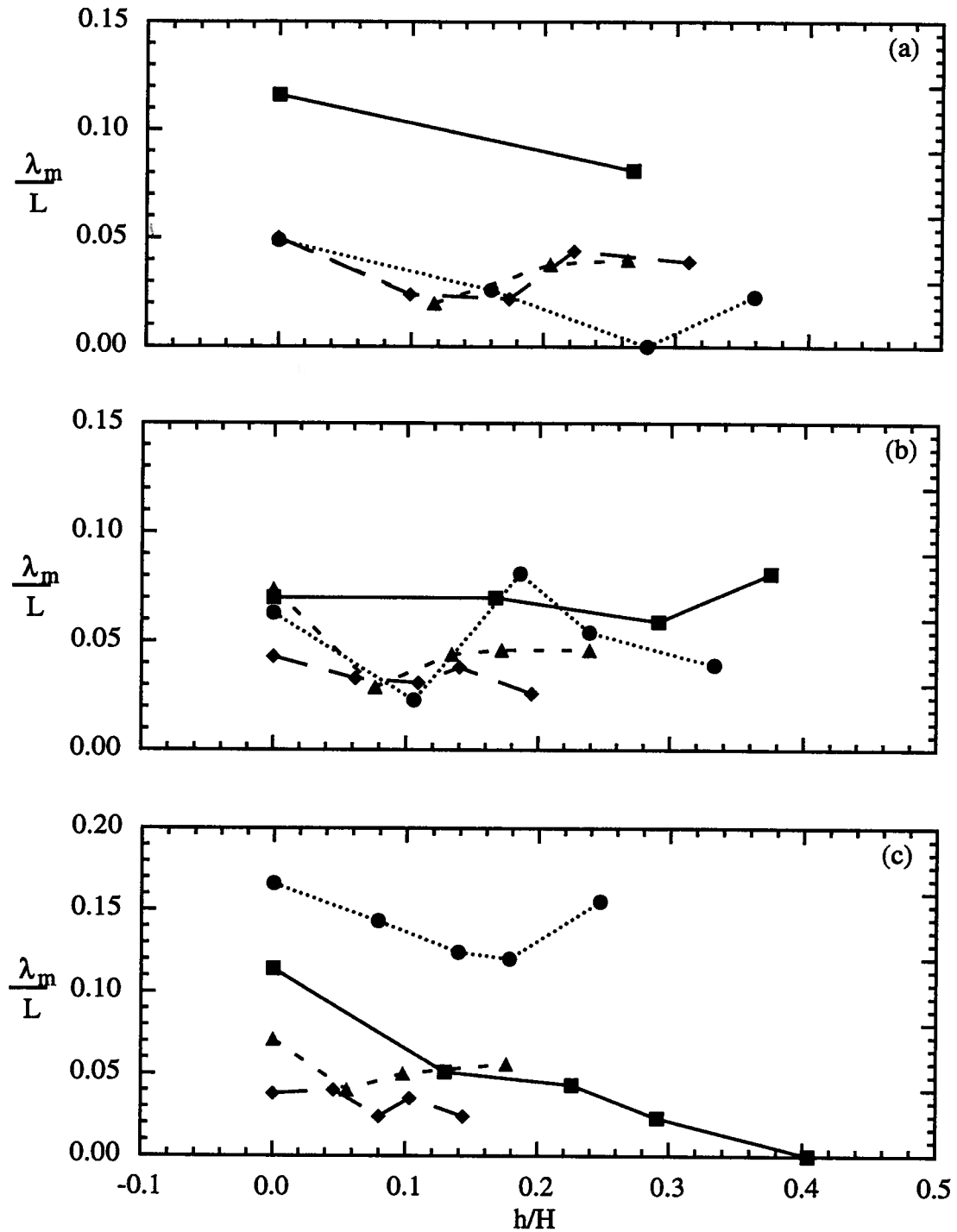


Fig. 4.18 Non-dimensionalised wetted length λ_m/L corresponding to maximum downward force as a function of relative plate clearance h/H and relative plate length ℓ/L . (a) $0.016 < H/L < 0.020$; (b) $0.026 < H/L < 0.030$; (c) $0.035 < H/L < 0.041$.

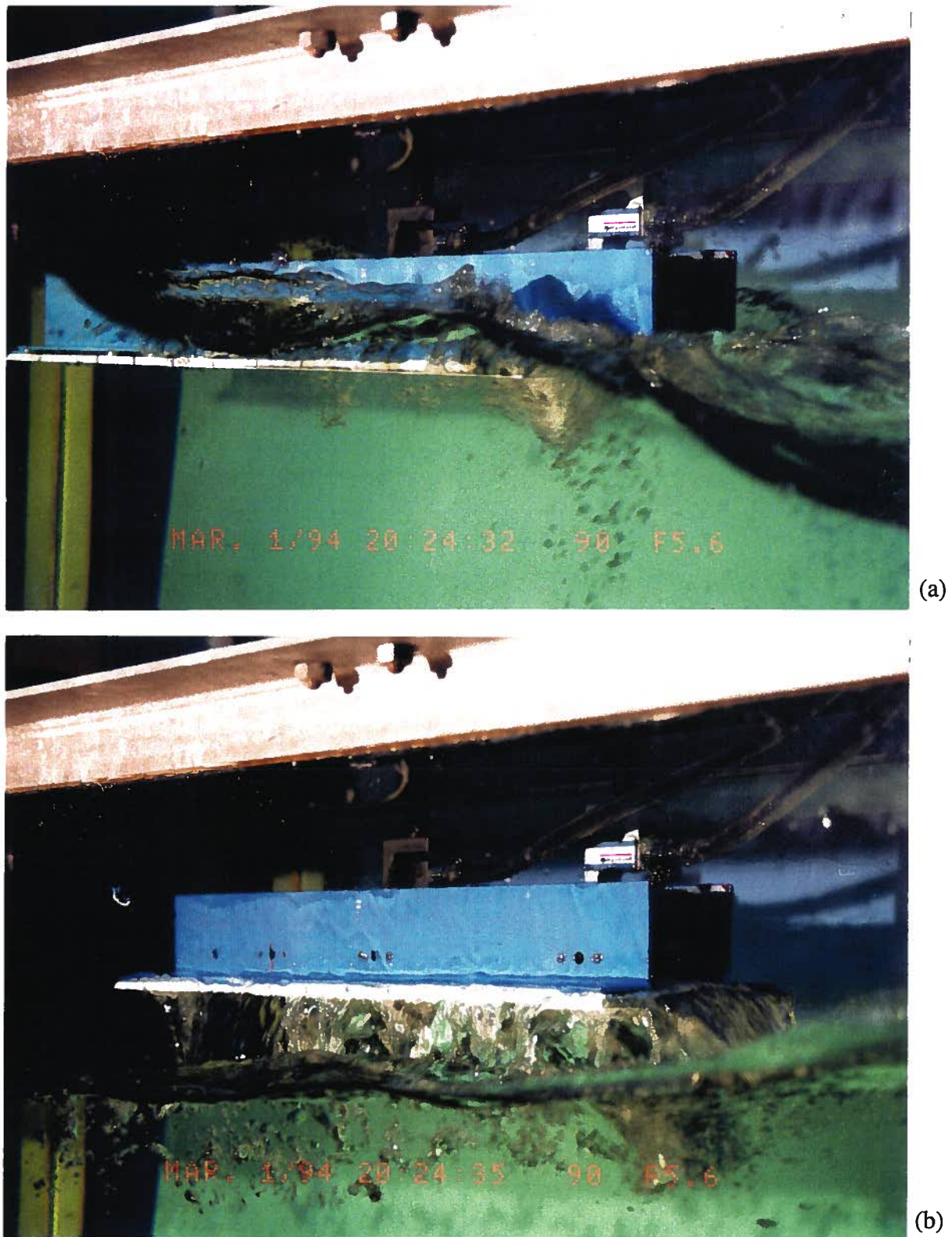


Fig.4.19 Photographs of wave impact. (a) instant of complete submergence; (b) water drainage following submergence.

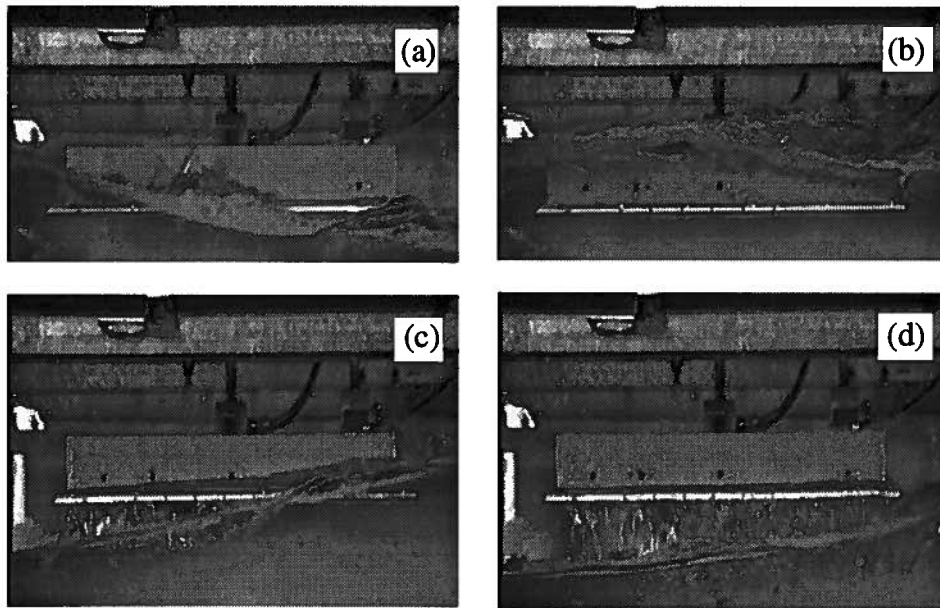


Fig. 4.20 Video images indicating various stages of wave impact during one wave cycle. (a) partial submergence; (b) complete submergence; (c) wave recession; (d) water drainage.

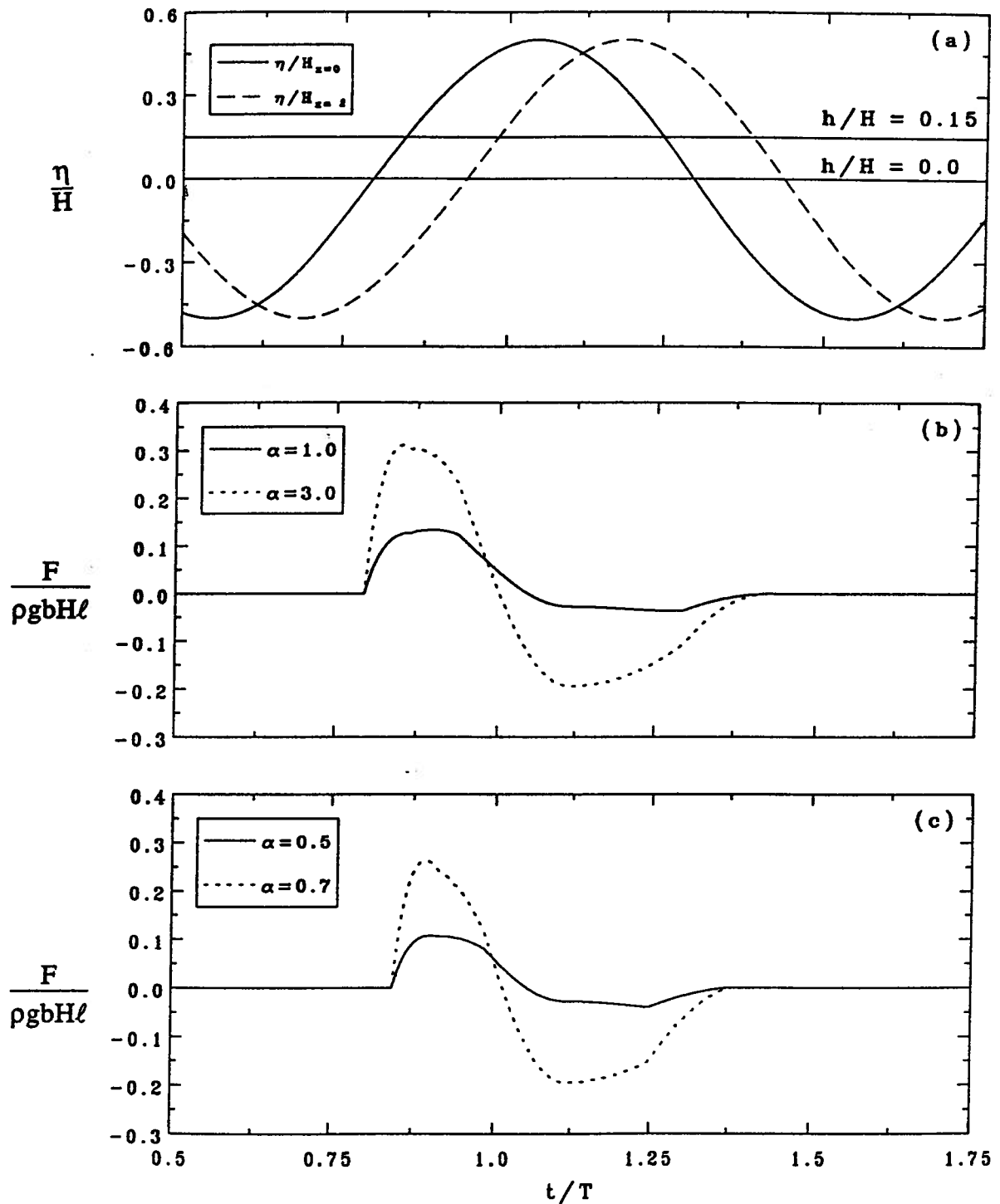


Fig. 4.21 Variation of normalized free surface elevation and predicted vertical force based on Eq. 2.23 for $H/L = 0.04$, $\ell/L = 0.146$ with two different plate clearances. (a) free surface elevation; (b) vertical force for $h/H = 0$; (c) vertical force for $h/H = 0.15$.

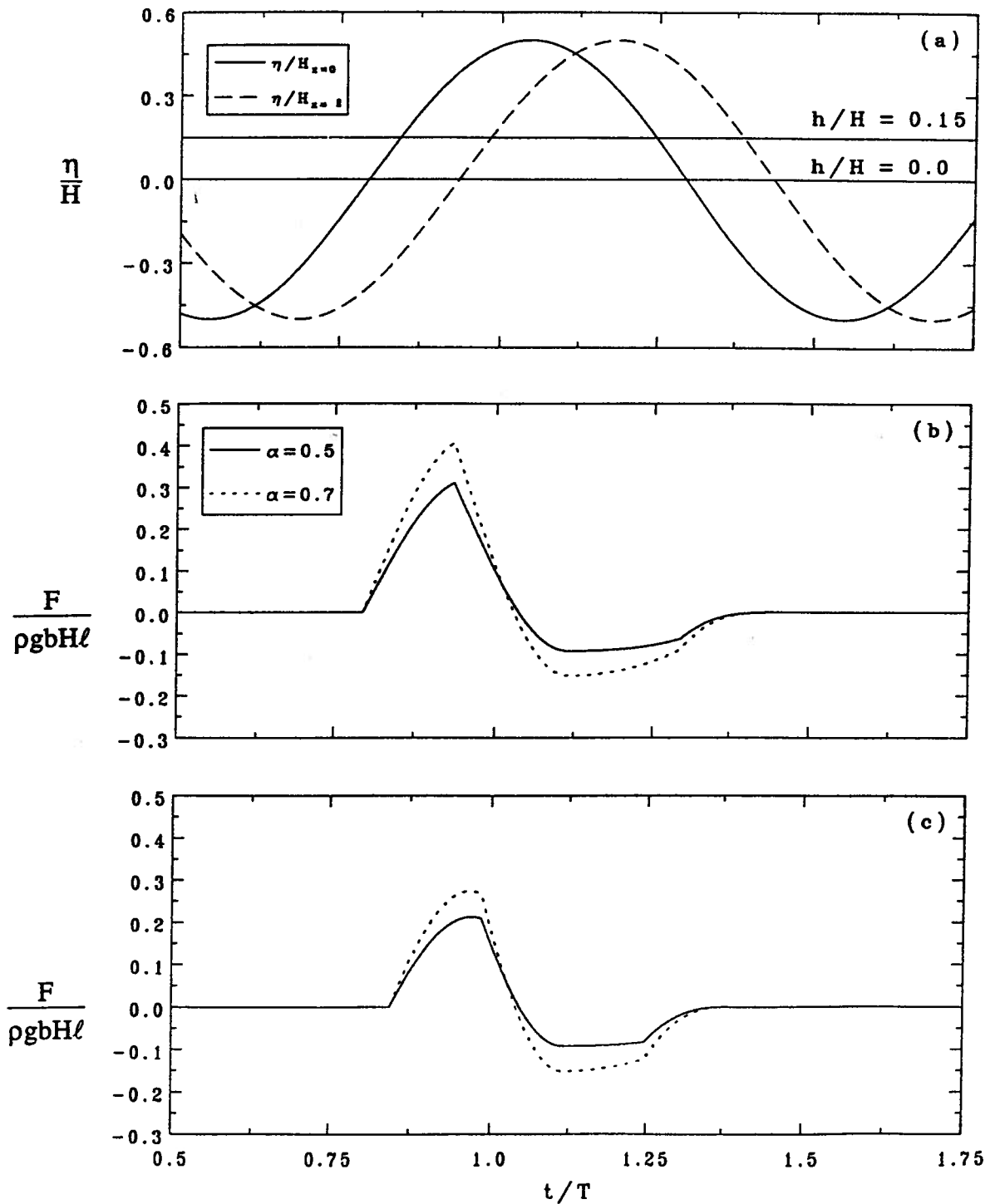


Fig. 4.22 Variation of normalized free surface elevation and predicted vertical force based on Eq. 2.27 for $H/L = 0.04$, $\ell/L = 0.146$ with two different plate clearances. (a) free surface elevation; (b) vertical force for $h/H = 0$; (c) vertical force for $h/H = 0.15$.

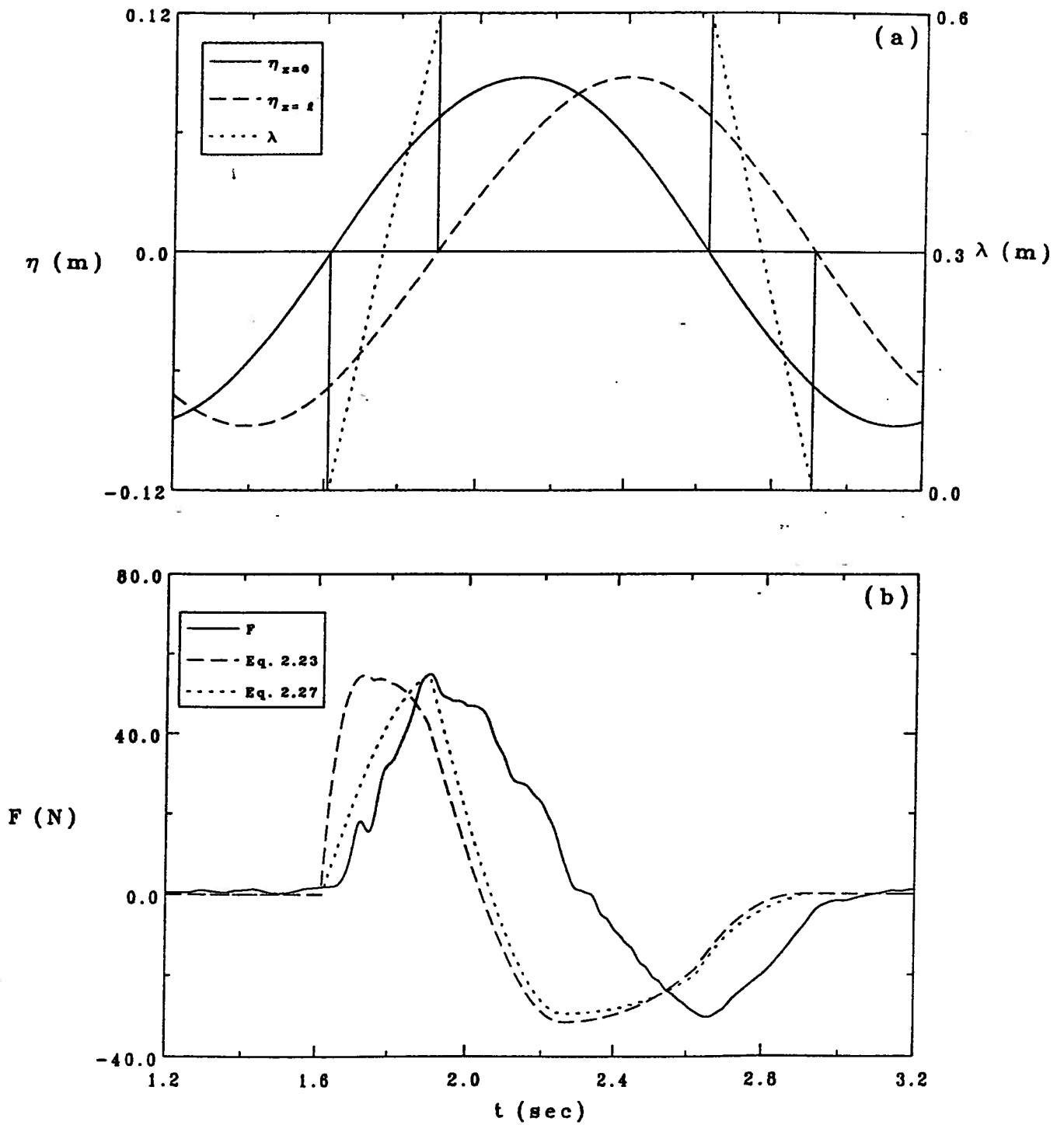


Fig. 4.23 Comparison of vertical force predicted by analytical models with experimental observation for $h = 0$ cm, $T = 2.02$ sec, $H = 17.5$ cm. (a) free surface elevation and the wetted length; (b) vertical force.

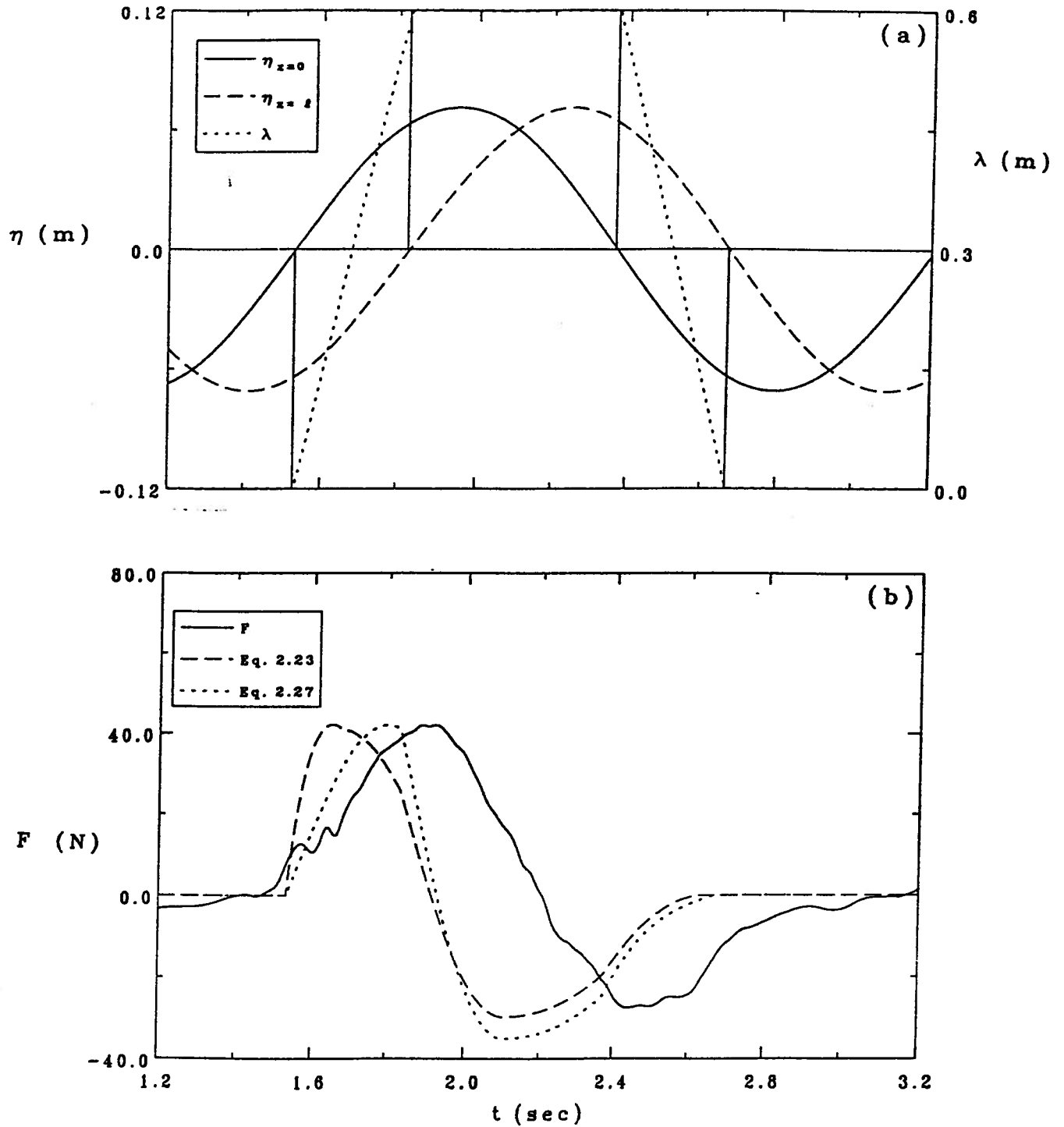


Fig. 4.24 Comparison of vertical force predicted by analytical models with experimental observation for $h = 0$ cm, $T = 1.68$ sec, $H = 14.2$ cm. (a) free surface elevation and the wetted length; (b) vertical force.

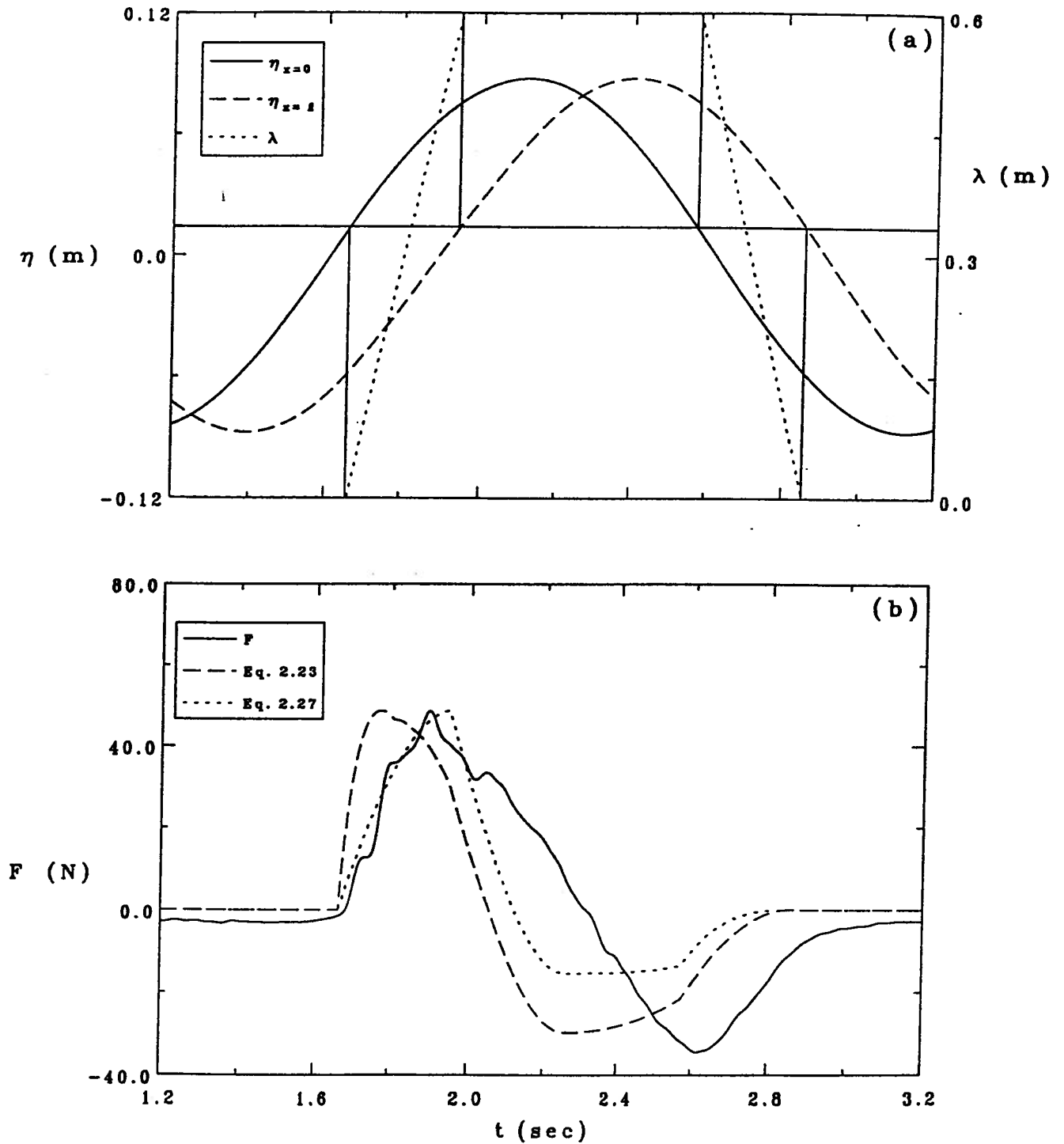


Fig. 4.25 Comparison of vertical force predicted by analytical models with experimental observation for $h = 1.4$ cm, $T = 2.02$ sec, $H = 17.5$ cm. (a) free surface elevation and the wetted length; (b) vertical force.

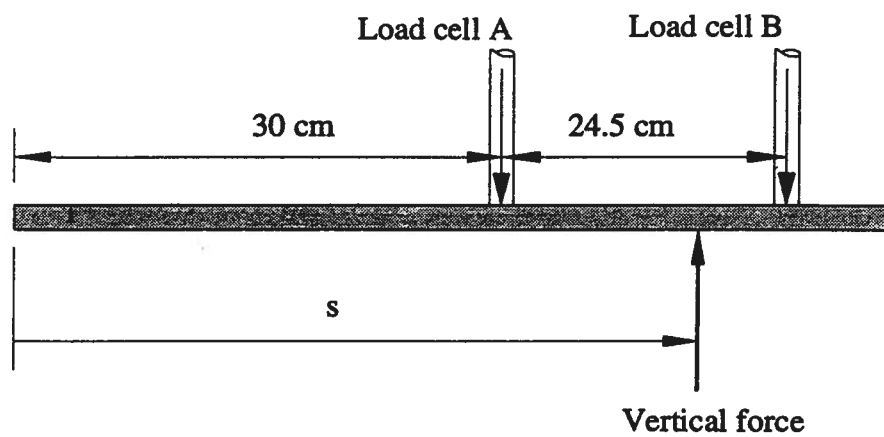


Fig. A1 Free body diagram of the plate indicating support forces and the line of action of the vertical force.